Alma Mater Studiorum - Università di Bologna

DOTTORATO DI RICERCA IN

BIOLOGIA CELLULARE E MOLECOLARE

Ciclo 33

Settore Concorsuale: 05/E1 - BIOCHIMICA GENERALE

Settore Scientifico Disciplinare: BIO/10 - BIOCHIMICA

DEVELOPMENT OF 3D CANCER CELL MODELS TO TEST METABOLIC INTERVENTIONS AS AN ANTICANCER STRATEGY

Presentata da: Ana Catarina Da Silva Almeida

Coordinatore Dottorato

Giovanni Capranico

Supervisore

Anna Maria Porcelli

Esame finale anno 2021

Abstract

In recent years, it has become evident that the role of mitochondria in the metabolic rewiring is essential for cancer development and progression. The metabolic profile during tumorigenesis has been performed mainly in traditional 2D cell models, including cell lines of various lineages and phenotypes. Although useful in many ways, their relevance can be often debatable, as they lack the interactions between different cells of the tumour microenvironment and/or interaction with the extracellular matrix [1,2]. Improved models are now being developed using 3D cell culture technology, contributing with increased physiological relevance [3,4].

In this work, we have improved a method for the generation of 3D models from healthy and tumour colon tissue, based on organoid technology, and performed their molecular and biochemical characterization and validation. Further, in-plate cryopreservation was applied to these models, and optimal results were obtained in terms of cell viability and functionality of the cryopreserved models. We have also cryopreserved colon fibroblasts with the aim to introduce them in a co-culture cryopreserved model with organoids. The utilization of this technology allows the conversion of cell models into "plug and play" formats. Therefore, cryopreservation in-plate facilitates the accessibility of specialized cell models to the universe of cell-based research and application, in cases where otherwise such specialized models would be out of reach. Finally, we have briefly explored the field of bioprinting, by testing a new matrix to support the growth of colon tumour organoids, which revealed promising preliminary results.

To facilitate the reader, we have organized this thesis into chapters, divided by the main points of work which include development, characterization and validation of the model, commercial output, and associated applications. Each chapter has a brief introduction, followed by the results and discussion and a final conclusion. The thesis has also a general discussion and conclusion section in the end, which covers the main results obtained during this work.

Contents

List of Abbreviations

AG	Antigen
ATP5A1	ATP synthase F1 subunit alpha
BME2	Basement membrane matrix type 2
BSA	Bovine serum albumin
CPA	Cryoprotectant
CRC	Colorectal cancer
DAB	3′-Diaminobenzidine
DAPI	4′,6-diamidino-2-phenylindole
DMEM	Dulbecco’s modified eagle medium
DPBS	Dulbecco's phosphate-buffered saline
DTT	Dithiothreitol
EBSS	Earle's balanced salt solution
ECAR	Extracellular acidification rate
ECM	Extracellular matrix
EDTA	Ethylenediaminetetraacetic acid
EdU	5-Ethynyl-2´-deoxyuridine
EGF	Epidermal growth factor
FBS	Fetal bovine serum
FCCP	Carbonyl cyanide-4-(trifluoromethoxy)phenylhydrazone (mitochondrial oxidative phosphorylation uncoupler)
FDA	Fluorescein diacetate
FFPE	Formalin-fixed, paraffin-embedded
H&E	Haematoxylin and Eosin
HCl	Hydrochloric acid
HEPES	4-(2-hydroxyethyl)-1-piperazineethanesulfonic acid

LGR5	Leucine-rich repeat-containing G-protein coupled receptor 5
MTCO1	Mitochondrially Encoded Cytochrome C Oxidase I
NDUFS4	NADH:Ubiquinone Oxidoreductase Subunit S4
OCR	Oxygen consumption rate
PBS	Phosphate buffer saline
PGE2	Prostaglandin E2
PI	Propidium acetate
qRT-PCR	Real time reverse transcribed polymerase chain reaction
RT	Room temperature
SDHA	Succinate dehydrogenase complex, subunit A
ULT	Ultra-low temperature
UQCRC2	Cytochrome b-c1 complex subunit 2
VDAC1	Voltage-dependent anion-selective channel 1
VIL	Villin

Introduction

An overview on colon function

The homeostasis of the intestine depends on the balance between cell production and cell death. Astonishingly, most of the epithelial cells of the intestinal lining are renewed in the space of only a week [5]. The intestinal epithelium is composed of invaginations, called the crypts, with intestinal stem cells (ISCs) residing on its lower part. ISCs give rise to daughter cells that mature and differentiate into epithelial cells such as colonocytes, goblet cells, tuft cells and enteroendocrine cells, in the case of the colon. These epithelial cells migrate to the top of the crypt over the course of several days and eventually dye and shed off [6] (Figure 1). The intestinal epithelium layer is also surrounded by mesenchymal cells such as fibroblasts, and it is also in contact with cells of the immune system.

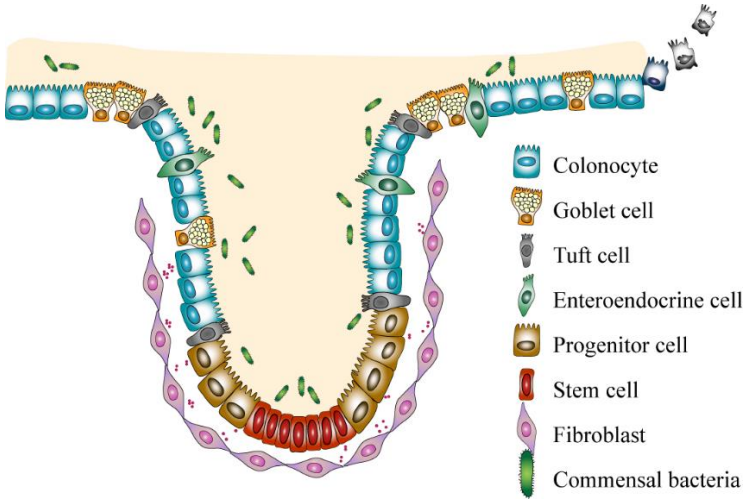

Figure 1: Schematic representation of the healthy colon crypt.

The colon crypt is composed of intestinal stem cells (ISCs) that reside on the bottom of the crypt. Stem cells give rise to progenitor cells that proliferate up the crypt and differentiate into epithelial cells such as tuft, enteroendocrine, goblet and colonocyte cells. Reaching the top of the crypt, these cells dye and shed off [6]. Original figure by Catarina Silva-Almeida.

The regulation of the intestinal epithelium renewal is largely attributed to the ISCs and depends on the spatial organization of signals originated from both the underlying mesenchymal cells and surrounding epithelial cells [5]. The markers that identify ISCs can originate some debate. However, LGR5 is considered one of the main markers of ISCs [7].

The niche in which ISCs reside provides the cells with an array of signals that control the crypt maintenance, mainly originated by the morphogenetic pathways Wnt, Notch, bone morphogenetic proteins (BMPs) and Hedgehog [5]. Several evidences suggest that the Wnt pathway has a crucial role in maintaining the homeostasis of the ISCs. For example,

inactivating mutations in the adenomatous polyposis coli (APC) or activating mutations in β-catenin, which are both key Wnt factors, drive intestinal hyperplasia [8]. Likewise, overexpression of the Wnt activator R-spondin, induces ISCs expansion in vivo [9].

The Notch pathway, mainly regulated through cell to cell contact, determinates lineage decisions in the intestine. For example, its inhibition results in an increase of differentiated goblet cells and its activation in an inhibition of cell differentiation [10,11]. Furthermore, along with the Wnt pathway, Notch can have a dual effect in either activation or depletion of this pathway [10–12].

Evidence shows that BMP pathway also has an important role over the control of crypt homeostasis. Mice deficient in a BMP receptor, or mice overexpressing Noggin, a BMP inhibitor, evidence hyperproliferation and crypt fission. In the top of the crypt, where cells are differentiated, BMP is active, whereas in the bottom of the crypt, BMP activity is controlled by BMP inhibitors produced by mesenchymal cells [13].

Finally, the Hedgehog pathway also has a role in the control of the crypt homeostasis. The conditioned deletion of the Hedgehog inhibitor patched, inhibits Wnt pathway and thus induces enterocyte differentiation is the small intestine [14]. However, the role of this pathway is still the source of some confusion, and further studies are needed to better define its function in the crypt.

Colorectal cancer features

Despite the detailed regulatory mechanisms that exist in the intestine, the high incidence of patients with colorectal cancer (CRC) suggests that these mechanisms can sometimes fail. Not only environmental factors such as diet and medical history of inflammatory bowel disease [15], but also genetic factors and family history of associated syndromes [16,17] are involved in the source of CRC.

The original model developed by Fearon and Vogelstein, where CRC develops by the accumulation of serial mutations that induce the transition of adenoma to carcinoma, is still the prevailing model for CRC [18]. The events that drive transition from normal mucosa to adenocarcinoma are mainly controlled by the Wnt pathway. In normal cells, transcriptional regulator β-catenin is controlled by a multiprotein complex containing the tumour suppressor APC [19]. Wnt ligands can activate the Fizzled receptors, disrupt the complex and induce the translocation of β-catenin to the nucleus. β-catenin is then able to associate with the T-cell factor/lymphoid enhancer factor (TCF/LEF) family of transcription factors and activate

specific Wnt-target genes, such as regulators of stem cell fate (*LGR5, ASCL2*), cell proliferation (*C-MYC*), and cell cycle (*cyclin D1*) [20–22]. Wnt pathway is then crucial for the homeostasis of the crypt, but it is also associated with pathogenic settings. For example, APC mutations result in a defective degradation of β-catenin by the complex, and thus lead to the permanent transcription of Wnt-target genes [23]. Although the first hint that induces the transition of healthy tissue to adenoma is associated with the Wnt pathway, progression to carcinoma is pushed forward by mutations affecting other pathways such as the RAS/mitogen-activated protein kinase (MAPK), TP53, phosphoinositide 3-kinase (PI3K), transforming growth factor (TGF), SMAD4 and PTEN [24,25].

Interestingly, tumourigenicity induced by mutations is proposed to be different depending on which cells they appear. Therefore, some models support a bottom-up theory, where ISCs are in the origin of CRC, whilst others support the top-down theory, with differentiated cells in the origin of mutations that lead to CRC [5]. Experimental evidence is stronger for the first. For example, the specific deletion of the *Apc* gene in ISCs of recombinant mice, leads to the development of adenomas [26–28] whilst a similar deletion of *Apc* in differentiated cells only leads to the appearance of sporadic or slow-developing adenomas [28].

Human CRCs contain a large genetic heterogeneity, presenting a significant range of mutations [29]. Also, there is evidence that the tumour microenvironment is composed by a self-renewing population of cancer stem cells (CSCs) and differentiated tumour cells, which further increases the complexity and heterogeneity of tumours [30]. Because CSCs are able to self-renew and have a multilineage differentiation ability, capable to generate the entire population of the original tumour when transplanted, they are defined as the driving force of the tumour itself [30,31]. Several studies have also indicated that CSCs in CRC are more resistant to therapy than differentiated tumour cells, which drives a general current interest in therapies that target specifically CSCs [20,32,33].

Despite clear evidence of the role of genetic mutations in the appearance of CRC, the tumour microenvironment also plays a crucial role. For example, the addition of dextran sulphate sodium in *Apc*^{Min} mice, strongly increased the formation of intestinal polyps [34]. Hyperplasia was induced in the same mice model, by the treatment with phospholipase A_2 [35,36]. Further, mice that carry the *Apc* mutation plus a deletion of *Smad4*, are unresponsive to differentiation induced by BMP signals from the microenvironment, and have very invasive adenocarcinomas with stromal proliferation [37]. Also, in mouse models of human juvenile polyposis and Peutz-Jeghers, characterized by the appearance of hamartomatous polyps, the

ectopic expression of Noggin and *Smad4* deletion in T cells, results in the generation of polyps [38,39]. Although this data is associated with mice models, that can sometimes not represent the real time evolution of CRC in humans, there is also evidence in humans for the importance of the tumour microenvironment in the appearance of CRC. The most common comes from the fact that patients with history of chronic inflammation due to Chron's disease or ulcerative colitis, have more predisposition to the development of cancer in the gut [40]. The involvement of immune cells is also evidenced by the fact that administration of anti-inflammatory drugs lowers the risk of CRC-associated mortality [41].

Metabolism rewiring in CRC

Cancer occurs due to the transformation of healthy cells into malignant cells by several molecular and biochemical changes that are common to several types of cancers, and that confer survival advantages to cancer cells. These changes define characteristics of cancer cells or "The Hallmarks of cancer", and can be divided into seven: self-sufficiency in growth signals, insensitivity to anti-growth signals, evasion of programmed cell death, limitless replicative potential, sustained angiogenesis, tissue invasion and metastasis, and reprogramming energy metabolism [42,43].

The most recent hallmark, "reprogramming energy metabolism", arise from early observations made by Heinrich Warburg, that noted that cancer cells have high glycolysis, even in the presence of oxygen [44]. This behaviour was later named as "aerobic glycolysis" or "Warburg effect". Currently, there are several explanations for the metabolic reprogramming observed in cancer cells. One of them is that cancer cells grown many times within limited blood supply, leading to hypoxia. In these conditions, cancer cells are still able to survive, by switching their metabolism from the less advantageous aerobic respiration, to glycolysis [45,46]. Nevertheless, glycolytic metabolism can occur even before exposure to hypoxia, as it was observed for leukemic cells residing in the bloodstream with large oxygen concentrations [47,48], or lung tumours likewise subjected to high oxygen concentrations [49,50]. Oncogene activation of tumour suppressor inactivation can also be in the origin of metabolic reprogramming observed in cancer cells [51–56].

CRC is one of the cancer types that is described has presenting the "Warburg effect". Evidence is described by a high rate of glucose consumption, high intratumour levels of lactic acid [57,58], and overexpression of glucose intermediates in CRC tumours [59–63]. However, there is proof that some CRC tumours still use oxidative phosphorylation as their main source of

energy [64], and that respiration rates and mitochondrial content is higher in tumour cells, comparing to healthy colon cells [65].

A hypothesis that can explain these observations is named as the "reverse Warburg effect" [66]. According to this theory, there is a metabolic connection between tumour cells and stomal cells, where cancer cells induce the metabolic reprogramming of neighbour stromal cells, such as fibroblasts (Figure 2). Fibroblasts differentiate into myo-fibroblasts and secrete lactate and pyruvate, that are used by tumour cells to produce energy [66]. Therefore, the metabolic reprogramming occurs in the stromal compartment and supports tumour growth and angiogenesis [66]. Similar behaviour was also observed by other authors, in myofibroblasts from skin [67], in breast cancer [68,69] osteosarcoma, ovarian cancer, head and neck tumours and malignant lymph nodes [70–72]. Likewise in CRC, studies by Chekulayev et al. compared the glycolytic activity and oxidative phosphorylation of both tumour and stromal cells, and demonstrated that tumour cells have an effect over metabolism of stromal cells, in order to support tumour growth [65].

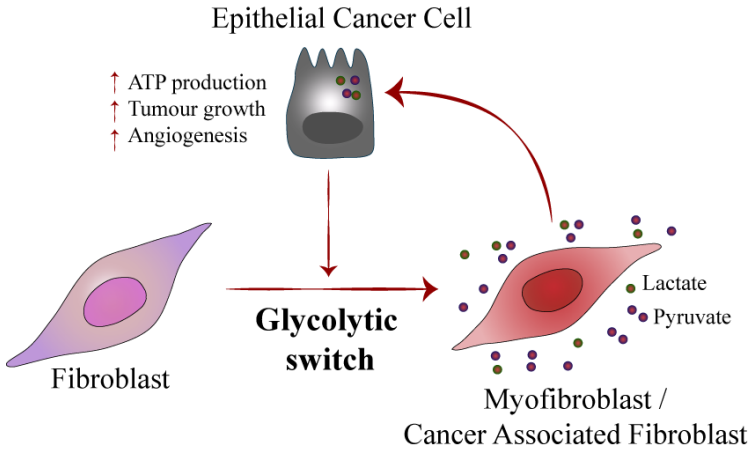

Figure 2: Schematic representation of the "Reverse Warburg effect".

Cancer cells induce a metabolic reprogramming (glycolytic switch) of neighbour fibroblasts. Fibroblasts differentiate into myofibroblasts and produce lactate and pyruvate, used as "fuel" by cancer cells which increase their ATP production, tumour growth and angiogenesis. Original figure by Catarina Silva-Almeida.

Organoids as *in vitro* 3D cancer models

Cancer cell lines have existed for many years to model cancer research and to perform drug screenings in order to identify drug sensitivity related to genetic alterations [73,74]. These models are easy to use, not expensive, and can provide reliable information when used for the study of specific topics. However, they present several limitations, such as the lack of signals from the exterior microenvironment which can lead to changes in the cells phenotype and does

not represent their *in vivo* behaviour, or the accumulation of genetic mutations along time and passages, which stops them from recapitulating the heterogeneity of the tumour of origin [1]. Furthermore, it is many times difficult or inaccurate to find a direct relationship between drug sensitivity and a specific genetic variation, utilizing these models. Co-culture methods can add some interest to 2D cultures, as they can include more than one cell type in culture. However, these cultures still lack the communication with the extracellular matrix and the spatial configuration of the tissue of origin.

More advanced models in cancer research include patient-derived tumour xenografts. These models are characterized by the transplantation of pieces of tumour or single-cell suspensions from tumour tissues into patients or most commonly, into immunocompromised mice [75]. Xenografts present many advantages such as the maintenance of cellular and structural characteristics of the tumour of origin, and the preservation of the genetic profile [75–77]. However, some limitations include high costs and longer times required for culture formation and thus to obtain results. Furthermore, they can present some challenges in the study of the tumour microenvironment, as cells derived from the stroma of the original tissue are generally substituted by cells of the host [75].

The development of three-dimensional (3D) technology introduced several advantages in research, specifically in cancer research. These models allow the study of the tumour microenvironment, by the use of cultures within an extracellular matrix, or by the establishment of gradient concentrations of components within the culture [78]. Furthermore, these cultures are adaptable as platforms for high-throughput studies [79].

The advances in the development of 3D models and the technology developed to support these models, has led to the appearance of the term "organoid" [80]. Although the correct and universal definition of the term organoid has been subjected to much debate, in our opinion, the most precise definition was made by Fatehullah et al. in 2016 and describes: "Here we define an organoid as an *in vitro* 3D cellular cluster derived exclusively from primary tissue, embryonic stem cells or induced pluripotent stem cells, capable of self-renewal and self-organization, and exhibiting similar organ functionality as the tissue of origin" [81].

Independently of the discussion behind nomenclature, it is important to mention that these advanced 3D models brough many advantages to cancer research [81–83] (Figure 3). Further, organoids could fill the gap between the use of cancer cell lines that facilitate high throughput

drug sensitivity studies, and the use of physiologically more relevant models such as xenografts [4].

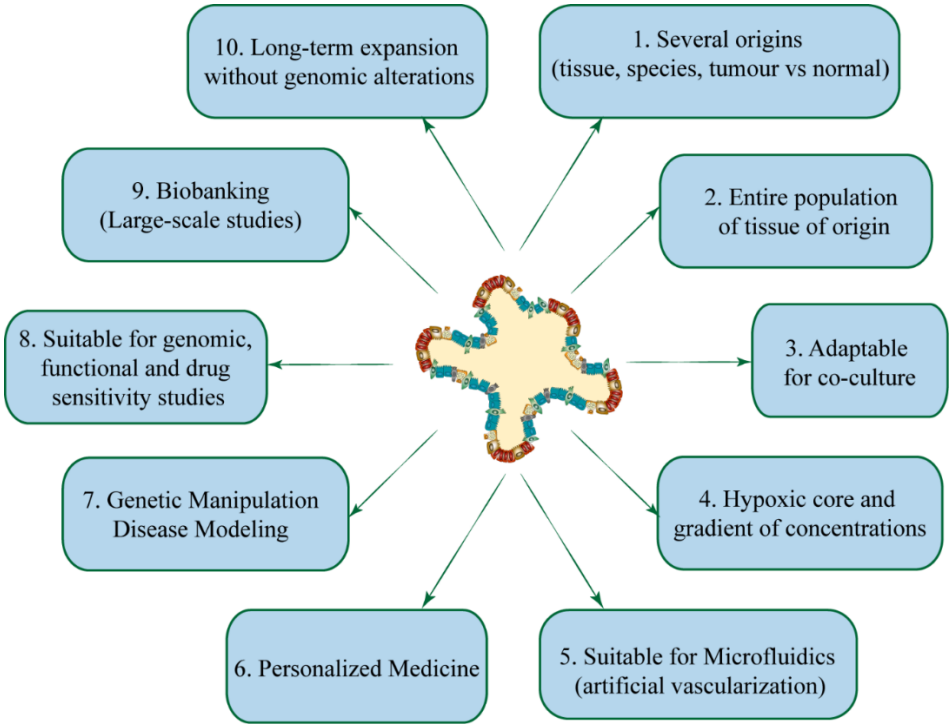

Figure 3: Advantages of the use of organoids in cancer research.

Some advantages of the use of organoids in cancer research are as follows: 1) organoids can be derived from several tissues and species, and allow a comparison between both healthy and tumour counter partners [84]; 2) they can generate the entire population of the tissue of origin, whilst conserving their spatial organization, morphology and genetic composition [85–88]; 3) they are adaptable for co-culture studies with cells of the immune system [89], fibroblasts [90–92] and cells of the nervous system [93]; 4) the 3D structure of the organoid allows the generation of a hypoxic core and a gradient of concentrations of components, which closely represents the conditions observed in the tissue of origin [93,94]; 5) organoids can be adapted to microfluidics systems, allowing the inclusion of artificial vasculature [95,96]; 6) organoids can be used for personalized medicine and to study human diseases difficult to model using conventional models [97–99]. Proof-of-concept for the use of organoids in personalized medicine has already been showed for cystic fibrosis (CF). Dekkers et al. has used rectal organoid models to study CF in human patients, and has observed the selective swelling effect of the component forskolin in healthy organoids and not in CF-derived organoids [100]. Further, the same authors have followed-up this study and successfully predicted drug responses in patients by utilizing CF-derived rectal organoids [101]; 7) organoids can be genetically manipulated, allowing disease

modelling. Still in the context of CF, other authors have used CRISPR/Cas9 technology in CF-derived organoids to restore its physiological function [102]; 8) organoids can be utilized for genomic, functional and drug sensitivity studies [86]. The data produced by Van De Wetering et al. demonstrated a link between genetic alterations and drug sensitivity and can enable a predictive model of individual patient responses to therapy, as it was able to capture sub-clonal populations of organoid cultures. In another setting, tumour organoids were utilized to develop a 384-well assay system, applicable for drug screenings [103]. The use of tumour organoid models like this, allows the use of automatic seeding, drug administration and results collection, that connects the use of tumour organoid models with the most modern and technology-relevant settings [103]. In a similar study, tumour organoid cultures were utilized in a set of *in vitro* drug testing, allowing to predetermine the best drug treatment for specific patient-derived organoids obtained from tumour samples [85]; 9) organoids can be bio-banked, permitting the generation of large-scale drug studies. The ability to generate biobanks was previously demonstrated and allows the use of such cultures in long-term basic and translational research [86]. The generation of biobanks is crucial to support the production of a relevant number of drug testing in patient-derived samples [104]. Considering the numerous molecular and genetic variations between tumours, it is necessary to generate massive biobanks to produce relevant data. Therefore, the ability to create large biobanks of patient-derived organoid models is of high importance; 10) they can be expanded without genomic alterations [85,88,105–107]. The maintenance of the original genetic identity is a main problem in routine cell cultures and can be one of the causes for failure encountered in translating results obtained in drug discovery with results from early clinical trials [108].

Despite the clear advantages in the use of organoid models in cancer research, like other models, organoids also present some limitations. For example, organoids can develop into several sizes and shapes within the same culture, which can present some difficulties for high-throughput studies [81]. This can also be intensified by the lack of standardized techniques utilized to produce organoids between laboratories. New technologies such as live imaging or artificial intelligence could be helpful to overcome this limitation. Further, organoids require the use of an extracellular matrix of animal origin, which can add variability factors into the culture and prevent transplantation of organoids into humans [81]. However, we believe that technology will develop advanced synthetic or human-compatible matrixes that could be used instead of animal-derived. Although organoids are a structurally complex model, they lack the other cell types of the stroma such as fibroblasts and immune cells. The tumour

microenvironment can have a significant effect on drug responses, which many times is the cause of the discrepancy found between *in vitro* and *in vivo* studies [109]. To overcome this possible caveat of organoids, some authors have already demonstrate the ability to co-culture organoids with cells of the immune system [89], fibroblasts [90–92] and cells of the nervous system [93].

Organoids to dissect healthy and cancer colon

The understanding of the physiology of the crypt, where the microenvironment and the extracellular matrix (ECM) originate a serious of complex morphogenetic signals that control the maintenance of the crypt, allowed the generation of the first *in vivo* models of crypts. Both Ootani et al. [110] and Sato et al. [106], describe models that require a solid matrix (either collagen or Matrigel), are enhanced by R-spondin 1 (Wnt signalling activator), and produce a crypt-like structure containing ISCs and differentiated cells. However, both describe different niche requirements. For example, Ootani et al. collagen cultures require mesenchymal myofibroblasts [110], whilst Sato et al. Matrigel cultures do not [106]. However, Sato et al. introduces the use of Noggin that could replace the need for mesenchymal myofibroblasts.

The knowledge of the microenvironment of the healthy crypt was crucial for the discovery of the components necessary for the development of healthy organoids, which will be further explored over the next paragraphs. However, in the case of tumour organoids, the scenario is more complicated and variable. Because of the different landscape of mutations and characteristics of each individual tumour, the niche requirements of each can be quite different. Initial protocols to generate tumour organoids from mice or human tumour samples were developed by Sato et al. [107], based on the protocols already developed for healthy organoids. However, this led to the understanding that tumour organoids do not have the same niche requirements as healthy organoids, as it will be developed further ahead in this thesis.

Niche components for healthy colon organoids

As mentioned before, Wnt signalling is crucial for crypt proliferation. Therefore, Wnt activators should be one of the niche components necessary for the development of intestinal organoids. In fact, R-spondin-1 (Wnt activator) is also a ligand for LGR5, an essential factor to activate Wnt signalling in intestinal crypts [111]. In mice small intestinal organoids, the presence of R-spondin is enough activate Wnt signalling [107], as Paneth cells present in this tissue produce other Wnt ligands that are essential to maintain stem cells [112,113]. However, Paneth cells are not present in the colon, and external R-spondin is not enough to sustain the

maintenance of stem cells. Therefore, the addition of Wnt3A or Wnt3A-conditioned medium has proved essential to overcome this issue and sustain crypt formation *in vitro*. Furthermore, removal of Wnt3A from the culture medium is essential to induce enterocyte differentiation.[107].

Epidermal growth factor (EGF), being a stimulator of cell proliferation in epithelial and non-epithelial cell types, is also associated with intestinal proliferation [114] and proved to be a crucial component for crypt proliferation [107]. The vitamin nicotinamide, a form of vitamin B3 with ability to suppress sirtuin activity [115], has also proved essential to prolong human colon organoid culture for longer than a week. Also, removal of this component from the culture medium was crucial to induce differentiation of goblet and enteroendocrine cells [107]. The hormone gastrin, was also found to be useful to support the growth of human colon organoids, although its effect was not crucial [107]. The transgenic expression of noggin, an inhibitor of the BMP pathway, induced crypt formation *in vivo* [39]. This reinforces the role of BMP signalling in the maintenance of the crypt homeostasis and the importance of using BMP inhibitor noggin as a niche component for healthy organoids. Maintenance of the cell-matrix and cell-cell interactions is required for the maintenance of the integrity of the intestine, as loss of cell interactions results in cell death by anoikis [116–118]. In fact, the addition of Y-27632 (Rock pathway inhibitor) to single-sorted colonic epithelial cells was necessary to prevent anoikis and generate colon organoids [107]. The matrix surrounding the organoids is also very important to support their growth. In fact, laminin is expressed at the base of the mice intestinal crypt [119] and has demonstrated to be essential for the generation of intestinal organoids *in vitro* [107].

Two small molecule inhibitors, A83-01 and SB202190, were crucial to sustain the plating efficacy of human colon organoids and prolong their culture period to half a year [107]. A83-01 is a Alk4/5/7 inhibitor as well as inhibitor of epithelial to mesenchymal transition (EMT) induced by TGF-β [120]. SB202190 is a p38 mitogen-activated protein (MAP) kinases inhibitor, a pathway involved in cell differentiation, apoptosis and autophagy [121,122]. Importantly, removal of SB202190, along with Wnt and nicotinamide from the culture medium was crucial to induce differentiation of goblet and enteroendocrine cells [107].

Niche components for colon tumour organoids

Due to the mutational landscape of most colon tumours, it is to be expected that the niche requirements to develop tumour organoids is different from that of healthy organoids. Indeed, the presence of R-spondin-1, Wnt3a and noggin was superfluous for the generation of human colon cancer organoids [107]. Interestingly, EGF was not dispensable for all the organoid

cultures obtained from human tumour samples, as it slowed the progression of some organoid cultures [107].

Although the robust protocol developed by Sato et al. allowed the generation of several organoid cultures from tumour samples, this is not always the case. Colon tumours can present several subtypes, with different degrees of differentiation, invasion capacity or evolution stages. For this reason, a good strategy for the successful generation of tumour organoids could be the establishment of different culture conditions that would initially access the niche requirement for the specific subtype of tumour samples. In fact, this was the strategy adopted by Fujii et al., which developed eight combinatorial culture conditions for isolated cancer cells at culture initiation [25]. The culture conditions contained variations of medium formulation but also of oxygen availability. By adopting this method, the authors were able to generate CRC organoids with 100% efficiency, not accounting for external factors such as contaminations or poor-quality samples [25]. Interestingly, the authors confirm the great variability in niche component requirements depending on the original tumour type [25]. For example, organoids from adenomas propagated without the need of Wnt and R-spondin, but mostly required EGF [25]. Contrary, organoids derived from hyperplastic polyps and sessile serrated adenoma/polyps (HP/SSAPs) required Wnt and R-spondin but dispensed EGF [25]. This variation was even more accentuated in organoids derived from CRC patients, with different niche requirements depending on microsatellite stability and metastaticity [25].

This variability found in niche requirements of tumour organoids reflects the ability of tumour cells to adapt to the tumour microenvironment and proliferate in hostile conditions. Therefore, it would be advantageous to adopt a similar strategy as Fujii et al. describes, for the initial establishment of tumour organoid cultures, in order to reflect the individual characteristics and behaviour of the original tissue *in vitro*. Furthermore, medium composition can affect the genetic composition and clonal outgrowth of certain mutations, as removal of selected components from the culture medium lead to the selection of specific mutant populations [123,124].

Organoid technology applied to cancer metabolism

Oxygen concentration is one of the main factors affecting tumour metabolism. The balance of absorption and secretion generated by the tumour microenvironment generates a gradient of molecules, specially oxygen. In many tumour, the response to hypoxia within the core of the tumour leads to a reduction in mitochondrial respiration and increased glycolysis,

along with angiogenesis [125]. Therefore, being able to simulate such conditions in *in vitro* models is of great importance. Some 3D models have accomplished this, such as Fischbak et al., who cultures oral squamous cell carcinoma cells with a porous artificial scaffold that allowed the generation of an hypoxia core [126]. Other models use microfluidics scaffold that integrate perfusion channels for solutes and oxygen [95], or that simulate vasculature [96].

Another important aspect in the study of metabolism is the rapid turnover of metabolites. In order to measure metabolic responses, it is necessary to quickly collect samples for posterior analysis. Some 3D models of tumours account for this aspect by using a scaffold-tumour composite sheet, that can be unfolded after tumour formation and allows isolation of cells from different layers of the tumour that were subjected to different gradients of solutes and oxygen [127].

Considering all particularities of metabolic studies, it is not easy to find a model that can account for so many details and that can satisfy all study designs. Overall, a good model should account for the tumour microenvironment (including cell types and extracellular matrix), present a gradient of metabolites and oxygen within the tumour, introduce an intrinsic or simulated vascularization, and allow fast recovery of cells and/or samples for posterior analysis. Organoid models can account for the majority of these characteristics. However, it is yet not possible to quickly recover samples for metabolic analysis, particularly if the objective of the analysis is to recover cells and/or metabolites from the different layers of the organoid. Nevertheless, organoid models can still add many advantages to the study of cancer metabolism, overcoming simples cell models such as 2D cell lines, and reducing the use of animal models that do not represent the physiology of human tissues.

Aims of the study

The field of cancer research is evolving fast, and already allowed the generation of cell models and technology that improves drug therapies and treatments. However, relevant models are ultimately necessary to reach relevant data. With this work, we aim at generating a colon cancer cell model that can be utilized to test metabolic interventions. The model will be created utilizing organoid technology and generated from human colon tumour samples. In the context of the metabolism framework in which this project is included, we also aim to demonstrate the utilization of the organoid models for metabolic studies. Ultimately, as this work is performed in the industry, we also aim at generating a commercial product with associated organoid and cryopreservation technology.

Chapter 1: Development of 3D colon organoid models

Chapter Introduction

Human colon tumour and normal adjacent tissue samples were obtained with full ethical permission and processed for isolation as described in the methods section and illustrated in Figure 4.

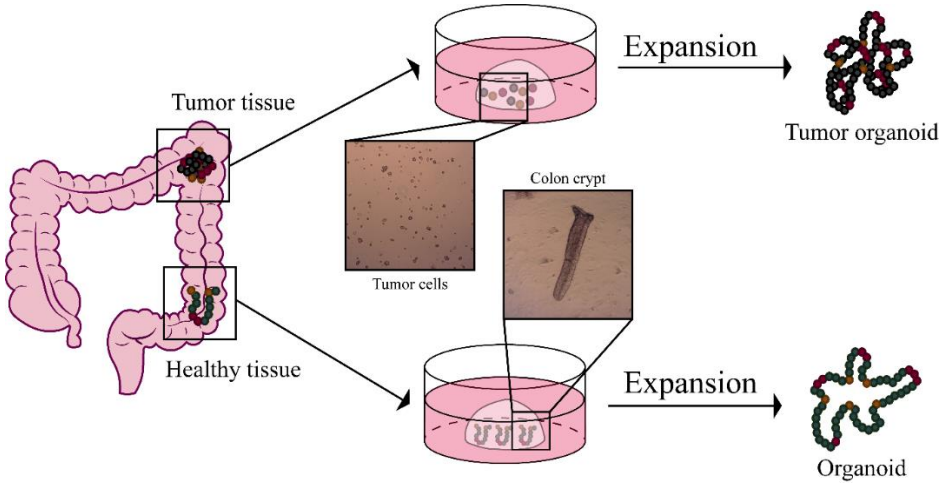

Figure 4: Cartoon illustration of the generation of tumour organoids and/or organoids.

Tumour cells or crypts are isolated from colon tumour tissue or adjacent healthy tissue, seeded in a 3D matrix, and expanded with specific culture medium for the generation of tumour organoids and organoids, respectively. Details of tumour cells or colon crypt were taken with an optic microscope (4x magnification).

In total we performed 3 isolations from different donors, from both colon tumour and normal adjacent tissues. The first isolation was successful, allowing the generation of both healthy and tumour organoids. The second isolation allowed the generation of both healthy and tumour organoids in the first week, but cultures started to dye-off and were discarded. The third isolation was lost due to contamination. Since we were only able to produce and expand both healthy organoids and tumour organoids from the first donor, all further work was performed on these cultures. This thesis involved many experimental techniques that needed optimization. Thus, our aim was to optimize new methods using the successfully expanded culture, and then use this knowledge to isolate and expand cultures from a wider range of tissue donors.

The success in the generation of organoid cultures from human tissue depends on several factors, such as underlying medical history of the patient, the heterogeneity of the tumour (which may contain areas of more necrosis or with differentiated cells intermixed with more proliferative areas), the use of adequate antibiotics during cell culture or the culture conditions that reflect particular existing mutations [86]. After the optimization of the protocols

used, along with the criteria for tissue acceptance and the optimization of culture conditions, we consider that we could reach a high success rate in the generation of organoid cultures.

This chapter describes the development and optimized procedure for the generation of healthy and tumour organoids.

Results and discussion

Healthy colon organoids can be generated from entire crypts

Colon organoids can be generated either from single sorted $Lgr5^+$ stem cells or by whole crypts [128]. The latter method was used in this study, due to the simplicity of the protocol and the lack of access to cell sorting equipment. To isolate crypts, healthy adjacent tissue from patients with colon cancer was washed and treated with a chelation solution under mechanic agitation. We found that the incubation of the mucosal stripes with chelation solution for 30 min, followed by 6 rounds of vortex was enough to remove most of the crypts. Although each isolation gave a different yield of crypts per gram of tissue, in average, the method utilized allowed the extraction of 12670 crypts/gram of tissue (Table 1).

Table 1: Crypt yield per tissue isolation.

	Tissue weight (g)	**Crypt number**	**Crypts/gram**
Isolation 1	2.941	36000	12240
Isolation 2	1.920	17555	9143
Isolation 3	1.283	21333	16627
			12670 (average)

The development of 3D structures is dependent of the existence of an ECM and adequate components in the medium to sustain the proliferation and expansion of the culture. The ECM is not only crucial for the support and growth of cells but also for the modulation of cell behaviour and tissue organization [129]. With these aspects in mind, we decided to seed the crypts (and organoid fragments after expansion) in a reduced growth factor basement membrane extract type 2 (BME2). The physical properties of this ECM allow to easily handle, seed and split the organoid cultures, while containing major components for stem cell growth such as laminin and collagen [129]. Furthermore, we found that a density of 500 crypts per 35 µL of BME2, was the optimal ratio for the development of organoid structures.

Regarding culture medium, we initially decided to use Intesticult^{TM} Organoid Growth Medium (Stemcell Technologies), a commercially available medium for the initial establishment of human intestinal organoids. Even though obtaining the culture medium from

a commercial source can signify a more controlled and less batch-variable product, we found that this involved high costs and stock dependence. For this reason, we also designed and tested in parallel an in-house culture medium (Table 4) for the development of our colon organoid cultures, exploiting those already established [4,86,107,128]. In order to understand if our in-house medium supported the growth of cultures in the same manner as the commercial medium, we measured organoid growth over 5 passages (Figure 5).

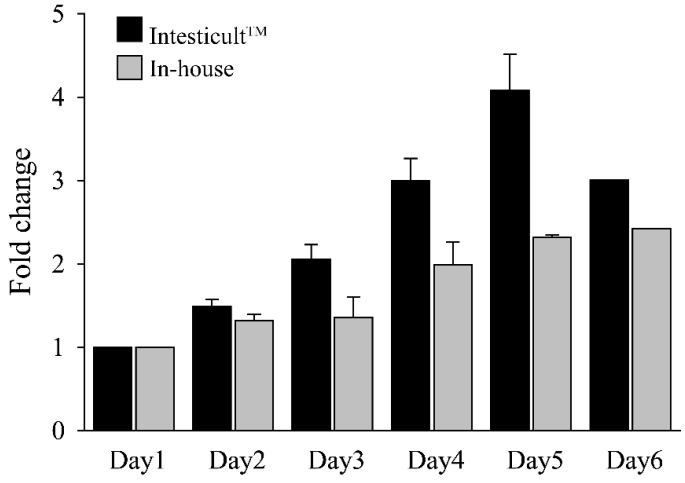

Figure 5: Colon organoids growth in the presence of in-house medium.

Organoids were expanded over 6 days per passage and maintained in culture for 5 passages. Data represent the fold change of the average values of diameter of 6 organoids per well per passage, considering Day 1. Results were obtained from one experiment.

At first glance, organoids cultured in Intesticult™ appear to expand more that organoids cultured in in-house medium. One of the components necessary for the culture of colon organoids, PGE_2, is a mediator of secretion by intestinal epithelial cells and can induce swelling of organoids [130]. Because the composition of Intesticult™ is not disclosed by the commercial source, we could be using different concentrations of this component in our in-house culture medium and this could explain the different measures of colonoid diameter. To explore this hypothesis, we also investigated the expression of stem cell, differentiation, and proliferation markers by qRT-PCR assay. The results obtained by qRT-PCR indicate that there are no relevant differences, in terms of gene expression of stem cell marker leucine-rich repeat-containing G-protein coupled receptor 5 (LGR5), differentiation marker villin (VIL) and proliferation marker MYC, between the commercial and the in-house media (Figure 6). This suggested that the differences in organoid growth could be due to the unalike concentration of components in the medium but were not causing important changes in the proliferative capacity of our organoid cultures. Considering these findings, along with the ability to expand the

organoid cultures using the in-house produced medium, we decided to use this as our expansion medium during further experiments.

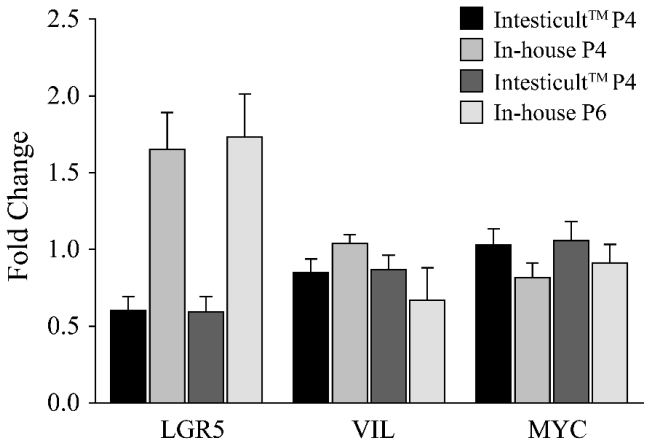

Figure 6: Gene expression is similar between organoids cultured in two different medium formulations.

Organoids were cultured with Intesticult™ or in-house medium along 4 passages. Samples were taken at passage 2, 4 and 6, and qRT-PCR was performed. Data represent the fold change of gene expression of passages 4 and 6, considering passage 2 as a fold change of 1. LGR5: Stem cell marker; VIL: brush-border microvilli marker; MYC: proliferation marker. Results obtained from one experiment.

Using the culture conditions optimized, including the use of in-house medium and BME2 as ECM, we were able to generate colon organoids from entire crypts, and expand these cultures over several passages (Figure 7). Organoids at passage 0 appear darker and smaller because the initial culture is made directly from crypts isolated from colon tissue, and thus present dead cells from original tissue that eventually are eliminated during the expansion process. The organoids were lifted and passaged according to the growth rate, approximately after 6 days of culture and at a ratio of 1:2-3. Organoids at passage 3 are spheric in shape, with a hollow middle, and can present various sizes. Some organoids may present a core with dead cells when they are originated from larger fragments (represented by an asterisk in the figure). The growth rate of the cultures was not always homogeneous and depended on random factors including the time of culture.

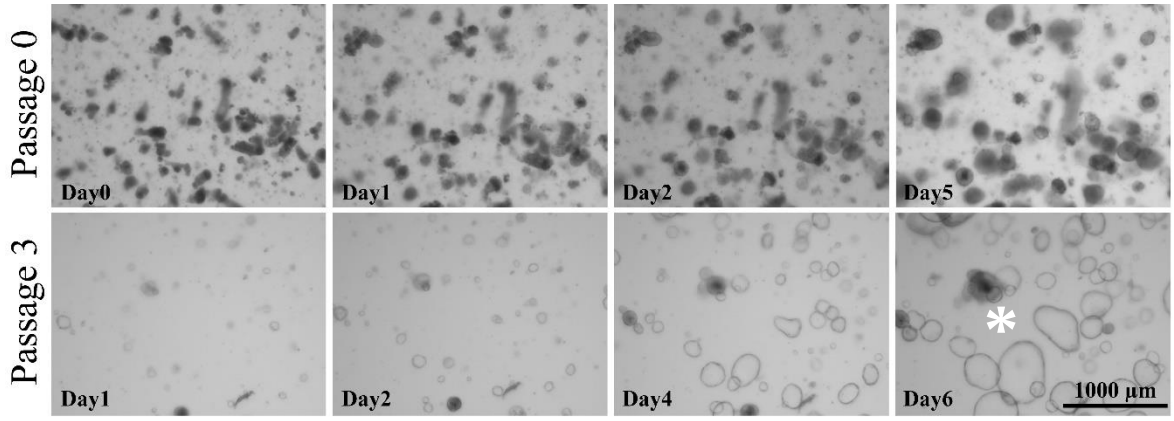

Figure 7: Organoid cultures derived from crypts expand over passages.

Organoids were cultured with in-house organoid medium and imaged at passage zero (top panel) and passage 3 (bottom panel), at the indicated days of culture. Organoid with a core containing dead cells is indicated with an asterisk. Images were obtained using an optical microscope (20x). Scale bar: 1000 µm.

Tumour organoid generation from whole tumour isolates

The generation of tumour organoids from whole human tumour samples was performed without recurring to cell sorting. The tumour was minced into small pieces, washed, and digested with a solution containing the enzyme liberase, due to the hardness of the tumour tissue. With this digestive solution, we found that 50 min incubation was necessary to digest the tissue into single cells. Although the yield of tumour cells from each tumour was variable, the average of tumour cells obtained was $11.97x10^6$ tumour cells per gram of tissue (Table 2).

Table 2: Tumour cell yield per tissue isolation.

	Tissue weight (g)	**Cell number**	**Cells/gram**
Isolation 1	0.522	$2.30x10^6$	$4.41x10^6$
Isolation 2	1.731	$45.28x10^6$	$26.16x10^6$
Isolation 3	1.112	$5.94x10^6$	$5.34x10^6$
			$11.97x10^6$ (average)

As for organoid cultures, BME2 was also used for the expansion of tumour organoid cultures. For the first isolation, we tested 4 different densities of tumour cells: 10000; 30000; 50000 and 100000 cells per 20 µL of BME2 (Figure 8). According to the density and growth or tumour organoids, we determined that the best concentration was between 50000 and 100000 cells per 20 µL of BME2, and thus used a concentration of 70000 cells per 20 µL of BME2 in the remaining isolations.

The success of the establishment of organoid cultures from colon epithelia arise from the discovery of the pivotal role of the Wnt pathway in the healthy crypt development.

However, over 90% of colorectal cancer cases have mutations that activate the Wnt pathway in an abnormal way [131]. Therefore, the need to add Wnt-activator components to the culture media is, in these cases, superfluous, and indeed could promote the outgrowth of normal organoids from healthy stem cells in the tumour sample [25]. On the other hand, a portion of colorectal tumours are in fact Wnt-dependent or even hypoxia dependency [25]. Taking these particularities into account, to obtain successful cultures of tumour organoids, we adopted a strategy of testing different culture settings in our initial cultures. For this, we cultured tumour cells either in normoxia (37 °C, 5 % CO_2) or hypoxia (37 ºC, 5 % CO_2 and 4 % O_2) conditions. We also used two different media formulations: Intesticult™ and complete tumour organoid expansion medium (Table 7). The complete tumour organoid expansion medium was produced in-house and does not contain Wnt or R-spondin. We were able to obtain tumour organoid cultures from the original tumour tissue, from all the conditions (Figure 8). The fact that we were able to obtain tumour organoids without the addition of external Wnt or Wnt-activators to the culture medium is an indicator of the tumourigenesis of the culture, as most colorectal cancers present an aberrant activation of this pathway [131].

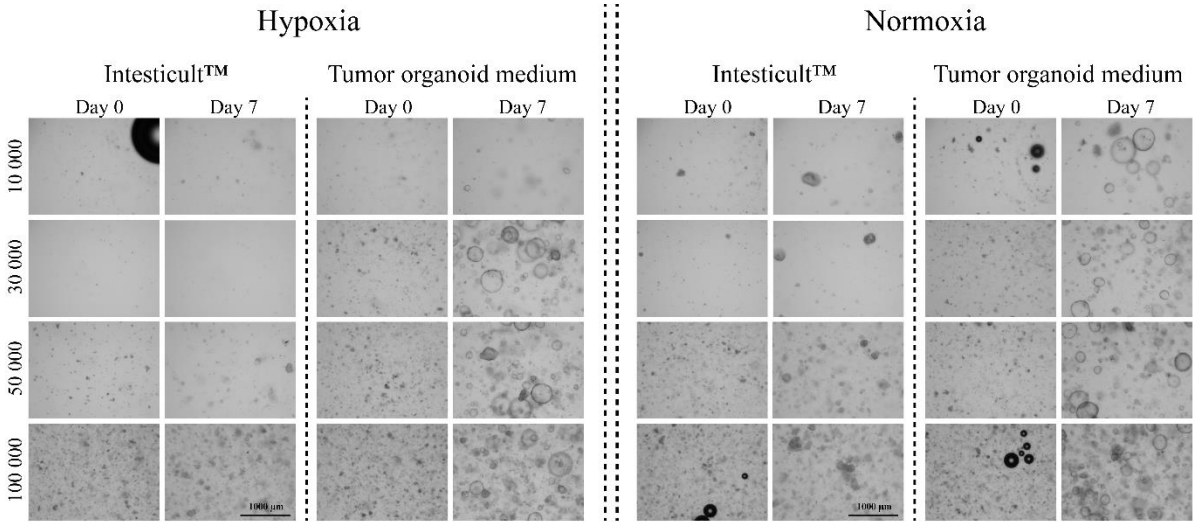

Figure 8: Tumour organoid can be expanded under different culture conditions.

Tumour cells were seeded at different densities (10 000 to 100 000 tumour cells per 20 µL of BME2), cultured either under hypoxia (5 % CO_2 and 4 % O_2) or normoxia (5 % CO_2) and fed with Intesticult™ or tumour organoid medium. Images were obtained using an optical microscope (20x). Representative images are shown.

To quantify the growth of tumour organoids in the different conditions, we measured their diameter over expansion (Figure 9A). Although we could obtain tumour organoids from all the conditions, normoxia plus in-house medium was the one in which tumour organoid growth was larger. We also observed that tumour organoids expanded in hypoxia plus

Intesticult™ eventually died off and thus excluded this condition from further experiments. Additionally, we also observed a slower growth of tumour organoid cultures in hypoxia conditions, irrespective of the medium. To explore if normoxia plus in-house medium was indeed the best medium condition, we performed qRT-PCR in the tumour organoid samples (Figure 9B).

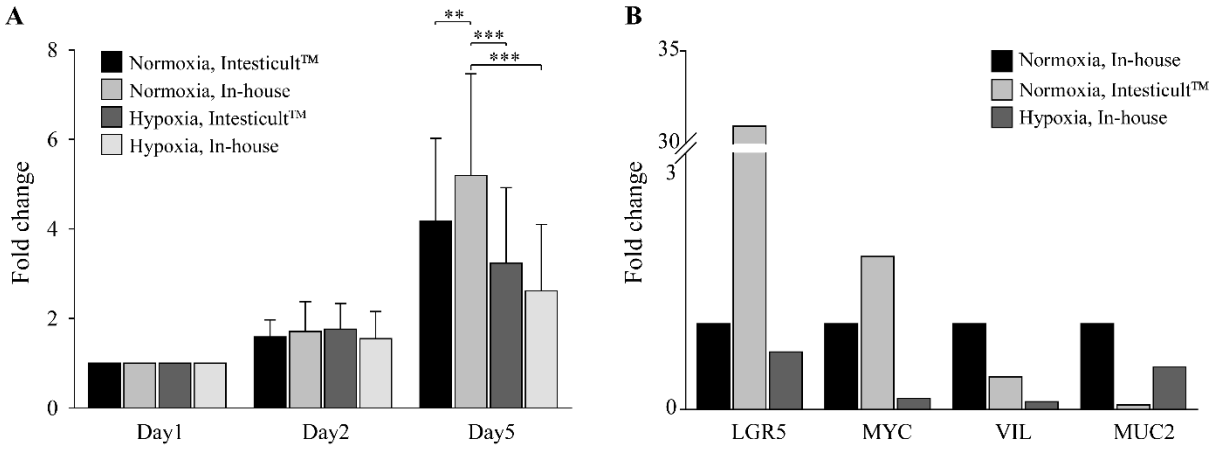

Figure 9: Tumour organoids diameter and gene expression varies under different culture conditions.

A: Tumour cells were seeded and cultured under different conditions over 5 days at passage 1. Data represents the fold change of diameter of 6 random tumour organoids per well, at different days, considering Day 1 with a fold change of 1. **B:** Tumour cells were seeded and cultured under different conditions for 5 days at passage 1; Total RNA was extracted and used to perform qRT-PCR assay with proliferation and differentiation markers. Data represents the fold change of gene expression under different culture conditions: "Normoxia, Intesticult™" and "Hypoxia, In-house", considering "Normoxia, In-house" with a fold change of 1. Hypoxia (5 % CO_2 and 4 % O_2); Normoxia (5 % CO_2). Results obtained from one experiment.

We observed an increase in the expression of proliferation markers LGR5 and MYC along with a decrease in the expression of differentiation markers VIL and MUC2, in the tumour organoids fed with Intesticult™ (Figure 9B). As mentioned before, Intesticult™ is a culture media optimized for the growth and expansion of colon organoids, that depends on the activation of Wnt pathway for the maintenance of stem cell expansion. Thus, this increase in the expression of LGR5 and MYC and decrease in expression of VIL and MUC2, in tumour organoid cultures, could be due to an over-activation of the Wnt pathway, that is leading the culture into a more undifferentiated phenotype. Due to these results, and to the fact that the presence of Wnt-activators could lead to the outgrowth of healthy organoid from contaminant healthy stem cells, we decided to exclude the culture condition normoxia plus Intesticult™. For all the remaining experiments, we used the in-house tumour organoid expansion medium under normoxia conditions.

Applying the culture conditions optimized, including the use of in-house tumour organoid medium under normoxia conditions and BME2 as ECM, we were able to generate colon tumour organoids from tumour cells, and expand these cultures over several passages (Figure 10). Tumour organoids at passage 0 are smaller in size because the initial culture is made directly from single cells, whilst successive passages are started from tumour organoid fragments, thus generating larger tumour organoid structures. Tumour organoids were lifted and passaged according to the growth rate, approximately after 5 days of culture and at a ratio of 1:4-5, much greater than for healthy organoids, due to their higher proliferative characteristics.

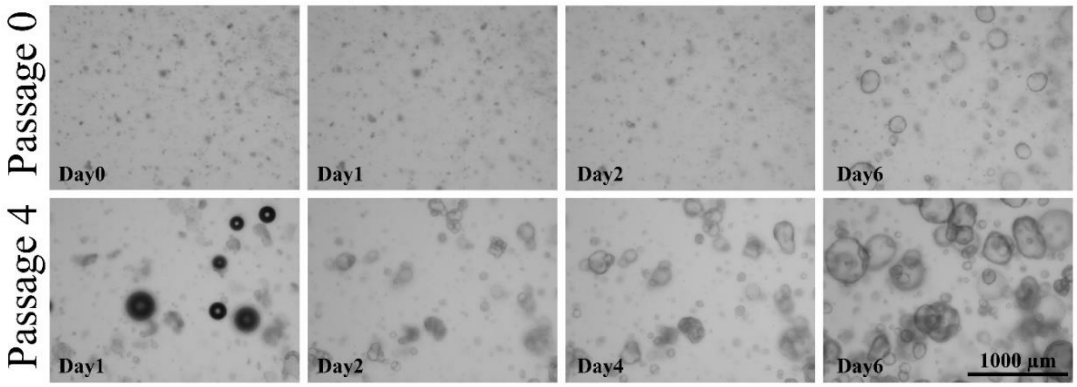

Figure 10: Tumour organoids derived from single cells expand over passages.

Tumour organoids were cultured with in-house tumour organoid medium in normoxia and imaged at passage zero (top panel) and passage 4 (bottom panel), at days zero, 1, 2 and 6 of culture. Images were obtained using an optical microscope (20x). Representative images are shown. Scale bar: 1000 µm.

Chapter Conclusion

In the present chapter, we explain the process that lead to the generation of healthy and tumour organoids from human colon tissue. We were able to generate colon organoids from entire crypts, by optimizing pre-established protocols and establishing a culture medium that supports the growth and expansion of organoids in the same manner as a commercially available culture medium. Similarly, we also generated tumour organoid cultures from tumour tissue samples. The medium optimization for the tumour organoids was based on the assessment of the best culture conditions for tumour organoid growth. This implied recreating either hypoxia or normoxia conditions and adding/removing components to the media that are responsible to maintain stemness. In this way, we reached an optimal culture condition for tumour organoids characterized by normoxia conditions in a medium without Wnt-pathway activators.

Chapter 2: Characterization of 3D colon organoid models

Chapter Introduction

The method of generating colon organoid models, described in the previous chapter and performed utilizing different medium and culture conditions, is based on the evidence that colon stem cells need certain external stemness factors to survive and proliferate, whilst cancer stem cells do not [107]. By doing this, in principle, we separate healthy from tumour cultures. However, to confirm that in fact we have two distinct cultures, we characterized the cultures by accessing both their structural and physiological characteristics. This was made by using paraffin-embedded immunohistochemistry, immunofluorescence, qRT-PCR assay, and assessment of mitochondrial respiration by measurement of oxygen consumption rate (OCR) with the Seahorse XF96 analyser. The work performed in this chapter was made in collaboration with SALK institute in Salzburg, namely the organoid clot formation, FFPE staining (H&E and immunohistochemistry) and assessment of mitochondrial respiration.

Results and discussion

Colon tumour and healthy organoids present different structural characteristics

With the aim to define the histological profile of healthy and tumour organoids, clots were prepared, and H&E staining performed. Whilst healthy organoids present an organized structure with a layer of cells and a hollow middle, resembling a transverse cut of the colon, tumour organoids pose as a disorganized mass of cells, generally without defined hollow middle (Figure 11). These structural differences between the two organoid models were the first evidence that these are two distinct cultures. Although it was not possible to perform the same histological analyses of the original tissues, this would have been a valuable result to further interpret the findings observed here. Nevertheless, it is already been demonstrated that tumour organoids preserve the histopathological characteristics of parental tumours [25,132].

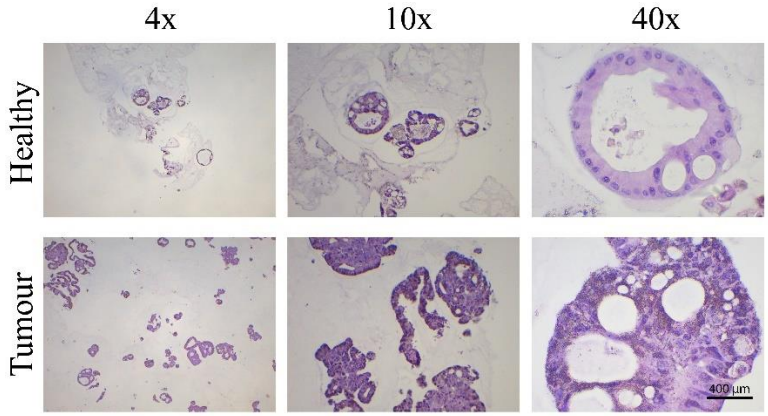

Figure 11: H&E staining shows different structures between healthy and tumour organoids.

Colon healthy and tumour organoids were clotted, dehydrated, paraffin embedded and sliced into 4 µm slices. The slices were used to perform H&E staining. The images were taken with 4x, 10x and 40x magnification, as indicated. Scale bar = 400 µm. Representative images are displayed.

To further analyse the structural characteristics of healthy and tumour organoids, we performed immunofluorescence in the FFPE tissue slices. We observed the same organised structure of healthy organoids, with hollow middle, and disorganized masses in tumour organoids (Figure 12). The immunofluorescence images were used to quantify the percentage of area stained per antibody and per sample (healthy or tumour) (Figure 13). We stained the organoids with Ki67, a proliferation marker that recognises the antigen present in the nuclei of cells in all phases of cell cycle except G0 and observed a higher number of positive cells for this marker in tumour organoids. In human colon tumour tissues, this marker can be used as a good indicator of proliferation and high levels of its expression are correlated with poor survival [133]. Although this marker is also present in healthy colon tissue, the high expression in tumour organoids indicates a higher proliferation rate, characteristic of tumours. Likewise, we also observed a higher expression of MUC2 in the tumour samples, a recognisable characteristic of mucinous phenotype of colon cancer [134]. The expression of epithelial marker CK18 and brush border marker microvilli VIL was similar between tissues.

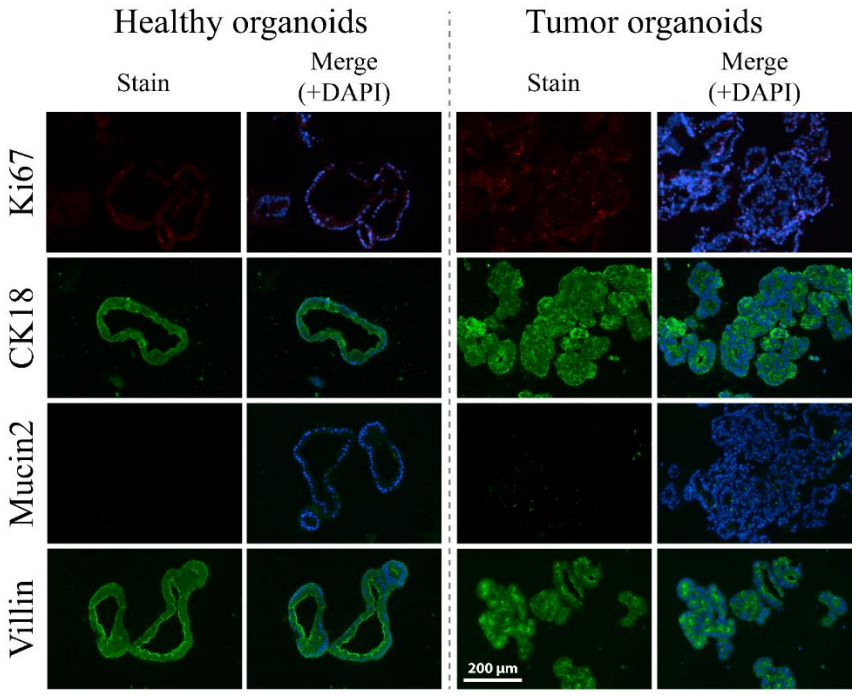

Figure 12: Immunofluorescence shows different structures and staining between healthy and tumour organoids.

Colon healthy and tumour organoids were clotted, dehydrated, paraffin embedded and sliced into 4 µm slices. The slices were used to perform immunofluorescence staining. The images were taken with 10 x magnification. Scale bar = 200 µm. Ki67: proliferation marker. CK18: cytokeratin 18 (epithelial marker). Mucin2: goblet cells marker. Villin: brush-border microvilli marker. Each image is representative of three pictures taken.

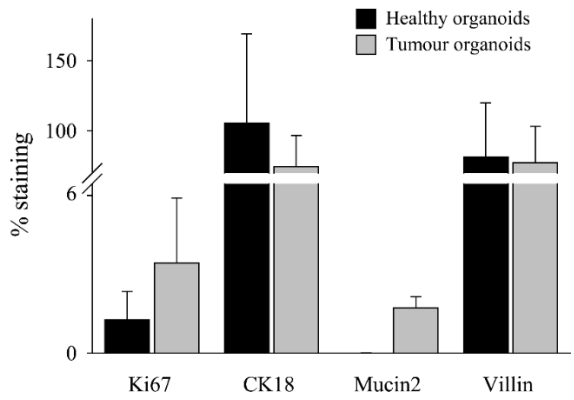

Figure 13: Quantification of immunofluorescence images confirms different staining between healthy and tumour organoids.

Colon healthy and tumour organoids were clotted, dehydrated, paraffin embedded and sliced into 4 µm slices. The slices were used to perform immunofluorescence staining. The graph represents the quantification of immunofluorescence images, as analysed with ImageJ. The % staining was quantified per antibody in each sample and normalized with the % area of DAPI staining. A total of 3 images were analysed per antibody, per tissue, in one experiment. Data is mean ±SD; n=1. Ki67: proliferation marker. CK18: cytokeratin 18 (epithelial marker). Mucin2: goblet cells marker. Villin: brush-border microvilli marker.

The immunofluorescence data, showing increased proliferation and mucus production by the tumour organoids, was also confirmed by qRT-PCR, through increased expression of

stem cell marker LGR5, proliferation marker MYC and goblet cells marker MUC2 (Figure 14A). We also observed downregulation of colonocyte marker carbonic anhydrase 1 (CA1) in tumour samples, suggesting a more undifferentiated state. BAMBI, a target of canonical Wnt-signalling pathway and cancer-associated gene, was also upregulated in tumour organoids, suggesting the overactivation of the Wnt pathway [135]. The overexpression of glucose transporter 1 (GLUT1) and pyruvate kinase 2 (PKM2) in the tumour samples, suggest a higher metabolic state of these cultures. However, these genes were chosen as a mean to perform an initial screening and we did not explore the metabolic state of cultures at this point. Interestingly, we also found that APCDD1, a cancer-associated gene and a Wnt target gene, is not expressed in healthy organoids but highly expressed in tumour organoids (not shown in the graph because it is not expressed in healthy organoids) [86,136].

To perform studies in any type of cell culture, it is crucial that the culture remains as stable as possible over passages. To evaluate if the tumour organoid cultures were in fact stable over passages, we collected samples of these cultures at passage 5 and 7, and analysed the expression of several genes by RT-PCR (Figure 14B). We did not observe significative differences between the fold change of gene expression at passage 7 to passage 5, for the total of 3 experiments performed and for most of the genes analysed. For LGR5, we did observe a significative difference between experiments. However, expression of LGR5 can vary significantly over the evolution of colorectal tumour and it highly depends on the factors such as the tumour stage, stem cell hierarchy or the tumour microenvironment [137]. Therefore, we do not consider that the variation in LGR5 expression indicates an instability of our culture, but instead a biological characteristic of the tumour itself. We also found significative differences for the expression of GLUT1 between two of the experiments performed. However, even though there is a difference in statistics, we do not attribute a biologically significative difference, as the values of fold change of expression are still very low to be considered.

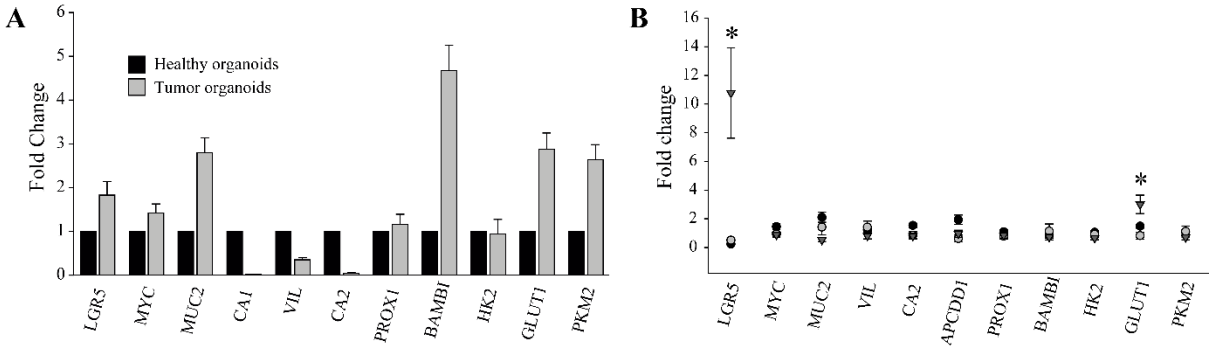

Figure 14: Healthy and tumour organoids present different gene expression and tumour organoids expression is maintained over passages.

A: Gene expression of healthy and tumour organoids at passage 1 and 5 days of culture was determined by qRT-PCR assay. Data represents the fold change of tumour organoid expression, considering healthy organoids with a fold change of 1. One experiment was performed. **B**: Gene expression of tumour organoids at passage 7 and 5 days of culture was determined by qRT-PCR assay. Data represents the fold change of tumour organoid gene expression at passage 7, considering passage 5 with a fold change of 1. LGR5: Stem cell marker; MYC: proliferation marker; MUC2: goblet cells marker; VIL: brush-border microvilli marker; CA2, PROX1 and BAMBI: cancer-associated genes; HK2, GLUT1, PKM2: metabolic markers. Data are expressed as means ± SD (n=3; * $P < 0.05$). Differences between tumour organoids at different passages were assessed using one-way ANOVA followed by Tukey test.

Colon tumour and healthy organoids present similar expression of mitochondrial markers

In the context of this project, we were looking for a comparison of metabolic characteristics between the tumour organoid model and the healthy counter partner. For this, we first performed immunohistochemistry staining using a 3′-Diamidobenzidine (DAB) substrate, according to the protocol described in the methods section. We investigated the expression of porin (mitochondrial membrane marker) and some subunits of complexes I to V of the respiratory chain. Immunohistochemistry analysis reveals a similar expression of mitochondrial markers between healthy and tumour organoids (Figure 15). This finding was supported by a search in "The Human Protein Atlas" [138], confirming that the proteins VDAC, NDUFS4, SDHA, UQCRC2, MTCO1 and ATP5A1, are expressed both in colon healthy and cancer tissues.

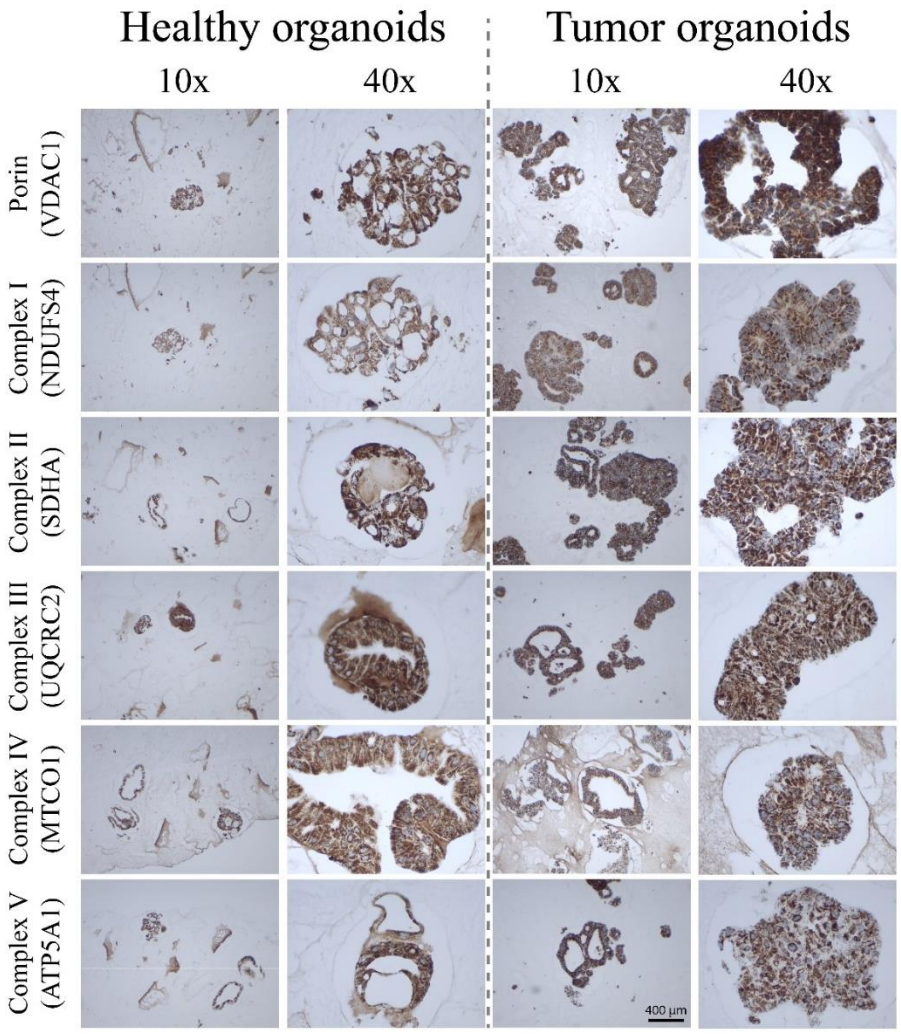

Figure 15: Immunohistochemistry reveals a similar staining of mitochondrial markers between healthy and tumour organoids.

Colon healthy and tumour organoids were clotted, dehydrated, paraffin embedded and sliced into 4 µm slices. The slices were used to perform immunohistochemistry with DAB substrate. The images were taken with 10x and 40x magnification, as indicated. Scale bar = 400 µm. Representative images are displayed. VDAC1: Voltage-dependent anion-selective channel 1. NDUFS4: NADH:Ubiquinone Oxidoreductase Subunit S4. SDHA: Succinate dehydrogenase complex, subunit A. UQCRC2: Cytochrome b-c1 complex subunit 2. MTCO1: Mitochondrially Encoded Cytochrome C Oxidase I. ATP5A1: ATP synthase F1 subunit alpha.

Optimization of a protocol for evaluation of mitochondrial function of tumour organoids with the Seahorse XF extracellular flux analyser

To assess the bioenergetic profile of 3D models, the rate of oxygen consumption was measured in real time using the Seahorse XF analyser. Initial protocols used in this work were based in the protocol developed by Fan et al. [139] and original Agilent user guides (Courtesy of Agilent Technologies, Inc.). Following these procedures, we made several adaptations and optimized a protocol for the use of the Seahorse XF96 analyser in tumour organoids. The final

protocol required several optimization steps, that are going to be explored over the next paragraphs. The different conditions utilized in every experiment are also resumed in Table 3.

Non-modified steps during the optimization procedure are the use of the Seahorse XF96 analyser, corresponding cartridges and plates, and the assay medium composed of 1 mM pyruvate, 2 mM glutamine and 10 mM glucose in DMEM (Table 7). Rotenone plus Antimycin A (specific complex I and complex III inhibitors, respectively) were used at 0.5 µM. Further, oligomycin (a specific inhibitor of complex V), was used generally at a concentration of 2 µM, unless when tested for its functionality, whereas cyanide-4-(trifluoromethoxy)phenylhydrazone (FCCP) required titration starting with a range of concentrations from 0.125 to 4 µM.

Table 3: Optimization steps for assessment of bioenergetic profile of tumour organoids

Trial	Plate utilised	Coated plate	Date of seeding (to assay day)	Organoid density	Drugs concentrations	Results
1	Spheroid plate	Yes Matrigel 1:10 (vol/vol) in assay medium	Day 0	15 µL suspension in Matrigel with 38 or 75 organoids/well	Oligomycin (2 µM) FCCP (0.125; 0.25; 0.5; 1; 2; 4 µM) Rotenone + Antimycin A (0.5 µM)	No curves detected None or very few and small organoids in wells
2	Spheroid plate	No	Day 0	6 µL suspension in Matrigel with 1:3 ratio from original culture	Oligomycin (2 µM) FCCP (0.125; 0.25; 0.5; 1; 2; 4 µM) Rotenone + Antimycin A (0.5 µM)	No curves detected None or very few and small organoids in wells
3	Spheroid plate	No	Day 0	6 µL suspension in Matrigel with 1:1 ratio from original culture	Oligomycin (2 µM) FCCP (0.125; 0.25; 0.5; 1; 2; 4 µM) Rotenone + Antimycin A (0.5 µM)	No curves detected None or very few and small organoids in wells
4	2D plates	No	Day 0	6 µL suspension in Matrigel with 1:1 ratio from original culture	Oligomycin 2 different batches (2; 4 and 6 µM) FCCP (0.5; 1; 2 µM) Rotenone + Antimycin A (0.5 µM)	Response for wells with higher organoid density
5	2D plates	No	Day 0	10 µL suspension in BME with 1:1 ratio from original culture Two 2D cell lines at a density of 105 cells/well seeded Day -1	Oligomycin 2 different batches (6 µM) FCCP (1; 2 µM) for cell lines FCCP (2 µM) for organoids Rotenone + Antimycin A (0.5 µM)	Response for wells with higher organoid density Good response for cell lines
6	2D plates	No	Day -4	10 µL suspension in BME with 1:1 ratio from original culture	Oligomycin (6 µM) FCCP (2 µM) Rotenone + Antimycin A (0.5 µM)	Good response

The initial experiment was performed in spheroid microplates, coated overnight with 30 µL/well of a solution of Matrigel 1:10 (vol/vol) in assay medium. After coating, the plate was washed with assay medium and filled with 15 µL of organoid suspension (in two concentrations tested, 38 or 75 organoids per well) plus 15 µL of assay medium. After 30 min incubation, assay medium was added, and the experiment was run according to the protocol

described in the material and methods section. The results of this experiment did not show any response to the inhibitors of oxidative phosphorylation (Figure 16).

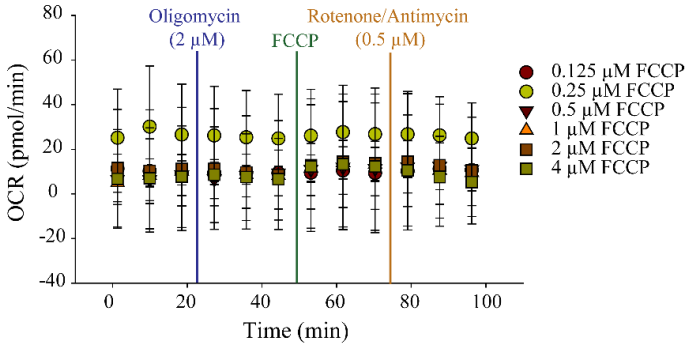

Figure 16: Oxygen consumption rate of tumour organoids seeded in matrigel coated spheroid plates did not show response to OXPHOS inhibitors.

Tumour organoids were seeded in matrigel coated plates and assayed on the same day. The timepoints represent the oxygen consumption rate (OCR) at different concentrations of FCCP. Data is mean ± SD; n=1. The vertical coloured lines indicate the timepoints of injection of 2 µM oligomycin, FCCP (0.125 – 4 µM) and 0.5 µM rotenone + antimycin A.

Since very few organoids were observed within the wells, we increased their concentration by using a ratio of 1:3, which is a ratio generally used in normal organoid expansion. We also decided not to coat the plates because the adherence of the matrix-containing organoids (Matrigel) was prejudiced due to the plate being wet. Because no coating was necessary, the seeding was performed at the day of assay and a smaller amount of Matrigel was used. Under this condition, no response in terms of OCR was observed after inhibitors injection and only few and small organoids were observed in the wells (Figure 17).

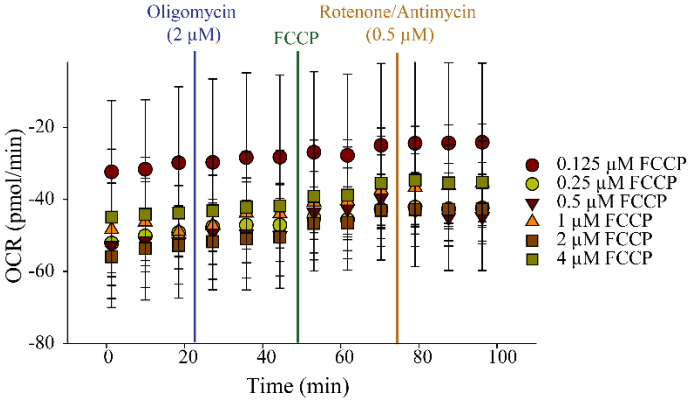

Figure 17: Oxygen consumption rate of tumour organoids seeded in matrigel and in spheroid plates did not show response to OXPHOS inhibitors.

Tumour organoids were seeded in matrigel and assayed on the same day. The timepoints represent the oxygen consumption rate (OCR) at different concentrations of FCCP. Data is mean ± SD; N=1. The vertical coloured lines indicate the timepoints of injection of 2 µM oligomycin, FCCP (0.125 – 4 µM) and 0.5 µM rotenone + antimycin A.

Similar result was obtained also with a density of the organoids at a ratio of 1:1 (Figure 18). We decided to change the microplates used, because the organoids can be smaller structures than typical spheroids and spheroid microplates are designed to support bigger spheroids and not to allow adherence. Thus, the spheroid plates could be causing the organoids to move within the wells during measurement and causing alterations in the readout values. To overcome this technical issue, we used conventional 2D assay microplates and we also tested two different batches of oligomycin at higher concentrations (4 and 6 µM). Regarding FCCP, we decided to choose only the 0.5; 1 and 2 µM concentrations. Under this experimental condition, a decrease of OCR was observed in some of the wells, containing larger organoids or higher organoid density. We did not observe a difference depending on the oligomycin batch or its concentration used (Figure 19). These findings suggested us to use 2D microplates for further experiments.

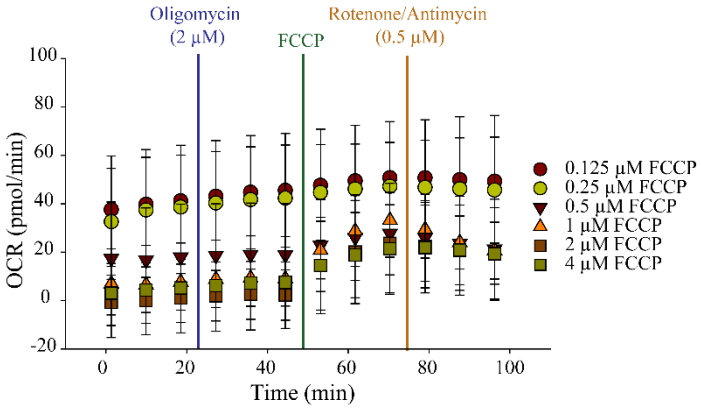

Figure 18: Oxygen consumption rate of tumour organoids seeded at higher density in matrigel and in spheroid plates did not show response to OXPHOS inhibitors.

Tumour organoids were seeded in matrigel and assayed on the same day. The timepoints represent the oxygen consumption rate (OCR) at different concentrations of FCCP. Data is mean ± SD; N=1. The vertical coloured lines indicate the timepoints of injection of 2 µM oligomycin, FCCP (0.125 – 4 µM) and 0.5 µM rotenone + antimycin A.

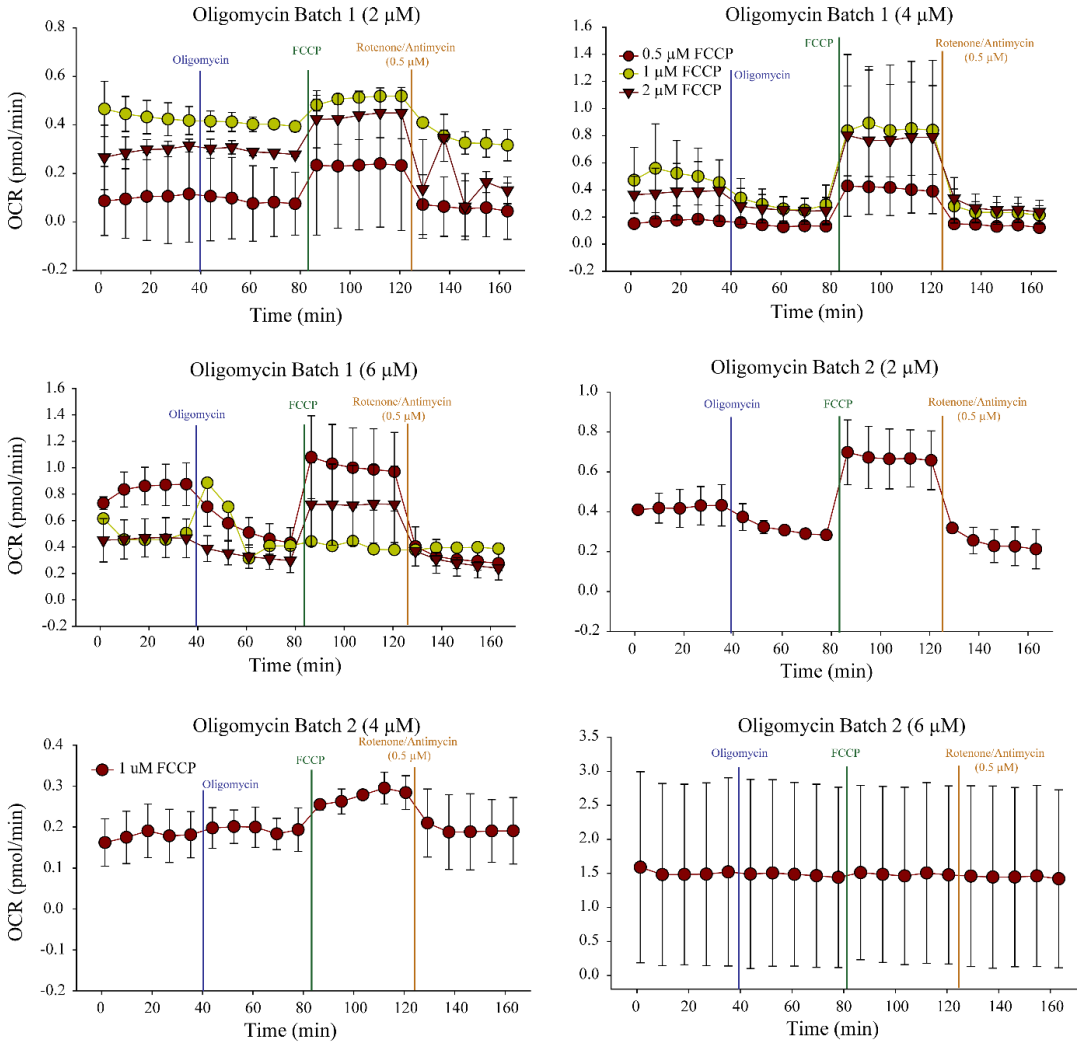

Figure 19: Oxygen consumption rate of tumour organoids seeded at higher density in matrigel using conventional plates show response to inhibitors.

Tumour organoids were seeded in matrigel and assayed on the same day. The timepoints represent the oxygen consumption rate (OCR) at different concentrations of FCCP and/or oligomycin batches. Data is mean ± SD; N=1. The vertical coloured lines indicate the timepoints of injection of oligomycin (2, 4 or 6 µM), FCCP (0.5, 1 and 2 µM) and 0.5 µM rotenone + antimycin A.

To verify if the oligomycin used is working we included as internal control 2D melanoma cell lines, namely A375 and WM3000. Furthermore, to ameliorate the adhesion support of tumour organoids in the microplate, we decided to use BME2 instead of Matrigel and increased the amount of matrix to 10 µL. Under these conditions, both cell lines responded to both oligomycin batches suggesting that they are functioning. Regarding the organoids, we observed again a response in the wells that contained bigger organoids or at a higher density (Figure 20).

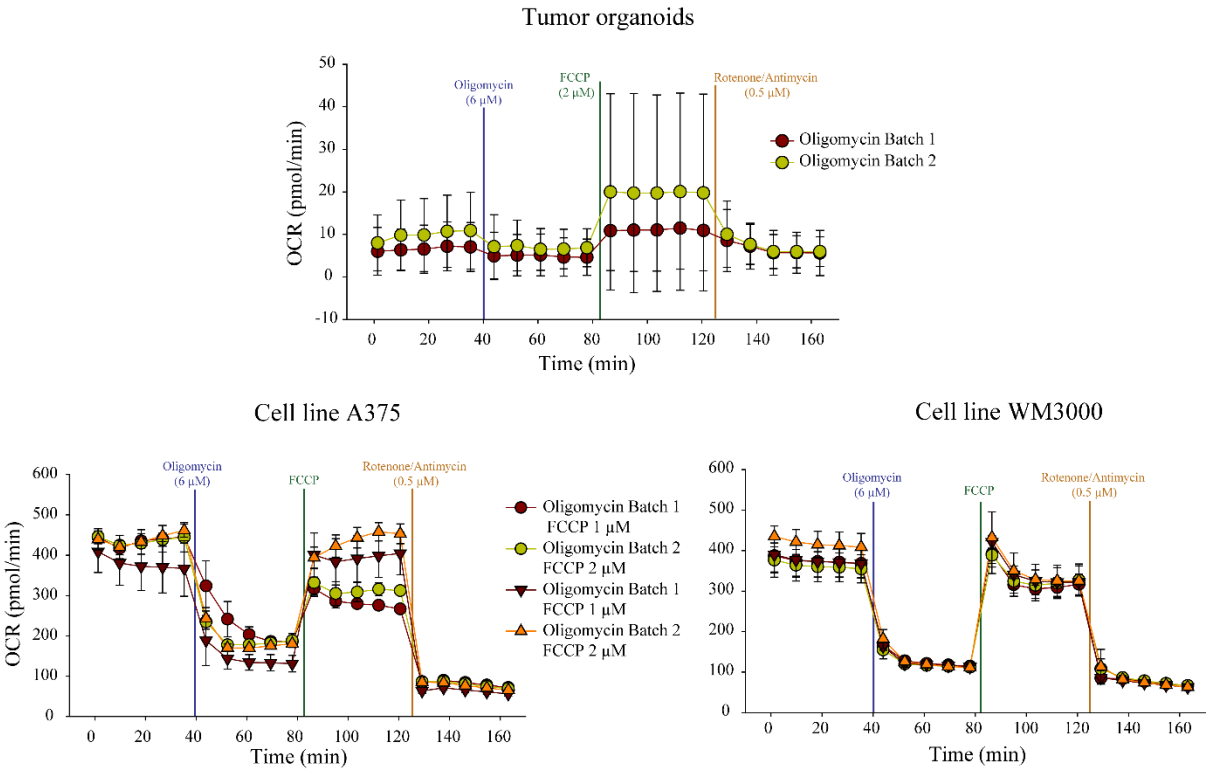

Figure 20: Oxygen consumption rate of tumour organoids seeded in BME2 using conventional plates, and 2D cell lines, show response to inhibitors.

Tumour organoids were seeded in BME2 and assayed on the same day. Cell lines were seeded at a density of 10^5 cells/well and assayed the day after. The timepoints represent the oxygen consumption rate (OCR) at different concentrations of FCCP and/or oligomycin batches. Data is mean ± SD; n=1. The vertical coloured lines indicate the timepoints of injection of 6 µM oligomycin, FCCP (1 and/or 2 µM) and 0.5 µM rotenone + antimycin A.

Since we observed that the organoids were still small and some wells presented low density, we decided for the next experiment to seed the organoids at day -4, in the 2D microwell plates. After 5 days of expansion the organoids had grown into larger structures, which resulted in a response in OCR in reaction to inhibitors (Figure 21).

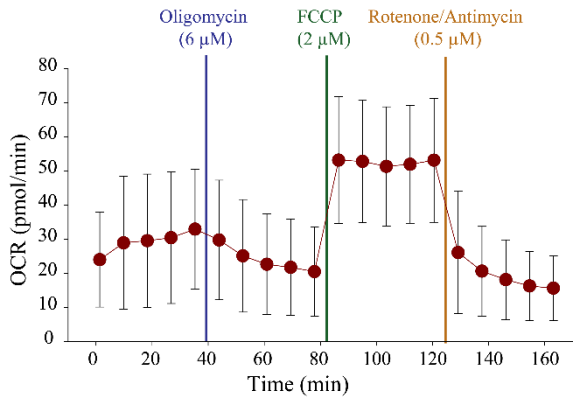

Figure 21: Oxygen consumption rate of tumour organoids seeded in BME2 at day -4 and using conventional plates show response to inhibitors.

Tumour organoids were seeded in BME2, 4 days before assay. The timepoints represent the oxygen consumption rate (OCR) of tumour organoids. Data is mean ± SD; N=1. The vertical coloured lines indicate the timepoints of injection of 6 µM oligomycin, 2 µM FCCP and 0.5 µM rotenone + antimycin A.

These optimization experiments led us to the final protocol presented in the material and methods section, and that we used for further experiments described in following chapters. The most important adaptations during the optimization steps were the use of 2D microplates without coating, BME2 as the matrix, seeding 4 days prior to assay day and using optimal drug concentrations (6 µM Oligomycin; 2 µM FCCP; 0.5 µM Rotenone + Antimycin A). Although we were able to optimize a protocol that could be used to further evaluate the mitochondrial respiration of the organoid models, within the context of the project, time was an issue. We utilized the tumour organoids for the optimization of the protocol due to their faster growth rate comparing with their healthy counter partners. Unfortunately, by the time the protocol was optimized, it was not possible to complement our study with the evaluation of mitochondrial respiration of healthy organoids. Further studies can be however performed in these and similar models, using the protocol optimized here.

Chapter Conclusion

In the present chapter we present results that contributed to the characterization of the organoid models. Both models presented different structural characteristics as evidenced by imaging assays. While healthy organoids present an organized structure with a layer of cells surrounding a hollow middle, tumour organoids are very disorganized and present as a mass of cells. Immunofluorescence and qRT-PCR studies further demonstrated that both models express different amount of proliferative and epithelial cells, with tumour organoids being more proliferative and expressing more mucin markers. However different in structural terms, both models presented same levels of expression of mitochondrial membrane and respiratory complex markers. To study mitochondrial respiration of organoid models, we optimized a protocol for the use of the Seahorse XF96 to define the bioenergetic profile of healthy and tumour organoids.

Chapter 3: Validation of 3D colon organoid models

Chapter Introduction

Chapter 3 describes the methods utilized to validate both healthy and tumour organoid models. To perform this, we first demonstrate the differentiation of healthy organoids after removal of stem cell components. As mentioned previously, the capacity to expand a colon organoid culture is dependent on the existence of critical niche factors that activate the Wnt pathway [107,140]. Upon removal of these factors, the cultures undergo differentiation into the tissue-specific cell types, reflecting the diversity of the tissue of origin [107]. Differentiated colon epithelial cells can exert their functions in vivo, such as nutrient absorption by absorptive colonocytes or mucus production by goblet cells [141]. Differentiated 2D cultures from monolayers can be utilized for membrane permeation screening of test compounds [142]. Due to their 3D structure, differentiated colon organoid cultures are more difficult to utilize for drug absorption studies due to their morphology [143]. More specifically, in colon organoid cultures the apical side where absorption is common to occur, is inside of the organoid. However, recent studies have shown that 3D colon organoid structures can also be cultured in monolayer, allowing the formation of a permeable membrane for the apical application of test drugs [144].

High throughput screening assays are a crucial tool to evaluate drug efficacy and pharmacological safety in early phase clinical trials of novel drugs. Traditional cell lines or 2D cell models have been routinely used for this purpose, and although useful in many ways, their relevance can often be debatable [1,2]. More recently, the discovery of the importance of the tumour microenvironment and the 3D aspect of tumours, promoted interest in developing more advanced models that could mimic tumour development in the original tissue. In this context, organoid models are of much interest. Organoids are 3D structures that contain the several cell types of the tissue of original and that self-organize into similar structures as the tissue of origin [145]. Furthermore, they also reflect the genetic landscape of the original tumour [97]. The application of such physiologically relevant cultures into drug discovery could thus improve cell-based assay systems in the context of drug discovery and pharmacological safety. In the second part of this chapter, we develop the context of drug testing and demonstrate the utilization of tumour organoids in two different cytotoxicity studies, facing three different components. Finally, we used tumour organoids to test the effect of sodium butyrate (NaBt), a bacterial biproduct that exists naturally in the gut.

Results and discussion

Healthy organoid cultures are differentiated after removal of stem cell components from the culture medium

To assess the ability of our colon organoid models to differentiate into epithelial cultures, we cultured healthy organoids in a culture medium without Wnt-activating compounds. This colon differentiation medium (Table 7) was obtained by removing Wnt conditioned medium, R-spondin conditioned medium, Noggin, A83-01, SB202190, CHIR99021, Nicotinamide, N-acetylcysteine and PGE2. Healthy colon organoids were seeded and expanded for 5 days and then culture medium was changed to complete differentiation medium for 3 days, with daily medium changes (Figure 22). To evaluate the proliferative capacity of cultures, we performed a proliferation stain with ethidium bromide (EdU stain). We initially observed that after 2 days with the differentiation medium, there were still some cells positive for the proliferation marker. However, after 3 days, the culture was completely differentiated, and no positive cells were observed for EdU marker. Immunocytochemistry analysis at 3 days of differentiation confirms the presence of epithelial marker CK18 and goblet cell marker MUC2. Furthermore, we performed a live/dead staining in the undifferentiated and 3 days differentiated cultures and observed that cells maintained their viability after differentiation.

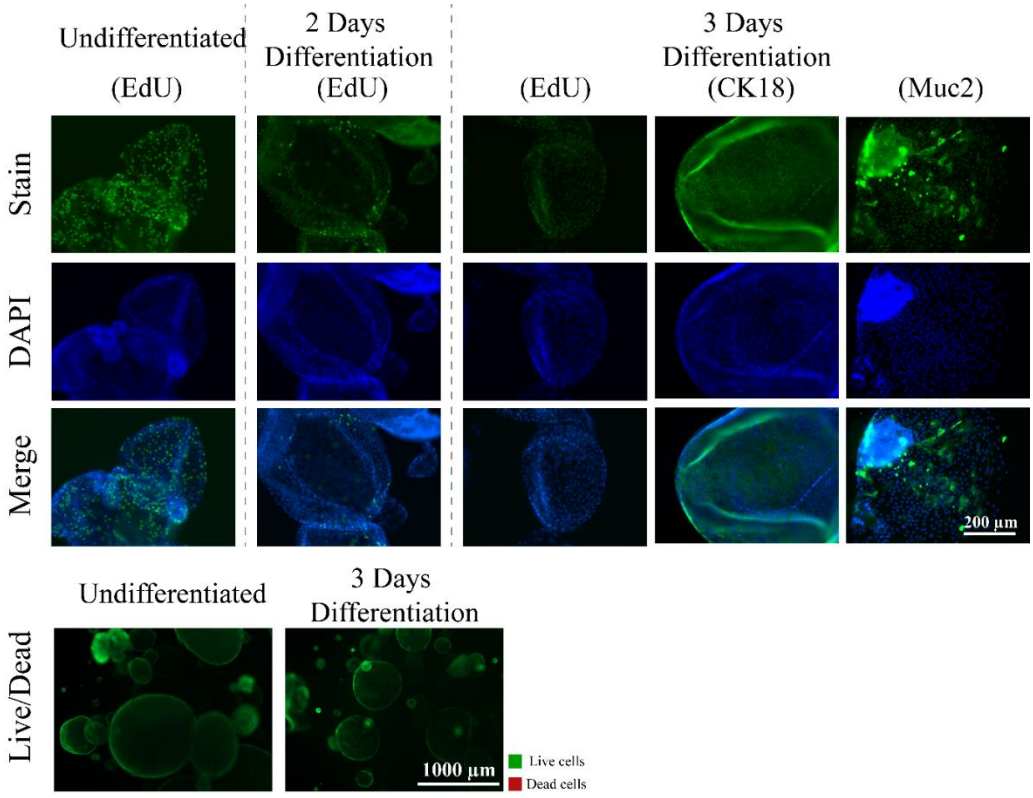

Figure 22: Healthy colon organoids are differentiated after removal of stem cell components.

Organoids were seeded and expanded for 5 days in expansion medium. After this, medium was changed into differentiation medium and organoids were kept in culture for 2 or 3 days, as indicated, with daily medium changes. EdU staining was used to stain for proliferative cells in green. DAPI was utilised to stain nuclei. The images are representative of results observed from a total of 4 experiments. Immunofluorescence was performed against epithelial cytokeratin18 (CK18) and Muc2 proteins. Live/Dead (green/red) staining was also performed in undifferentiated and differentiated cells. Images were obtained using an optical microscope (20x).

To further support this data, we performed qRT-PCR in both undifferentiated and differentiated cultures (Figure 23). We observed a significative reduction of expression of stem cell marker LGR5 and proliferation marker MYC in differentiated cultures. Further, a significative increase of expression of epithelial markers VIL, MUC2 and CA1 after differentiation, was determined. Overall, this data suggests that a viable and completely differentiated culture was successfully obtained.

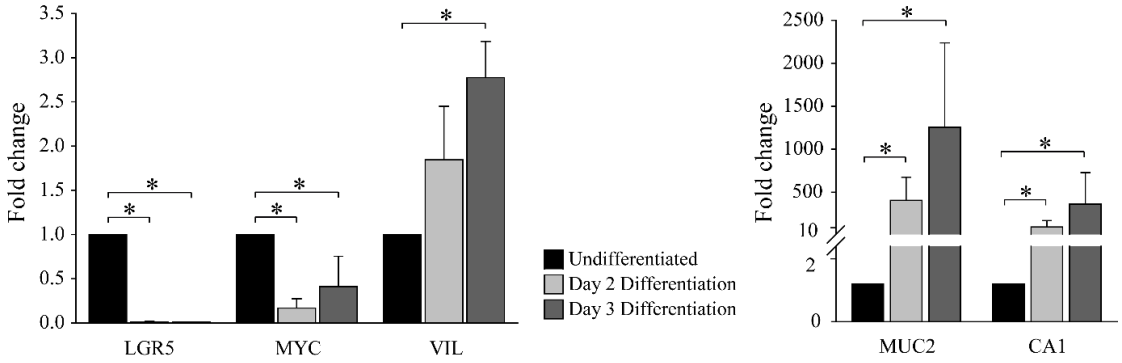

Figure 23: Gene expression of healthy organoids indicates a differentiated culture.

Organoids were seeded and expanded for 5 days in expansion medium. After this, medium was changed into differentiation medium and organoids were kept in culture for 2 or 3 days, as indicated, with daily medium changes. Gene expression of differentiated and undifferentiated healthy organoids was determined by qRT-PCR assay. Results represent the average of the fold change of differentiated organoids gene expression, considering undifferentiated organoids with a fold change of 1, for a total of 3 experiments with 3 technical replicates each. LGR5: stem cell marker; MYC: proliferation marker; VIL: brush-border microvilli marker; MUC2: goblet cells marker; CA1: colonocyte marker. Results are expressed as means ± SD (n=3; * $P < 0.05$). Differences between differentiated and undifferentiated groups were assessed using one-way ANOVA followed by Dunnett test.

Application of tumour organoids for cytotoxicity assays

To validate the utility of the developed tumour organoid models in drug studies, we performed several cytotoxicity assays. We started by testing the effect of staurosporine, a routinely laboratory inducer of cell death. Although staurosporine has shown, in early studies, an inhibitory effect over proliferation of human colon adenocarcinoma cells [146], we mainly choose this drug because of its easy accessibility to perform initial cytotoxic tests. To evaluate the effect of staurosporine over the viability of tumour organoids, we utilized the CellTiter-Glo® 3D cell viability assay after treatment with different concentrations of staurosporine (from 10 pM to 10 µM) (Figure 24A). Staurosporine treatment was able to decrease the viability in a dose dependent manner (IC50 = 0.00576 µM). However, because the assay is based on the amount of ATP present and produced by the cells, it is dependent on the metabolic state of the cells and thus does not account for secondary effects over metabolism, not necessarily associated with viability. Second, because the organoids, and specially tumour organoids, can present variable sizes within each well, the results can be misleading, indicating that there are more viable cells present in a determinate well, when in fact, there are only more cells.

To address these issues, we decided to explore another viability assay, named the live/dead assay. This is a fluorescence-based assay and it is very simple to perform, consisting

on treating the cells with a solution composed of fluorescein diacetate (FDA) and propidium iodide (PI), which stains viable or dead cells, respectively (Table 7). Based on image analysis, it is possible to calculate the % of dead cells per well treated, and thus reducing the variability originated by having organoids from different sizes. Furthermore, it is also not dependent of cell metabolism, as PI only passes through the membrane of dead cells. To perform this assay, we treated the tumour organoids with doxorubicin, a chemotherapeutic utilized in the treatment of various cancers, including colon cancer [147,148]. Treatment with a range of concentrations from 20 nM to 200 µM induced an increase of cell death in a dose dependent manner (IC50 = 28.288 µM) (Figure 24B). The reduction of the influence of organoids size utilizing this assay its reassuring of more reliable results. However, this is a more time-consuming assay, as it requires image and data analysis, contrary to the CellTiter Glo assay. We believe that both assays could be used in parallel and can support each other by providing more reliable and relatable results in terms of drug cytotoxicity testing.

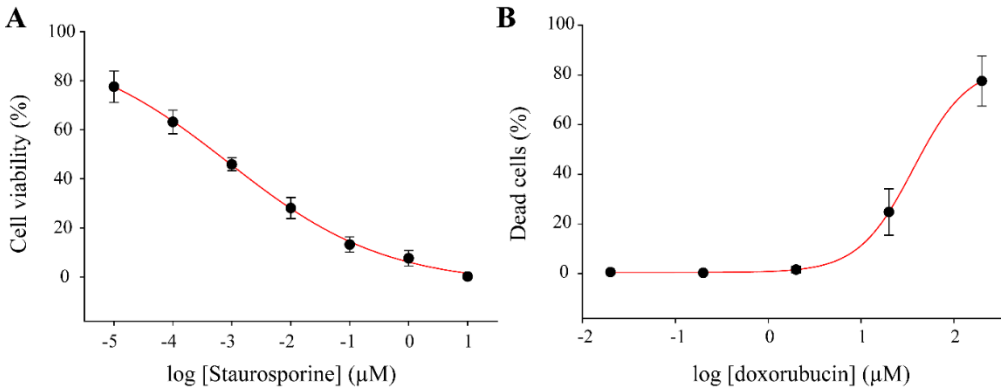

Figure 24: Tumour organoids are sensitive to treatment with staurosporine and doxorubicin.

Tumour organoids were seeded in 96 wells plates, expanded for 5 days, and then treated for 24 hours with (A) staurosporine (10 pM to 10 µM) and (B) doxorubicin (20 nM to 200 µM). **A:** Cell viability was determined using the CellTiter-Glo® 3D cell viability assay after treatment with staurosporine. Data (mean ± SD, n= 3) are expressed as % viable cells per well, considering non-treated cells as 100%. **B:** Cell viability was performed by using live/dead assay after treatment with doxorubicin. Data (mean ± SD, n= 3) are expressed as % of dead cells, considering non-treated cells as 100% and normalized per total number of cells per well.

Tumour organoids present higher sensitivity to cytotoxic agent sodium butyrate

As mentioned previously, tumour microenvironment is a topic of increasing interest, and whilst studying cell lines can be very useful, it does not account for this factor. To explore this hypothesis, we performed cytotoxic assays with NaBt in a 2D colon cancer cell line (CACO2) and in 3D tumour organoids. NaBt is a natural by-product of anaerobic fermentation by bacteria existing in the gut and has been shown to have anti proliferative effect in several

types of cancer, namely in colon cancer [149–151]. Since the live/dead assay could not be utilized in the 2D culture of CACO2 cells because it is an adherent monolayer culture and cells are removed during the wash steps, we used the CellTiter Glo assay to measure cell viability in both models. After testing several concentrations of NaBt, we decided to use a range of concentrations from 10 to 150 mM of NaBt and were able to obtain dose-response curves for both models (Figure 25). Analysis for both dose-response curves indicates that the IC50 for CACO2 cells is 128 mM, while the IC50 for tumour organoids is at 63 mM, almost half. This difference could be due to the presence of several types of cells in tumour and/or to the tumour microenvironment. Furthermore, there is evidence that NaBt induces differentiation and cell death in colon cells [152–154]. As tumour organoids have a high proliferation capacity as discussed in chapter 1, and as stem cells or undifferentiated cells are possibly the main target of NaBt, it is reasonable to find that the sensitivity of the tumour organoids to NaBt is higher than CACO2 cells.

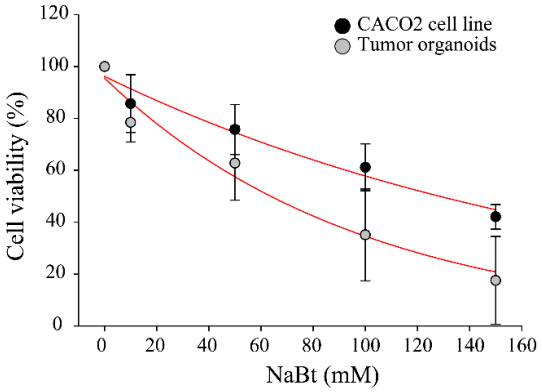

Figure 25: Colon tumour organoids are more sensible to sodium pyruvate than CACO2 cells.

Tumour organoids were seeded in 96 wells plates, expanded for 5 days, and then treated for 24 hours with NaBt (10mM to 150 mM). CACO2 cells were seeded at a density of 6000 cells/well, expanded for 48 hours, and then treated for 24 hours with NaBt, at the same concentrations. Cell viability was determined using the CellTiter-Glo® 3D assay. Data (mean ± SD, n= 3) are expressed as the % of viable cells per well, considering non-treated cells as 100%.

To understand whether extracellular matrix interferes with the sensitivity of the cells to NaBt, it would be very interesting to compare the effect of NaBt in 3D models obtained with CACO2 cells, which was unfortunately not possible within the time frame of this thesis.

The effect of NaBt over tumour organoids occurs in a permanent manner

We were also interested to understand if the effect of NaBt over the tumour organoids occurred in a temporary or permanent manner. For this, we treated cells for 24h with NaBt and then either replaced the culture medium with fresh medium without NaBt and cultured the cells for another 48 hours before assay, changing medium daily (medium change), or stop the culture

without medium change (no medium change). As reported in Figure 26, the percentage of viable cells of the tumour organoids when the medium is changed is similar to that when medium is not changed, suggesting that tumour organoids do not recover from treatment with NaBt. However, after performing the live/dead assay, the results are slightly different, as that the percentage of dead cells in the plate were the medium was changed was higher than in the plate were medium remained the same (Figure 26B). As previously mentioned, these two assays represent two different types of outputs. Whilst CellTiter Glo accounts for metabolically active cells, the live dead assay accounts for the number of dead cells, with compromised cell membrane. The higher number of dead cells observed by the live/dead assay in the plate were the medium was changed could be due to the fact that this plate is maintained for an extra 48 hours in culture, and cells continue to die (Figure 26C).

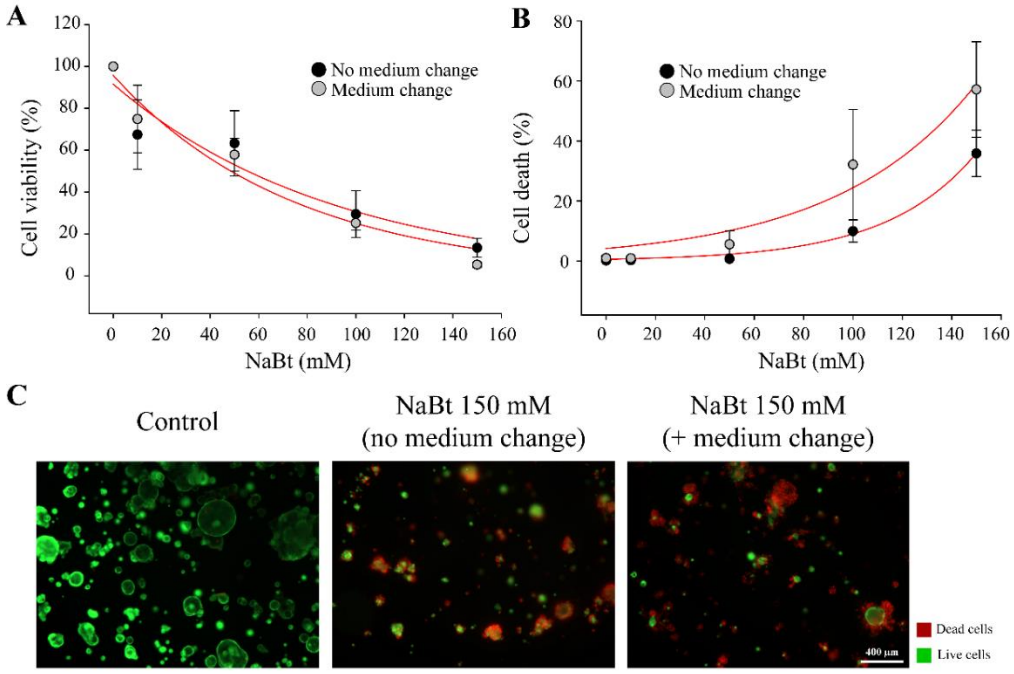

Figure 26: Tumour organoids display a cytotoxic dose-response to NaBt.

Tumour organoids were seeded in 96 wells plates, expanded for 5 days, and then treated for 24 hours with NaBt, ranging from 10 mM to 150 mM. In the case where the medium was changed, organoids remained in culture for an extra 48 hours, with daily medium changes without NaBt and assayed the day after. **A:** Cell viability was measured by using the CellTiter-Glo® 3D assay. Data (mean ± SD, n=3) are expressed as the % viable cells per well, considering non-treated cells as 100%. **B:** Cell viability was measured by the live/dead assay. Data (mean ± SD, n=3) are expressed by the % of dead cells, considering non-treated cells, and normalized per total number of stained cells per well. **C**: Representative images of the live/dead assay of control organoids and organoids treated with NaBt 150 mM, with or without medium change. Images were obtained using an optical microscope (20x).

NaBt effect could be dependent on the proliferation and differentiation state of colon cells

Another interesting point in the context of the study of the effect of NaBt in the organoid cultures, is to evaluate whether healthy colon organoids are sensible to NaBt. In this context, we have to consider that the cellular composition of tumour organoids is different from healthy organoids, being the latter less proliferative and more differentiated. Further, the anti-proliferative effect of NaBt is observed mainly in cells with a high proliferative ability, such as cancer cells, and the effect of NaBt in the colon epithelial proliferation can be very complex and depend on factors such as exposure level or availability of other substrates of the intracellular background [151]. Thus, the evaluation of NaBt effect on healthy colon organoids could allow to elucidate whether this compound is effective also on the differentiated cells and not only on high proliferative cells.

To understand if the behaviour of healthy organoids in response to NaBt is different from that observed in tumour organoids, we measured cell viability of both organoid cultures treated with NaBt and calculated that the IC50 for healthy organoids if of 99 mM, whilst it is 63 mM for tumour organoids (Figure 27A). This finding reinforces the previous concept that the anti-proliferative effect of NaBt is observed mostly in cells with a high proliferative profile, as is the case of the tumour organoids and that the latter are more sensitive to NaBt treatment. Further, treatment with NaBt induced only a shrinkage morphology without cell death (Figure 27B).

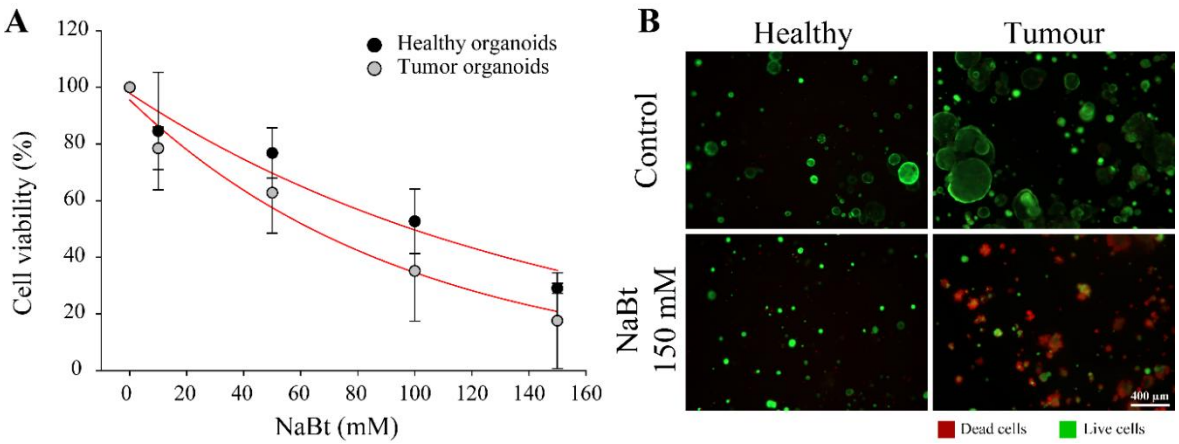

Figure 27: Tumour organoids are more sensitive to NaBt.

Tumour organoids and healthy organoids were seeded in 96 wells plates, expanded for 5 days, and then treated for 24 hours with 10 mM to 150 mM of NaBt. **A:** Cell viability was determined by using the CellTiter-Glo® 3D assay. Data for tumour organoids (mean ± SD, n= 3) and healthy organoids (mean ± SD, n= 2) is expressed by the % of viable cells per well, considering untreated cells as 100 %. **B:** Cell death was visualized by using the live/dead assay. Representative images of healthy and tumour organoids untreated (control) and treated with NaBt 150 mM are reported.

Chapter Conclusion

We presented evidence in this chapter that healthy organoids can be completely differentiated into the different colon epithelial types. These results were confirmed by proliferation assays, immunofluorescence, and RT-PCR, and indicate a complete differentiation of the healthy organoid culture after a period of 3 days without stem cell components, without compromising their cell viability. These results are relevant because they validate the versatility of the models and demonstrate the applicability of these models to perform drug absorption studies in the context of the function observed in the tissue of origin.

We also demonstrate the ability of the tumour organoid cultures to respond to several cytotoxic components, namely staurosporine, doxorubicin and NaBt. Further, we present results for the realization of two different cytotoxicity assays, one based in cell viability by the production of ATP (CellTiter Glo) and the other one based in cell death by disruption of the cell membrane (live/dead). Even though both can present similar results, they should be used in parallel. This is because they evaluate different parameters, and if studying for example components that affect cell metabolism, it is important to take into account that this can affect the production of ATP and result in mischievous results in terms of cell viability. This can be confirmed by the live/dead assay, that presents results in terms of cell death due to disruption of the cell membrane. However, this assay can be more time consuming, as it depends on image analysis.

Finally, we discuss in more detail the effect of an anti-proliferative bacterial bi-product, NaBt, over tumour organoids [149–151]. We were able to demonstrate the presence of a dose-response treatment with NaBt, and discuss the importance of the tumour microenvironment after verifying that the IC50 of the tumour organoids 3D model is lower from the IC50 of the CACO2 2D cell line. Because tumour organoids present a higher sensitivity to NaBt comparing to the cell line, we can discuss that this could be due to the contribution of the tumour microenvironment existent in the organoid model. However, further research should be performed to confirm this, for example by performing the same tests in a 3D model of CACO2 cells.

Still in the context of the study of NaBt, we also show preliminary results that the response observed in tumour organoids is different from the response observed in healthy organoids. This raised other questions related to the actual effect of NaBt over the different types of cells. Could the effect of NaBt in healthy organoids be directed towards metabolism

and thus appear to affect cell viability when analysed in terms of the CellTiter Glo assay? Is this effect reversible after removing the NaBt from the medium? Is the effect of NaBt the same after differentiating the healthy organoids? Even though we would like to address these questions in more detail during this work, this was not possible due to time limitations, context of the work and slow rate of growth of healthy organoids. However, we believe that it would be of great interest to address these questions in further research work.

Chapter 4: Commercial output – Cryopreservation of 3D models

Chapter Introduction

On the context of a PhD in industry, one of the important aims of this work was to develop a product that could be transformed into a commercial product with added value to the business. One of the technologies developed by the company at the time was cryopreservation. More specifically, the company developed technology that allowed cryopreservation of cells in situ, by the utilization of optimized cryoprotective (CPA) components, freezing protocols and thawing procedures. The concept of the technology is that different cell types can be cryopreserved *in situ*, in different multiwell platforms, stored for long term, and thawed when necessary for the realization of relevant studies (Figure 28). Amongst the advantages of this method is the improvement in automated analysis introduced by the reduction of preceding steps of cell isolation, propagation, and characterization. Furthermore, it also allows the utilization of assay-ready cells that involve more specialized or unconventional culture methods that would require specialized handling. Although in practice for other cell types, the technology was not yet optimized for 3D cultures of colon organoids at the start of this project.

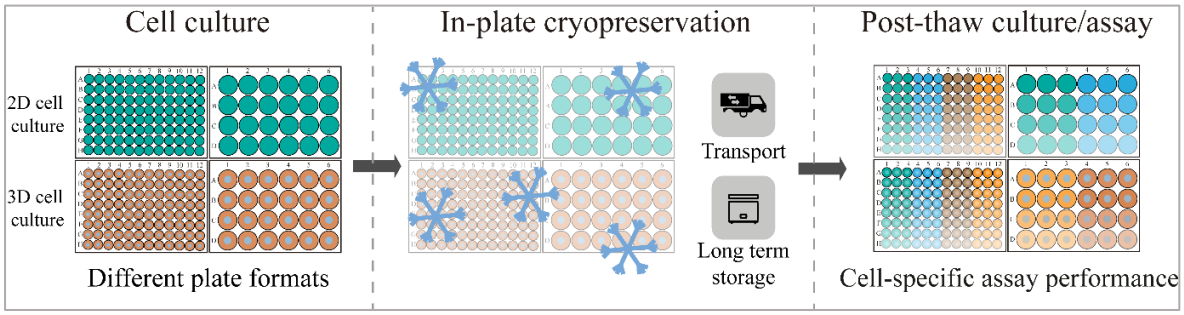

Figure 28: Schematic overview of in-plate cryopreservation technology.

Cryopreservation technology has been utilized for several years to produce cell stocks and protect cells from aging [155]. The technology itself has been mostly used as a method to cryopreserve cells in cryovials, but more recently, attempts have been made to apply this technology to monolayers or in-plate cell cultures [156,157]. Lately, and in a 3D context, it has been demonstrated that the technology can be applied for the in-plate cryopreservation of bovine cultures, with demonstrated maintenance of viability and functionality [144]. In chapter 4 we present and discuss the results obtained from the optimization and application of similar cryopreservation technology to 3D models of colon healthy and tumour organoids. The initial

results investigate the viability of healthy and tumour organoids after cryopreservation. These findings are complemented firstly by qRT-PCR results performed to access the effect of cryopreservation in gene expression and secondly by OCRs to access the types of respiration in both control and cryopreserved cultures. The chapter ends with cytotoxic studies performed with NaBt to study the effect of cryopreservation over the response to cytotoxic agent NaBt.

Results and Discussion

The viability of 3D colon models is not affected by the cryopreservation procedure

To initially access the viability of 3D colon organoid cultures after cryopreservation, both healthy and tumour organoids were seeded in 96 well plates, cryopreserved and thawed after 24 hours, according to the procedures defined in the material and methods section.

Alongside the in-house optimized cryopreservation medium utilized for the colon organoids (CPA-A), we also tested a commercial cryoprotectant existing in the market, CryoStor® (Figure 29). The viability of cultures was evaluated by the live/dead assay and results show the maintenance of viability of cells after cryopreservation. Both healthy and tumour organoid cultures remain viable after cryopreservation with both tested cryoprotective mediums. We did not find any significant differences for tumour organoids with either of the CPA comparing with control non-cryopreserved but found that CryoStor® as a cryoprotectant for healthy organoids is significative worse than CPA-A, comparing with non-cryopreserved (control) cultures.

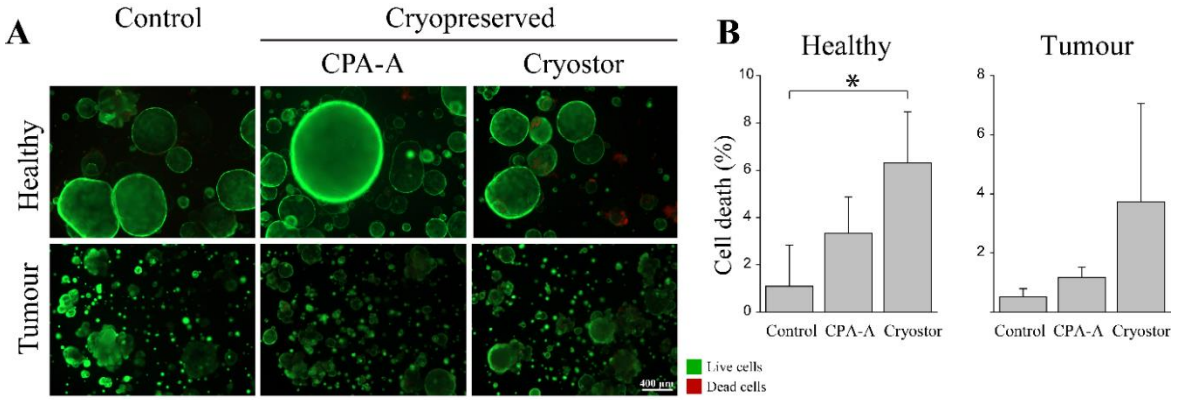

Figure 29: Cell viability of healthy and tumour organoids is not affected by **c**ryopreservation in-plate.

Organoids were seeded, cryopreserved in plate, thawed, and cultured for 6 days before assay. **A:** Representative images of non-cryopreserved (control) and cryopreserved healthy and tumour organoids. **B:** Cell death (%) was determined using the live/dead assay. Images were taken using an optical microscope (20x). Data are expressed as mean ± SD (n = 3; * $P < 0.05$) and represents % of dead (red stain), considering total number of stained cells (green + red) per well. CPA-A: Organoid

cryoprotective medium. Differences between non-cryopreserved (control) and cryopreserved groups were assessed using one-way ANOVA followed by Dunnett test.

As mentioned previously, the cultures were cryopreserved immediately one hour after seeding. The reasoning for this is that we have found that cryopreserving tumour organoid cultures after they are expanded decreases the viability of the cultures after thawing (Figure 30). To reach this conclusion, we cryopreserved tumour organoids either after seeding or after 5 days of expansion. We have found no significative differences in terms of percentage of death, between non-cryopreserved (control) and cultures cryopreserved after seeding. However, cryopreserving cultures at day 5, significantly increases the percentage of dead cells comparing to control cultures. We hypothesise that this decrease in viability is caused by the bigger size of expanded organoids where CPA may not be able to reach the cells within the inner portion of the organoid, thus leading to cell death induced by the freezing process. On the contrary, in the initial cultures, which are composed of small fragments of organoids, the CPA can reach each of the cells of the culture and exert its protective effect.

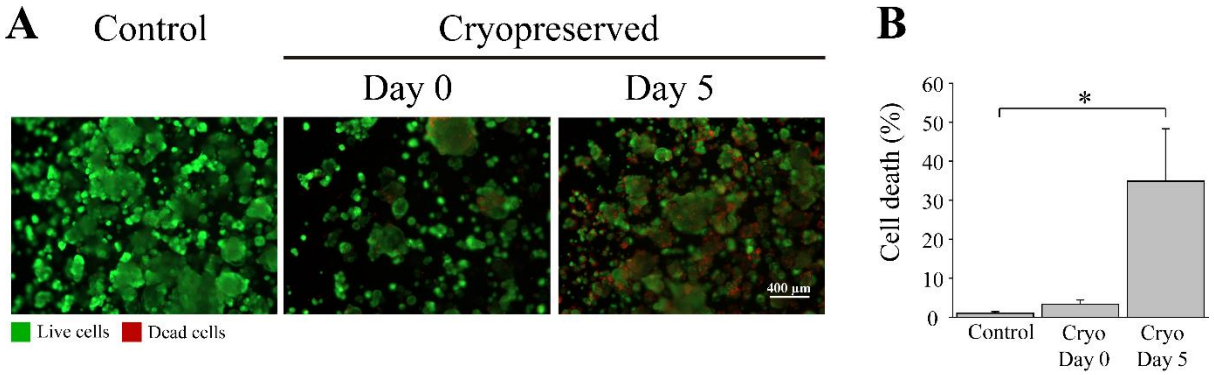

Figure 30: Cryopreservation of tumour organoid cultures at day 5 decreases viability of cultures.

Organoids were seeded, cryopreserved in plate at seeding day or after 5 days in culture, thawed and respectively cultured for 6 days before assay or assayed 24 hours post thawing. **A:** Representative images of non-cryopreserved (control) and cryopreserved tumour organoids. Images were taken using an optical microscope (20x). **B:** Cell death (%) was measured by using the live/dead assay. Data (mean ± SD) are expressed as % of dead (red stain), considering total number of stained cells (green + red) per well (n = 3; * $P < 0.05$). Differences between non-cryopreserved (control) and cryopreserved groups were assessed using one-way ANOVA followed by Dunnett test.

Gene expression of cryopreserved tumour organoids is not affected by cryopreservation

Besides examining viability after cryopreservation, we also wanted to analyse if the gene expression of the cultures was affected by the cryopreservation process. For this, tumour organoids were seeded in 24 wells, cryopreserved 1 hour after seeding, stored for 24 hours, thawed, and cultured for a further period of 7 days before collecting total RNA and running a reverse transcribed qRT-PCR. Prior to the discussion of these results, it is interesting to

mention that the structure of the 3D matrix, BME2, was not affected by the process of cryopreservation, as it is possible to see the structure of the matrix-containing tumour organoids (Figure 31A).

The analysis of gene expression of non-cryopreserved (control) and cryopreserved tumour organoid cultures show no significative difference, suggesting that the cryopreservation process itself does not affect the physiology of the culture (Figure 31B). In the context of metabolic studies, we also analysed the expression of metabolic-associated markers GLUT1 and PKM2. Again for these two markers, we did not observe differences for gene expression between control and cryopreserved cultures. This result is reassuring in the way that we could potentially use these cryopreserved cultures for metabolic studies, without concerns in respect to metabolic changes caused by the cryopreservation process. However, it is important to mention that metabolic state of the cultures cannot be accessed only by the expression of two metabolic genes. In this regard, we decided to further explore the metabolic pattern of these cultures.

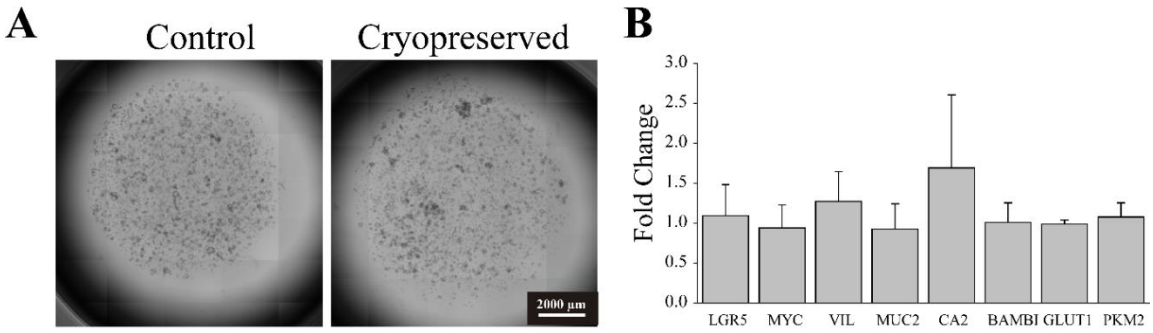

Figure 31: Cryopreservation does not affect gene expression of tumour organoids.

Organoids were seeded, cryopreserved in plate, thawed after 24 hours, and cultured for 7 days before collection of total RNA. **A:** Representative images of non-cryopreserved (control) and cryopreserved tumour organoids in 24 wells. Images were obtained using an optimal microscope (2.5x). **B:** Gene expression of cryopreserved tumour organoids was determined by qRT-PCR assay of total RNA samples. Data are expressed as mean ± SD ($n = 3$; $P < 0.05$) and represents the fold change of gene expression, considering non-cryopreserved (control) cultures as a fold change of 1. Differences between groups were assessed using one-way ANOVA followed by Tukey test. LGR5: stem cell marker; MYC: proliferation marker; VIL: brush-border microvilli marker; MUC2: goblet cells marker; CA2: colon cancer associated marker; BAMBI: colon cancer associated marker; GLUT1: glucose transporter marker; PKM2: pyruvate kinase 2 marker.

Cryopreservation did not alter the metabolic profile in both non-cryopreserved and cryopreserved tumour organoids

After the previous results obtained in terms of maintenance of the gene expression between control and cryopreserved cultures, we decided to further analyse the effect of

cryopreservation over the metabolic activity of cultures. For this, cryopreserved 96 well plates containing tumour organoid cultures were sent to the SALK institute, Salzburg, and stored at -150 °C. Following the protocol already optimized for the evaluation of mitochondrial respiration with Seahorse XF extracellular flux analyser, tumour organoids had to be seeded in the assay plates and expanded before assay. Because of this, it was not possible to measure respiration directly from the cryopreserved plates. However, cryopreserved plates were thawed, expanded for 6 days, seeded in the assay plates, and further expanded before assay. At the same time, non-cryopreserved tumour organoid cultures were seeded in the assay plates, expanded, and used as controls. The OCR was very variable between the different wells analysed (Figure 32A), likely due to the different size of tumour organoids in each well assayed. Because of this, it was not possible to average the results of all the wells in a single response curve, and then calculate the different types of respiration. Thus, we fist calculated the different types of respiration per well, and then averaged the results for all the wells (Figure 32B). By doing this, we decreased the variability caused by the size of the tumouroids. We based our calculations of the different types of respiration on the paper published by Divakaruni et al. [158], in the following way:

- Basal respiration = highest value before oligomycin injection – lowest endpoint value
- Proton leak-linked respiration = lowest value after oligomycin injection – lowest endpoint value
- ATP-linked respiration = basal respiration – Proton leak-linked respiration
- Maximal respiration = highest value after FCCP injection – lowest endpoint
- Reserve capacity = basal respiration – maximal respiration
- Non-mitochondrial respiration = lowest endpoint value

We did not observe differences related to the types of respiration between the control and cryopreserved tumour organoids.

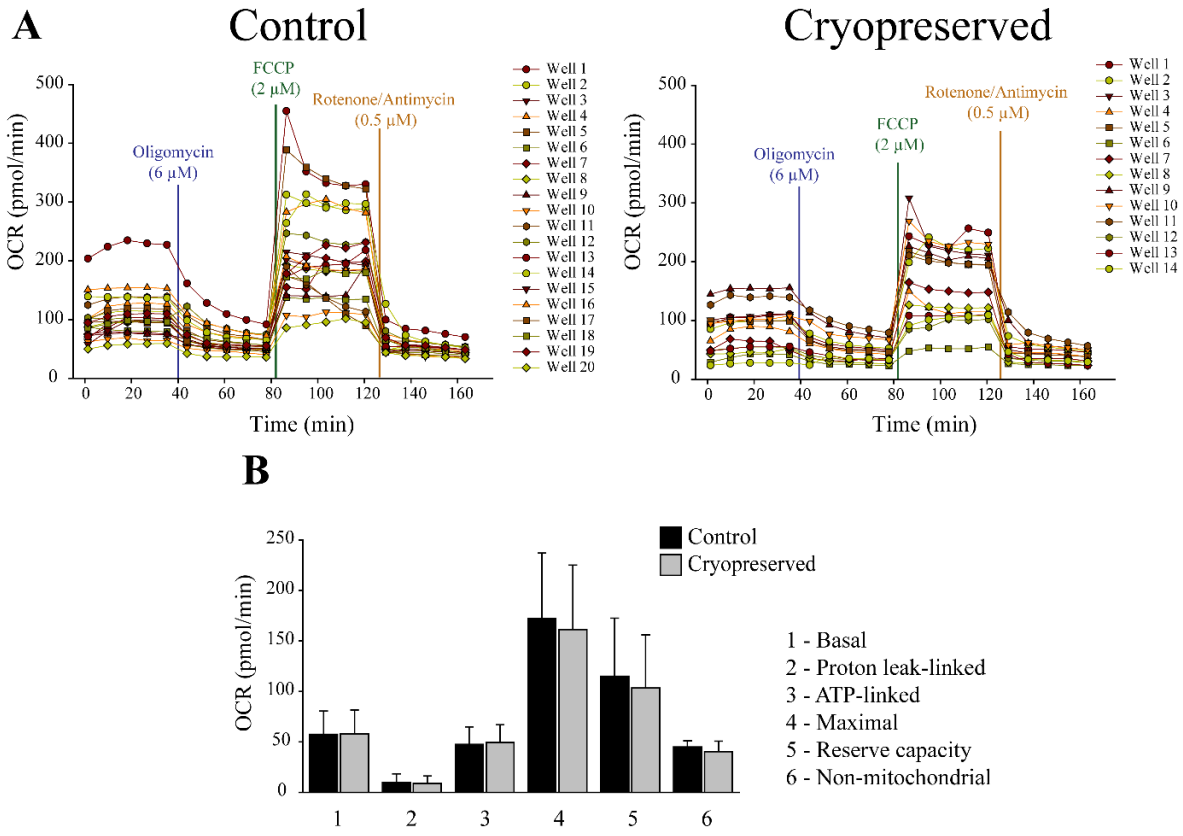

Figure 32: Non-cryopreserved and cryopreserved tumour organoids present similar bioenergetic profiles.

Tumour organoids were seeded in BME2 in assay plates and expanded for 5 days. **A:** The coloured timepoints indicate the oxygen consumption rate (OCR) of the different wells. The coloured vertical lines indicate the timepoints of injection of 6 µM oligomycin, 2 µM FCCP and 0.5 µM of Rotenone/AntimycinA. **B:** Data (mean ± SD; n = 2) represents the average of OCR measurements of non-cryopreserved (control) and cryopreserved tumour organoids per type of respiration.

It is important to mention that, because the tumour organoids needed to be seeded in the assay plates, they were not assayed directly as frozen cultures. They were instead thawed, expanded, and then seeded in assay plates for further expansion and assay. This was not anticipated a priori, as the method for determining respiration was not yet optimized when the plates were cryopreserved and sent to the laboratory. However, the same experiment can in future be performed in tumour organoids cryopreserved directly in the required assay plates.

Cytotoxicity response to NaBt is not affected by cryopreservation

It was demonstrated in chapter 3 that tumour organoids can be used to perform cytotoxicity assays. Here, we also wanted to investigate if this response was affected by cryopreservation. For this, we cryopreserved tumour organoids in 96 well plates, as described in the previous chapters and in the material and methods section. After thawing, we expanded the cultures for 5 days, treated the tumour organoids with NaBt and cell viability and cell death were evaluated (Figure 33A-B). No significative differences were observed between the

control and cryopreserved cultures, in terms of their response to NaBt, except for the higher concentration of 150 mM (Figure 33C). We also observed that the IC50 for control cultures is 128.70 mM and for cryopreserved cultures is 80.31 mM. However, as mentioned in the previous chapters, the CellTiter-Glo assay can introduce some variability associated with the differences in organoid sizes. Therefore, the differences in the IC50 values result from the slightly different curves observed for control and cryopreserved cultures, that can arise from variability introduced by the assay. Considering both the live/dead and the viability assay, we accept that these results were very encouraging and complete the previous indications that the functionality of cryopreserve cultures is not affected by the cryopreservation process.

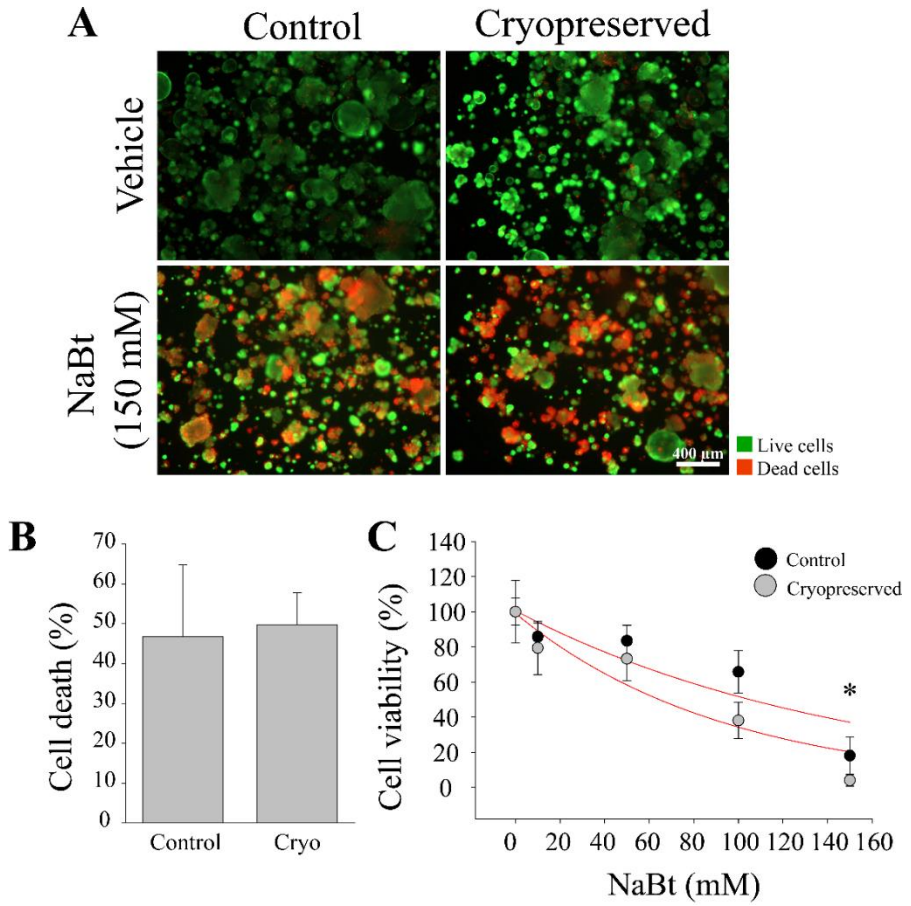

Figure 33: Cryopreservation does not affect the sensitivity of tumour organoids to NaBt.

Tumour organoids were seeded in 96 wells plates, cryopreserved, thawed, expanded for 5 days, and treated for 24 hours with 150 mM (A and B) or 10 to 150 mM (C) of NaBt. Non-cryopreserved cultures were used as controls. **A:** Representative images of non-cryopreserved (control) and cryopreserved, either treated or not with NaBt (150 mM), are reported. Images were taken using an optical microscope (20x). **B:** Data (mean ± SD; n = 3) expresses the % of dead cells (red stain), considering the total cells (green + red stain) per well as 100%. **C:** Cell viability was performed using the CellTiter-Glo® 3D assay. Data is indicated as mean ± SD (n = 3; * P < 0.05) and expresses the % of viable tumour organoids, treated with NaBt, considering non-treated tumour organoids as 100% viable. Differences between groups were assessed using t-test.

Chapter Conclusion

This chapter illustrates the work performed utilizing the previously characterized and validated organoids cultures, for the development of new applications. In the context of an industrial PhD thesis, one of the aims of the project was to develop a product that could produce commercial interest. The product develop here consists of the production of cryopreserved multiwell plates, containing pre-assembled organoid models. To initially access the capacity of the cryopreservation technology, both healthy and tumour organoids were cryopreserved in-plate, and after thawing, the cultures were accessed for their viability. The results indicate the maintenance of viability after thawing, with optimal results for the in-house produced CPA, in comparison with the commercial CPA Cryostor®. Furthermore, we also show evidence that viability is optimal if the cultures are cryopreserved within one hour after seeding, as opposite to 5 days after expansion.

We further analysed tumour organoid cultures in terms of their gene expression and demonstrate that the cultures maintain their gene expression after thawing. It was also interesting to observe that the process of cryopreservation does not affect the structure of the 3D matrix. After observing that the expression of the examined metabolic genes was not affected by the cryopreservation, we also decided to investigate further the respiration of these cultures. For this, we measured the OCRs profiles of control and cryopreserved cultures utilizing the Seahorse XF extracellular flux analyser revealing that no difference was found between control and cryopreserved cultures. Although this result is very encouraging, it is important to mention that, due to technical requirements, cryopreserved cultures were expanded and passaged once before assay. Because of this, the result does not exactly represent the behaviour of immediately thawed cultures, although it reflects the behaviour of a early passage of cryopreserved culture.

Finally, we also show that cryopreservation does not alter the response to NaBt in terms of cell viability and cell death. Overall, the results presented in this chapter reveal the generation of a cryopreserved colon organoid model, that maintains the characteristics of control cultures in terms of viability and functionality. Exploiting the technology here proposed, the organoid model can thus be produced in one location, cryopreserved, and transported to other locations. This allows the reduction of time-consuming steps of cell isolation and propagation and permits the utilization of assay-ready cells that would require specialized handling.

Chapter 5: Associated relevant applications

Chapter Introduction

As mentioned in Chapter 2, the organoid models produced in this project are composed of a culture of different cell types, that include stem cells and epithelial cells of the original tissue. However, these cultures still lack other cells usually present in the tumour microenvironment, such as fibroblasts, immune and blood cells. In a first attempt to upgrade these models to contain other cells of the microenvironment, we advanced with initial plans to co-culture organoids with fibroblasts. Since the final product of the project would be the generation of a cryopreserved model, we explored the optimization steps for the generation of a protocol that allows cryopreservation of fibroblasts in plate. Further, we also exploited the bioprinting technology for the generation of new bioinks that support the growth and expansion of tumour organoids.

Results and Discussion

Optimization of a protocol for in-plate cryopreservation of colon fibroblasts

To perform the cryopreservation experiments we characterized the fibroblast culture in terms of specific markers such as vimentin (fibroblast marker), alpha-smooth muscle actin (α-SMA, myofibroblast marker) and cytokeratin 18 (CK18, epithelial marker). The presence of positive signal for vimentin and negative for α-SMA and CK18, confirms the presence of a culture of fibroblast cells (Figure 34).

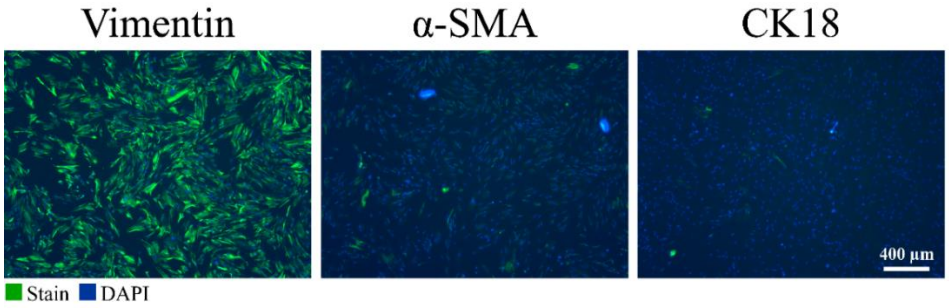

Figure 34: Immunofluorescence confirms presence of colon fibroblasts.

Colon fibroblasts were seeded at a density of 6000 cells per well in 96 wells plates and immunofluorescence assay was performed with antibodies specific for vimentin, α-SMA and CK18. Representative images are reported. Images were taken using an optical microscope (2.5).

For the initial protocol of cryopreservation of fibroblasts, cells were seeded in-plate and cryopreserved after 24 hours. A control plate was kept in routine conditions, non-

cryopreserved, and utilized as control. For cryopreservation, the culture medium was removed and replaced for cryopreservation medium. PBS was added to wells not containing cells, to ensure even freezing. We initially tested 3 different formulations of cryopreservation medium (CPA1, CPA2 and CPA1N). The cryopreservation medium is composed of the main CPA plus other nutrients. The main difference between CPA1 and CPA2 is the main cryoprotectant utilized. CPA1N is the same as CPA1 but with an added step of nutrient supply after thawing. After administration of cryopreservation medium, the plate was incubated for 30 min at 37 °C / 5 % CO_2. This time allowed the delivery of the CPA to the intracellular space. The plate was then cryopreserved in a gradient freezer utilizing a gradient freezing protocol, allowing a gradual cooling of the cells. After frozen, the plate was transferred to an ultra-low temperature freezer (-150 °C) for storage. For thawing, plates were transferred using a dry ice container, from the -150 °C storage to a -20 °C freezer for 30 min. After this, 100 µL of warm culture medium was added to all the wells and plate was incubated for 3 min at 37 °C in a static platform. Once thawed, the medium was completely removed and replaced with warm culture medium. In the case of cells treated with CPA1N, cells were incubated with medium containing extra-nutrients for 30 min before replacing with normal culture medium. Cells were then incubated overnight before assay.

Cell viability of cryopreserved 2D fibroblasts was determined by evaluating the caspase-3 activation, an indicator of apoptotic cell death. Cells cryopreserved only with culture medium show a low caspase 3 release (Figure 35A). However, this does not indicate a higher viability of cells cryopreserved in this matter, because cells cryopreserved with medium only are mostly dead and are release from the wells upon performing the assay. Amongst the 3 other cryopreservation mediums, CPA1N has the lowest value of caspase release, indicating a higher viability of cells cryopreserved with this formulation. We also observed high values of variability between the wells, which we believe are resultant from seeding variability and/or from the non-controlled release of adherent cells from the wells during the performance of the apoptosis assay.

To confirm these results, we performed the lactate dehydrogenase (LDH) assay to further assess the viability of cryopreserved fibroblasts. The cytotoxicity assay is based on the release of from the cells and accounts not only for cell death occurring by apoptosis but also by necrosis. We performed this cytotoxicity assay in non-cryopreserved (control) and cryopreserved fibroblasts and did not find significative differences between control cultures and cryopreserved cultures, except for fibroblasts cryopreserved with CPA2 (Figure 35B). As

verified for the apoptosis assay, we observed a low value of LDH release in cells cryopreserved with only medium, which we attributed to the loss of cells in these wells. We also observed in this assay that the formulation of cryopreservation medium that presents the best viability values is CPA1N.

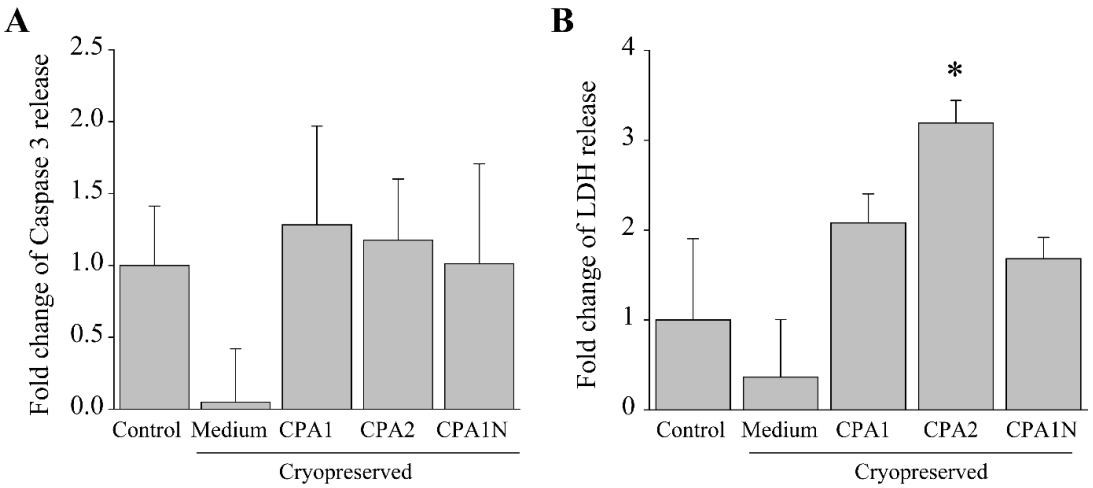

Figure 35: Caspase 3 and LDH release of cryopreserved fibroblasts relies on the cryopreservation medium.

Colon fibroblasts were seeded and cryopreserved in plate. Non-cryopreserved fibroblasts were used as control. 24 hours after cryopreservation, cells were thawed and assayed the day after. **A:** Apoptosis assay was performed in control and cryopreserved fibroblasts. Data are expressed as mean ± SD (n = 3; * P < 0.05) and represent the fold change of caspase 3 release of cryopreserved cultures, considering non-cryopreserved (control) cultures as a fold change of 1. **B:** Cytotoxicity assay was performed in control and cryopreserved fibroblasts. Data are expressed as means ± SD (n = 3; * P < 0.05) and represents the fold change of LDH release of cryopreserved cultures, considering non-cryopreserved (control) cultures as a fold change of 1. Differences between groups were assessed using one-way ANOVA followed by Dunnett test.

To better understand if the source of variability found was related to the number of cells present in the wells, we decided to perform a DNA quantification in control and cryopreserved fibroblast cultures. Independently of the cryopreservation formulation utilized, the variability in DNA amount is still high (Figure 36).

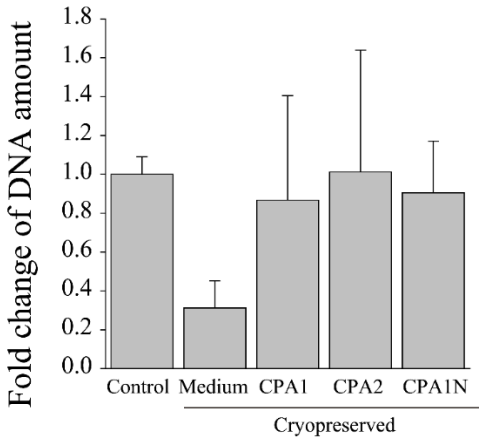

Figure 36: DNA quantification assay reveals variability in the amount of DNA of fibroblasts.

Colon fibroblasts were seeded and cryopreserved in plate. Control non-cryopreserved fibroblasts were used as control. 24 hours after cryopreservation, cells were thawed and assayed the day after. DNA quantification assay was performed in control and cryopreserved fibroblasts. Data are expressed as means ± SD (n=1) and represent the fold change of DNA amount of cryopreserved fibroblasts, considering non-cryopreserved (control) fibroblasts as a fold change of 1.

The low value observed for the fibroblasts cryopreserved only with culture medium is suggestive that cells are not surviving to cryopreservation with this formulation and that we are in fact not accounting for all the cells initially seeded. This supports the previously discussed values encountered in the apoptosis and cytotoxicity assays. In fact, images of wells taken at seeding day and after cryopreservation (assay day), show that the number of cells decreases after cryopreservation, and varies depending on the CPA formulation utilized (Figure 37). Control non-cryopreserved wells remain at similar numbers, but cells cryopreserved with medium or CPA2 significantly decrease their numbers.

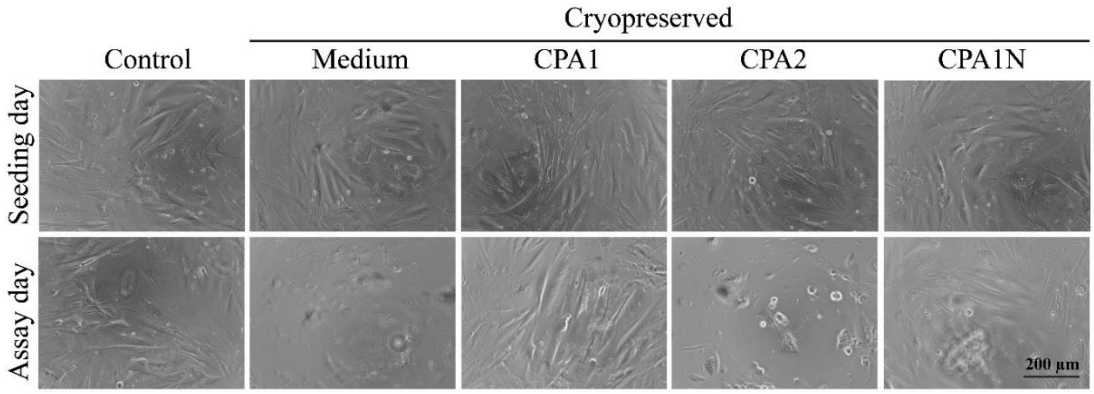

Figure 37: Fibroblast morphology and number is affected by cryopreservation.

Colon fibroblasts were seeded and cryopreserved in plate. Control non-cryopreserved fibroblasts were used as control. 24 hours after cryopreservation, cells were thawed and assayed the day after. Images were taken at seeding day and after cryopreservation (assay day), utilizing light microscope (40x objective).

We can still discuss that some of the variability illustrated by the standard error bars can be due to inconsistency of the seeding process. To account for this variability, we would have to use a method for in-plate cell counting before cryopreservation. However, we were not able to find a method such as this, that would not interfere with the cryopreservation process.

Regardless of the variability encountered between different wells corresponding to the same treatment, we observed that in general, CPA1N was the cryopreservation formulation that contributed to a higher viability of cells after cryopreservation. Because of this, we decided to only utilize this formulation in our next optimization experiments.

One of the most important events that affect cell viability after cryopreservation is ice nucleation [159]. This event is characterized by the formation of intracellular ice crystal due to

decrease in temperature below freezing point. If all cells reach this point at the same time, they will be cryopreserved at the same time. However, the range of ice nucleation temperatures can vary within cultures [159]. To decrease a possible variability due to different ice nucleation timepoints, we included CPA1N in the surrounding wells that did not contain cells. Until this point, we were filling these wells with PBS. However, the freezing point of PBS is not the same as the more complex cryopreservation medium. By applying the same cryopreservation medium in the surrounding wells and in the wells containing cells, we expected that all wells would freeze at the same temperature and thus reduce the variability found. Furthermore, we also reduced the incubation time with CPA1N before cryopreservation, from 30 min to 20 min. By doing this, we were also expecting to decrease a potential detrimental effect of the CPA over cell viability. We performed the cytotoxicity assay in cells treated using this approach and found that cells cryopreserved with CPA1N and with the adjustments mentioned above, presented cell viability values very similar as control non-cryopreserved cells (Figure 38). Furthermore, we also observed a very important decrease in variability amongst wells, which we attributed to the improved steps of addition of CPA1N in the surrounding wells and reduction of the incubation time with CPA1N.

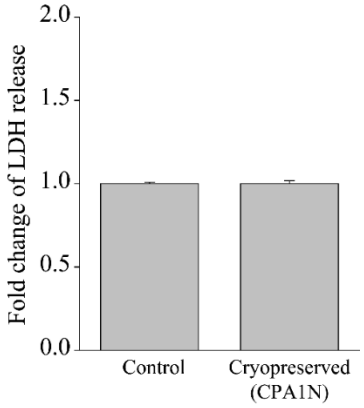

Figure 38: Cytotoxicity assay reveals no difference in LDH release between non-cryopreserved and cryopreserved fibroblasts with CPA1N.

Colon fibroblasts were seeded and cryopreserved in plate. Non-cryopreserved fibroblasts were used as control. 24 hours after cryopreservation, cells were thawed and assayed the day after. Cytotoxicity assay was performed in control and cryopreserved fibroblasts and data (mean ± SD; n = 2) are expressed as fold change of LDH release of cryopreserved fibroblasts, considering non-cryopreserved (control) cultures as a fold change of 1.

Bioprinting of tumour organoid models

Bringing the 3D technology further, we explored the application of bioprinting technology to our model. To optimize a new bioink that could support the growth of tumour organoids with the same or better performance than BME2, we collaborated with CELLINK,

a bioink company. The initial starting point was to use LAMININK 521 (LAM521), a bioink that supports different tissues types, including pluripotent and embryonic stem cells and induces their self-renewal [160]. Because LAM521 is temperature-sensitive, we warmed up the bioink to 37 ºC, mixed the ink with the tumour fragment suspension (proportions were the same as routine procedures), cooled down to room temperature in order to obtain a more viscous solution (easier to manipulate for seeding) and seeded the tumour organoids in 96 or 24 wells plates. After seeding, the plates were crosslinked by incubating cells with a few drops of a $CaCl_2$ solution for 2 min (as provided by CELLINK), washed once with PBS and feed with culture medium.

Simultaneously, we also wanted to understand which components of the culture medium were essential for tumour organoid growth. The rational for this, besides the research point of view, was to generate a specific culture medium that could be used as a commercial product. To do this, we seeded tumour organoids with either BME2 or LAM521, and at the same time, removed each of the tumour organoid medium components, one by one (Table 4).

Table 4: Composition of culture mediums.

*Basal components are: Advanced DMEM/F12; Penicillin/Streptomycin; Primocin; Glutamax; HEPES; N-acetylcysteine. ✓Component present. ×Component absent.

Medium / Component	Complete	Basal	Noggin	EGF	Gastrin	A83-01	SB202190	PGE2	Nicotinamide
Basal*	✓	✓	✓	✓	✓	✓	✓	✓	✓
Noggin	✓	×	×	✓	✓	✓	✓	✓	✓
EGF	✓	×	✓	×	✓	✓	✓	✓	✓
Gastrin	✓	×	✓	✓	×	✓	✓	✓	✓
A83-01	✓	×	✓	✓	✓	×	✓	✓	✓
SB202190	✓	×	✓	✓	✓	✓	×	✓	✓
PGE2	✓	×	✓	✓	✓	✓	✓	×	✓
Nicotinamide	✓	×	✓	✓	✓	✓	✓	✓	×

To access the viability of cultures we performed the live/dead assay (Figure 39A-B). We also performed qRT-PCR assay and analysed the expression of LGR5 and MYC, to understand if any of the medium components is essential to maintain the proliferation state of the cultures (Figure 39C).

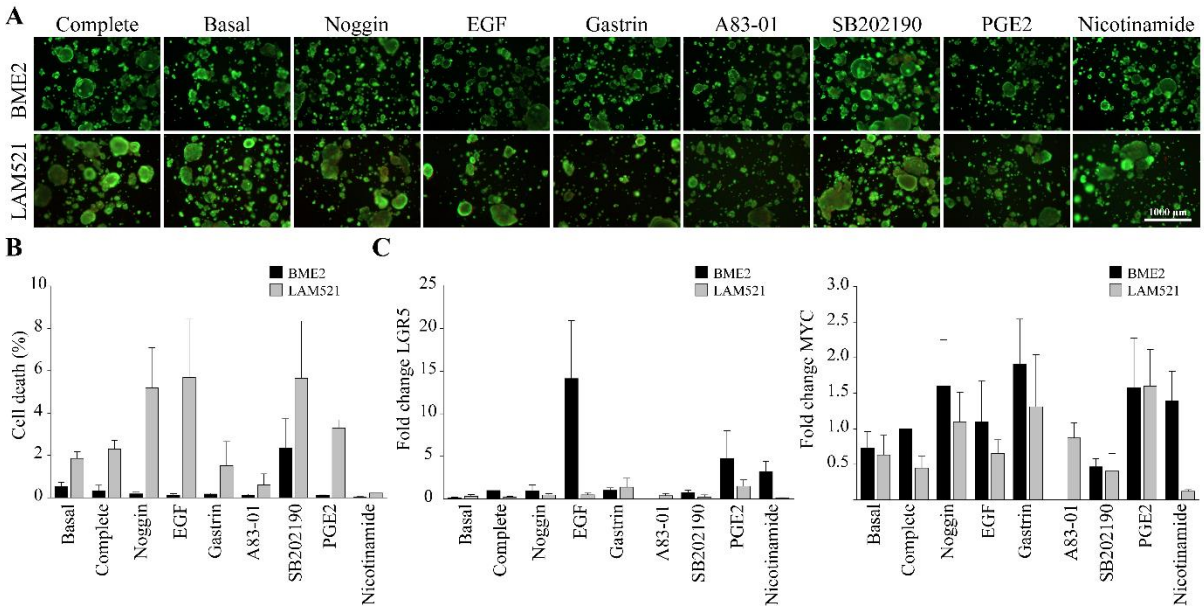

Figure 39: Tumour organoids present similar viability when seeded with LAM521 or BME2.

Tumour organoids were seeded in 96 (live/dead assay) or 24 wells plates (qRT-PCR assay), in either BME2 or LAM521 and feed for 6 days with different medium compositions: complete medium, basal medium and complete medium without a specific component (Noggin, EGF, Gastrin, A83-01, SB202190, PGE2 or Nicotinamide). **A:** Tumour organoids were subjected to the live/dead assay and images are representative of each of the studied conditions. Images were taken using an optical microscope (20x). **B:** Cell death were measured by using the live/dead assay. Data (mean ± SD) are expressed as the percentage of dead cells (red stain), considering the total number of cells per well (green stain + red stain) as 100% **C:** Tumour organoid samples were taken from each condition and processed with qRT-PCR assay. Data (mean ± SD) are expressed as the fold change of LGR5 (left) and MYC (right) expression levels, considering cells seeded with BME2 in complete medium as a fold change of 1.

Overall, the results obtained for the live/dead assay were very surprising. Considering cells seeded in BME2, it was unexpected to find such good viability by removal of components, especially for organoids cultured in basal medium. The highest % of dead encountered was for organoids cultured in complete medium without SB202190, even so, this value was only of 2%, a value we consider insignificant. The overall viability of organoids seeded in LAM521 was lower than organoids seeded in BME2. Even so, these values are also considered small. The highest values found in terms of % of dead in cultures seeded in LAM521 belonged to organoids seeded in medium without Noggin, EGF or SB202190. However, these results are puzzling, because their % of dead cells is higher than organoids cultured in basal medium, which do not contain any of the most relevant components. To have more relevant results, we would have to repeat this experiment, and to culture organoids for longer term in the same conditions, to access viability at long-term.

In terms of gene expression, we did not find relevant differences in terms of the expression of LGR5 or MYC, indicating an overall good proliferation state of all cultures.

Particularly regarding LGR5, we did find a high increase of its expression in organoids seeded in BME2 and cultured with medium without EGF. As these results were obtained from only one preliminary experiment, we would have to perform more repetitions and investigate this further. Despite the need for further research, we were very encouraged by these first results in terms of both viability and proliferation. Firstly, because they suggest that LAM521 could be a potential viable bioink to support the growth of tumour organoids. Secondly, because this can be a practical way to understand the specific component requirements of the culture.

Chapter Conclusion

As mentioned previously, this was a thesis performed in the context of the industry. The final product of the work performed during this time, was the generation of a cryopreserved model of organoids. Thinking ahead on the possibility of generating a more complex cryopreserved model, composed of organoids co-cultured with fibroblasts, we present here the optimization of the protocol for cryopreservation of fibroblasts in-plate. After accomplishing the cryopreservation of fibroblasts, the next step would be to cryopreserve the co-culture. Indeed, we were able to successfully cryopreserve fibroblasts in plate, in a 2D system, by optimizing both the cryopreservation medium and the cryopreservation protocol. This reassured us that these cells can be cryopreserved and thus would respond well when cryopreserved in co-culture. One of the main problems encountered during this process, was to find a method that could efficiently and accurately access the viability of the cultures after cryopreservation. Because fibroblasts are expanded and cryopreserved as adherent cultures, dead cells eventually detach from the plate during the different steps of the protocol. This, in the end, does not allow the correct evaluation of the viability of cells, either because there are less cells in the plate in the end of the protocols, or because dead cells detached, giving an incorrect notion of viability. The fact that these phenomena happened, contributed to some of the high variability encountered between assays or within the same assay performed.

Although fibroblasts were cryopreserved as 2D cultures in these experiments, they would eventually be cryopreserved in a 3D manner, in co-culture with organoids. This would decrease the problems encountered with the adherent culture, because in a 3D culture, cells are “trapped” within the matrix, which allows the accurate quantification of both live and dead cells. Even though we were not able to complete the generation of a co-culture model and its cryopreservation, we present here preliminary data that can be used for this end and leave a potential future application.

Associated relevant applications

Another possible application for this model, is in the context of bioprinting. This technology is being currently utilized to generate advanced tissue-like structures that mimic native tissue parts [161]. In this context, we tested this technology in the generation of organoid models. We worked in collaboration with a bioink company, CELLINK, and tested a bioink that supports pluripotent and embryonic stem cells and induces their self-renewal. The efficacy of this bioink, LAM521, was tested pairwise with the current utilized 3D matrix, BME2. At the same time, we also had interest in assessing the importance of each of the medium components, and thus cultured tumour organoids in the absence of each of the main components of the tumour organoid medium. In the preliminary experiments we performed, we observed a very good viability of tumour organoids cultured with LAM521, along with support of cellular proliferation, which suggested a potential use of this ink to sustain the growth or tumour organoids. Surprisingly, we also found that tumour organoids survived in the absence of the main components of the culture medium. However, these are preliminary results, and further research would be needed to confirm this. Most important would be to understand if the tumour organoid growth is supported at long term, by expanding tumour organoids in the same conditions over several passages.

General Discussion and Conclusions

The generation of models for cancer research is not without its challenges. Two-dimensional cell models are simple to use and can be very useful and adequate to study a defined cellular pathway or simple cellular mechanisms. However, cancer involves several cellular pathways, several cell types, and the interaction with the extracellular matrix. Further, the complexity metabolism of cancer adds another layer of difficulty. Therefore, 2D cell lines are no longer enough to produce reliable and representative results in cancer research. More complex models, that reproduce the characteristics of the tumour microenvironment of the original tissue or organ, are being developed and include organoid cultures. Despite some controversy that may exist regarding the nomenclature behind organoid cultures, an organoid model can be generated from stem cells or induced stem cells, from several tissues and organs, originates the cell types of the tissue of origin, and reproduces *in vitro* the structure and physiology of the tissue of origin.

In this thesis, we described the processes of generation, characterization, validation, and application of human colon organoid models. Healthy and tumour organoid cultures were generated by entire colon crypts or single tumour cells, respectively. The process of generation of healthy organoids required optimization of pre-established protocols and was complemented by the establishment of an in-house culture medium. Tumour organoids were likewise subjected to optimization of pre-established protocols but required a more complex process. This involved testing of several culture conditions to better reproduce the original requirements of the original tumour tissue, based on oxygen supply or specific medium components. We believe that this method of generating tumour organoids, that was also adapted by other authors previously, is a more adequate method than choosing a priori a specific culture condition. The reason for this is that tumours can present several subtypes, with different types of cellular differentiation, invasion capacity or mutational landscape. Therefore, establishing differentiated initial culture conditions and choosing the one more successful can improve the success rate in the generation of such cultures.

The existence of two different colon culture models, healthy and tumour, was confirmed by the presence of structural and physiological differences. Healthy organoids are characterized by having a round structure, with a hollow middle surrounded by a layer of cells. Contrary, tumour organoids have a very disorganized structure, and appear as a “clump” of cells. Further, the cell composition of these models is also different, with tumour organoids

presenting more undifferentiated and proliferative cells. Gene expression was also separate between the two models. However, both presented a similar expression of mitochondrial and respiratory complex markers, which is congruent with the literature. The interest of studying metabolic respiration in these models led to the optimization of a protocol for the assessment of the bioenergetic profile of tumour organoids with the Seahorse XF analyser. This is a method currently used to access the bioenergetic profile of several models, but usually in a 2D manner. Therefore, the process of optimization required a long time, and it was not possible to compare the bioenergetic profile of healthy against tumour cultures. However, this can be now performed in further studies by applying the optimized protocol to healthy and tumour cultures and comparing their OCRs.

The interest in generating organoid cultures stands, apart from other reasons, in the fact that the physiology of the tissue of origin can be reproduced. In the case of the colon, one of the most relevant studies that can be performed are drug absorption studies, usually performed in a monolayer of epithelial colon cells. Since the apical side where absorption occurs is in the internal side of organoids, this can be a challenge for the realization of such studies in these models. However, other authors have already demonstrated the ability to generate monolayers from colon organoid cultures. We have demonstrated in this thesis the ability to differentiate healthy organoid cultures into complete epithelial cell cultures, that can be therefore applied into drug absorption studies.

Drug discovery is one of the most critical fields in cancer research, and reliable and representative models are necessary to generate data that can be transposed to clinical trials. In this context, we have demonstrated that tumour organoids respond to staurosporine, doxorubicin and sodium butyrate. Interestingly, we reveal that two assays that are used to indicate cell viability have different outcomes for the same drug study, which is caused by the 3D structure of the organoid. This raises attention to the importance of utilizing assays that accurately reflect the behaviour of the model and normalizing these assays so that data can be compared between different laboratories. Regarding the studies performed with sodium butyrate, we have also demonstrated the different responses between 2D and 3D models, and between healthy and tumour organoids. This data can be explained by the contribution of the tumour microenvironment and by the effect of sodium butyrate in the different cells of the microenvironment, and raises understanding for the relevance that the adequate model can have in a drug response studies.

Utilizing the organoid technology for the development of new products in a commercial setting, we have also developed an in-plate cryopreservation protocol. We demonstrated the cryopreservation of organoids in several multiwell formats utilizing this protocol, with maintenance of cell viability, gene expression, 3D structure, mitochondrial respiration, and toxicity response. This technology allows organoid models to be produced in one location with expertise knowledge, cryopreserved, and transported to other locations, thus reducing time-consuming steps of cell isolation and propagation. We further explored this topic by optimizing a protocol for in-plate cryopreservation of fibroblasts. In follow-up studies, these cells could be co-cultured with organoid cultures, that lack the cells of the stroma, and further complement the cryopreserved 3D model. This also opens the door to the realization of similar studies with other cells of the tumour microenvironment, such as immune cells.

We ultimately performed preliminary research into the area of bioprinting, by testing new bioinks to support the growth of tumour organoids. This work is not only important because it intended the discovery of new bioinks that could be used in a commercial setting, but also because it explores the importance of the different matrixes and the different components in the development of tumours. Although this work showed very promising preliminary results, it required more time for its development, which can be picked up for follow-up studies.

In conclusion, we believe that the work performed in this thesis contributed to the field of cancer research, by developing relevant models of colon cancer, and demonstrating its application in several pertinent settings, including the metabolic field. This work also leaves important questions that can be used to continue research in this field, namely regarding the different sensitivities of healthy and tumour organoids to NaBt. Furthermore, the technology described in this work can also be applied to other cell culture models.

Future perspectives

- Compare histology of original tissue with histology of organoid cultures
- Analyse genetic profile of organoid cultures and compare with tissue of origin
- Compare mitochondrial respiration of healthy organoids with tumour organoids utilizing Seahorse XF analyser
- Analyse mitochondrial respiration of organoids directly cryopreserved in Seahorse XF assay plates
- Sodium Butyrate: Perform a 3D model of CACO2 cells to compare dose-response with 3D tumour organoid model; Perform cytotoxicity studies in differentiated healthy organoid cultures to better understand the effect of NaBt towards proliferative versus differentiated cells
- Develop co-culture model with fibroblasts and perform cryopreservation of the model

Material and Methods

Cell cultures

Human colon tissues were obtained under ethical approval from the West of Scotland Research Ethics Committee, and in compliance with UK Human Tissue Authority guidelines. Tissues were procured as anonymized material indirectly through specialist intermediary suppliers from sources adhering fully to legal and ethical requirements of the country of collection, which included prior donor consent. Tissue specimens were collected from individuals suffering from colorectal cancer, from the original tumour and/or from normal adjacent tissue. Acceptance criteria consist of donors under 75 years old with primary colorectal tumour, without history of radiotherapy, minimum tissue weight of 0.25 grams and delivery within 48 hours after sample collection.

Human colon organoids

Methods for the isolation of colon crypts were adapted from the protocols developed by Sato et al. [106,107]. The study described here uses these initial protocols, but with the addition and/or implementation of some steps. Upon delivery, tissue was weighted, placed in a 70 µM filter, washed with cold wash tissue solution (Table 7), and the upper mucosal layer was dissected from the tissue by cutting into small mucosal stripes of approximately 1x3 mm. The mucosal stripes were recovered and washed with cold wash tissue solution for at least 3 times followed by 30 min incubation with chelation buffer (Table 7) at 4 ˚C to release the colon crypts. The chelation step was stopped once crypts could be visualized on the microscope. After removal of chelation buffer, colon crypts were washed with cold tissue wash solution and gently vortexed (1-2 seconds). A small sample was taken to observe the presence of crypts and the washing plus vortex procedure was repeated until no more crypts were observed. Crypts were seeded at a density of 500 per 35 µl of cold BME2 per well of a 24 well culture plate. BME2 domes were allowed to polymerize at 37 ˚C in a humid atmosphere with 5% CO_2 for 15 min before they were overlaid with 500 µl of human colon organoid complete medium (Table 7). Embedded crypts were cultured at 37 ˚C in a humid atmosphere with 5% CO_2 and culture media was replaced every 2 days. After approximately 10 days after seeding, colon organoids were ready for passage. All material utilized to work with colon organoids was previously coated with a solution of 1 % BSA. For passaging, the media was removed, the BME2 domes were destroyed using 1mL of ice cold human colon basal medium (Table 7), recovered to a 15 mL plastic tube, centrifuged at 300g for 5 min at 4 ºC, and the pellet was disrupted using

TrypLE™ Express with 10 µM Rock Inhibitor (Y-27632) for 10 min. Basal medium was added to stop the disruption of the organoids and the cell suspension was centrifuged at 300 g for 5 min at 4 ºC. Organoid fragments were re-embedded in 35 µl of BME2 in a 24-well plate format, using a splitting ratio of 1:2-1:4, and cultured in 500 µl of human colon organoid complete medium.

Human colon tumour organoids

Methods for the isolation of cells from tumour tissue were adapted from previous protocols [4,25,86,106,107,162]. Following a maximum period of 48 hours after surgical excision, tissue was weighted, placed in a 70 µM filter, washed with colon tumour tissue wash solution, dissected into 0.5-1 mm^3 pieces and washed with colon tumour tissue wash solution at least four times to remove any pieces of fat and blood. Tumour pieces were digested in a tumour organoid digestive solution (Table 7) until approximately 80 % of the cell suspension was composed by single cells. In order to do this, 4-5 mL of digestive solution was added per gram of tissue and incubated at 37 ºC using a magnetic stirrer for 30 min. The solution was checked for the presence of single cells every 10 min and returned to the incubator until most of the solution was composed of single cells. When digestion was complete, colon tumour tissue wash solution containing 2 % of human serum was added to stop the enzymatic reaction. The material was centrifuged at 300 g for 3 min at 4 ºC and washed 4 more times with colon tumour tissue wash solution in the same manner. Cells were seeded at a density of 5 x 10^4 cells per 20 µl of cold BME2 per well of a 48 well culture plate. BME2 domes were allowed to polymerize at 37 ˚C in a humid atmosphere with 5 % CO_2 for 15 min before they were overlaid with 200 µl of human colon tumour organoids complete medium (Table 7). Embedded single cells were cultured at 37 ˚C in a humid atmosphere with 5 % CO_2, and culture media was replaced every 2 days. After approximately 8 days after seeding, colon tumour organoids were ready for passage. All material utilized to work with colon tumour organoids was previously coated with a solution of 1 % BSA. For passaging, the media was removed, the BME2 domes were destroyed using 1mL of ice cold human colon basal medium, recovered to a 15 mL plastic tube, centrifuged at 300 g for 5 min at 4 ºC, and the pellet was disrupted using TrypLE™ Express with 10 µM Y-27632 for 15 min. Basal medium was added to stop the disruption of the tumour organoids, and the cell suspension was centrifuged at 300 g for 5 min at 4 ºC. Tumour organoid fragments were re-embedded in 35 µl of BME2 in a 24-well plate format, using a splitting ratio of 1:3-1:5, and cultured in 500 µl of human colon tumour organoid complete medium.

Drug treatments

For cytotoxicity assays, cultures were treated with Staurosporine (cat.S6942, Sigma-Aldrich, Irvine, UK), Sodium Butyrate (NaBt) (cat. B5887, Sigma-Aldrich, Irvine, UK) or Doxorubicin (cat.324380, Sigma-Aldrich, Irvine, UK). Concentrations and treatment duration were used as specified per case. Cytotoxicity was accessed as specified in the results and discussion section, using either the CellTiter Glo 3D assay, the live/dead assay or the LDH assay.

Differentiation of organoid cultures

For differentiation experiments, organoids were cultured for approximately 5 days until their outgrowth was visible. Culture medium was removed, cultures were washed with DPBS was differentiation was induced by changing the medium to complete organoid differentiation medium (Table 7), for 3 days with daily medium changes. Differentiated organoid cultures were then processed for gene expression analysis, EdU staining and live/dead staining.

Fibroblast cell lines

Fibroblast cell lines were isolated from tissue samples obtained from patients undergoing medically prescribed surgery, utilizing the explant method. Colon fibroblasts utilized in this project belonged to batch number 12-C402C. Fibroblasts were seeded at a density of $0.5x10^6$ cells per T75 flask in 10 mL of fibroblast medium. For cell passaging, cells were detached from the flask by incubation with 1 mL of 0.25 % Trypsin-EDTA, for 5 min incubation at 37 ºC. The enzymatic reaction was stopped with 9 mL of fibroblast medium, cells were centrifuged at 300 g for 5 min and seeded at a density of $0.5x10^6$ cells per T75 flask in 10 mL of fibroblast medium. For experimental assays, cells were seeded in 96 well plates at a density of 6000 cells per well.

Preparation of conditioned media

Wnt-3A conditioned media

The Wnt-3A secreting cell line L-Wnt-3A (ATCC® CRL-2647™), purchased from ATCC, MNZ, USA, was cultured according to manufacturer's instructions.

Cell seeding was performed at a density of $2x10^6$ cells per T75 flask, in L-cell media (Table 7). Twenty-four hours later, medium was replaced with L-cell selective complete medium (Table 7), which was renewed every 2 days. When confluent, cells were lifted with 2 mL of Trypsin-EDTA (0.25 %) for 5 min at 37 ºC, split in a ratio of 1:10 into 4xT175 tissue culture flasks and fed with 25 mL of L-cell medium. Seeding in L-cell medium is crucial for

cell attachment. Twenty-four hours later, flasks were washed with HBSS and medium replaced with 25 mL of L-cell conditioning medium (Table 7). L-cells grow in conditioning medium whilst secreting Wnt-3A. Three days after seeding, Wnt-3A conditioned medium was removed, centrifuged at 300 g for 7 min to remove cell debris, sterile filtered through a 0.22 µM filter and stored at 4 ºC. Fresh L-cell conditioning medium was added to the flasks and collected in the same manner after 3 days of culture. The 2 batches of conditioned medium were merged and an equal amount of fresh L-cell conditioning medium was added, making up 50 % of conditioned medium. Aliquots of this medium were prepared and stored at -80 ºC for a maximum period of 3 months.

R-spondin conditioned media

The R-spondin1 secreting cell line Cultrex ® HA-R-Spondin1-Fc 293T, purchased from AMS Biotechnology Ltd, Milton Park, UK, was cultured according to manufacturer's instructions.

Cell seeding was performed at a density of $1x10^6$ cells per T75 tissue culture flask, in R-spondin basal growth medium (Table 7). After overnight incubation, medium was replaced with R-spondin selection growth medium (Table 7), and replaced every 2 days. After reaching 80-90 % confluency, cells were split using 3 mL of TrypLE for 3 min, and seeded at a density of $5x10^6$ cells in T175 tissue culture flasks. After reaching 80 % confluency, medium was replaced with R-spondin basal medium with Penicillin/Streptomycin (100 µg/mL) for 24 hours and with R-spondin conditioning medium (Table 7) for 10 days at 37 ºC, 5 % CO_2. After approximately 7 days, cells start detaching from the flask, but are still producing R-spondin and growing in suspension. After 10 days, conditioned medium was collected, centrifuged at 300 g for 10 min at 4 ºC to remove cell debris, sterile filtered through a 0.22 µM, aliquoted and stored at -80 ºC for up to 3 months.

Cryopreservation

Cryopreservation of cells in suspension

Crypts, colonoid fragments and tumour organoids fragments in suspension, were cryopreserved in 1 mL Cryostor ® CSR supplemented with 10 µM Y-27623, in 2 mL cryovials. Vials were cryopreserved in a Mr. Frosty™ freezing container at -80 ºC overnight and transferred to a ULT freezer (-150 ºC) for long term storage. Colon crypts were cryopreserved immediately after tissue isolation, at a concentration of 2000 crypts per cryovial. Colon organoids and tumour organoids were harvested and disrupted in TrypLE™, as previously

described. Fragments were cryopreserved at a density of 1-3 wells (24 well plate) per cryovial for colon organoids and 1 well (24 well plate) per cryovial for colon tumour organoids. Cryopreserved organoid and tumour organoid fragments were rapidly thawed at 37 ºC in the water bath and re-suspended in 10 mL of respective culture medium. After centrifugation at 300 g for 5 min at RT, fragments were res-suspended in BME2 and seeded as for passaging.

Fibroblasts were harvested in 0.25 % Trypsin-EDTA, as previously described, counted, and cryopreserved in 1 mL of Cryostor® at a density of $0.5x10^6$ cells per cryovial. Cryopreserved fibroblasts were rapidly thawed at 37 ºC in the water bath and re-suspended in 10 mL of fibroblast culture medium. After centrifugation at 300 g for 5 min at RT, cells were seeded as for splitting.

In-plate cryopreservation of 2D cultures

Human colon fibroblasts were passaged applying standard procedure and seeded into 96 well plates at a density of 6000 cells per well. After 24 hours, culture medium was exchanged with 100 µL cryopreservation media (CPA1, CPA2 or CPA1N) for 30 min at 37 ˚C / 5 % CO_2. Wells not containing cells were filled with cryopreservation medium to ensure even freezing. After CPA equilibration, temperature was gradually decreased to a final temperature of -80 ˚C using an EF600 controlled rate freezer. Cryopreserved plates were transferred to a cryogenic ULT freezer at -150 ˚C for long term storage. For the thawing process, cell cultures were pre-incubated at -20 ˚C for 30 min, 100 µL of pre-warmed culture media was added to each well and the plate was transferred to a heated static platform at 37 ˚C until completely thawed (3 min). Once the plate was thawed, media was immediately replaced with fresh cell culture media and cultures incubated at 37 ˚C, 5 % CO_2. Cells treated with CPA1N were incubated for 30 min with a medium containing extra nutrients, prior to feeding with normal culture media.

In-plate cryopreservation of 3D cultures

Human colon organoids and tumour organoids were passaged applying standard procedure and seeded into 96 or 24 well plates within 6 µL or 35 µL of BME2, respectively. After a period of 2 hours, culture medium was exchanged with 100 µL/500 µL CPA supplemented with 10 µM Y- 27623 for a period of 20 min at 37 ˚C / 5 % CO_2. Wells not containing BME2 cultures were filled with CPA to ensure even freezing. After CPA equilibration, temperature was gradually decreased to a final temperature of -80 ˚C using an EF600 controlled rate freezer. Cryopreserved plates were transferred to a cryogenic ULT

freezer at -150 ˚C for long term storage. For the thawing process, cell cultures were pre-incubated at -20 ˚C for 60 min, 100 µL/500 µL of pre-warmed culture media was added to each well and the plate was transferred to a heated static platform at 37 ˚C until completely thawed (3 min for the 96 well plate and 3.5 min for 24 well plates). Once the plate was thawed, media was immediately replaced with fresh cell culture media and cultures incubated at 37 ˚C / 5 % CO_2.

CellTiter-Glo ® 3D Cell viability assay

Cell viability was determined by quantification of ATP present in metabolically active cells, using the CellTiter-Glo® 3D cell viability Assay. Organoids and tumour organoids were harvested and split as described previously, and seeded in 96-well, black walled, transparent bottom, culture plates. For quantitative analysis, an ATP standard curve was included to the plate immediately prior to adding the CellTiter-Glo® reagent. Luminescent signal was detected by Synergy ™ H4 Hybrid Multi-Mode Microplate reader. Viability was measured as the fold change of ATP production in treated wells comparing to control wells.

Live/Dead staining

Live/dead staining is a fluorescence-based assay utilizing fluorescein diacetate (FDA) and propidium iodide (PI) to stain live and dead cells, respectively. To perform this assay, culture medium was removed, cultures were washed once with PBS and incubated to a freshly prepared solution of FDA/PI in PBS (Table 7) for 4 min at room temperature. After incubation, cells were washed twice with PBS and immediately imaged. Images were analysed with Image J (National Institutes of Health, MD, USA) and the percentage of dead cells was quantified as % area positive for PI/(% area positive for PI + % area positive for FDA). All images were acquired using Cytation™ 5 Multi-Mode Cell Imaging reader (BioTek Instruments Inc., VT, USA).

DAPI staining

DAPI nuclear staining was performed using Fluoroshield™ and following the manufacturer's instructions. Briefly, some drops of Fluoroshield™ were added directly to the cultures, following 25-30 min incubation in the dark and washing twice with PBS. Cells were immediately imaged. All images were acquired using Cytation™ 5 Multi-Mode Cell Imaging reader (BioTek Instruments Inc., VT, USA).

EdU proliferation

To perform this assay, 3D cultures were seeded into 96 well, black walled, transparent bottom cell culture plates. The assay was performed using the EdU HTS Kit 488, according to manufacturer's instructions. The assay was performed at RT, cells were always kept protected from light and washed with a 1 % BSA solution between treatments. Briefly, cells were incubated with 5 µL of EdU for 2 hours, fixed with 100 µL of 4 % PFA for 30 min, permeabilized with 0.5 % Triton-X100 for 15 min, incubated with the reaction kit for 30 min at RT and washed with 1 x rinse buffer. Finally, DAPI staining was performed in the same wells and cells were imaged after 30 min. All images were acquired using Cytation™ 5 Multi-Mode Cell Imaging reader (BioTek Instruments Inc., VT, USA).

Apoptosis assay

This assay was performed only in 2D cultures of fibroblasts. For this assay, fibroblasts were seeded at a density of 6000 cells per well. A standard curve of caspase 3 was prepared in 2x caspase buffer (Table 7), in the concentrations ranging from 0 to 10 ng/5 µL (0; 0.077; 0.155; 0.31; 0.62; 1.25; 2.5; 5 and 10). These concentrations were then diluted in culture medium in the assay well, to make their final concentrations in a proportion of 5:100. At the day of assay, a caspase substrate (DEVD-Rh110$_2$) was diluted in 2x caspase buffer and 100 µL were added to each well of the assay plate to make up a final volume of 200 µL. The plate was gently mixed and incubated in the dark for 4 hours at 37 ºC / 5 % CO_2. The substrate is converted in a fluorescent product in the presence of caspase3/7, and the result is measured as fluorescence units (excitation 485 nm/emission 528 nm). Fluorescence units are converted in units of caspase 3 (µg/well) utilizing the standard curve. Ideally, higher results of caspase release indicate a higher apoptotic state of the cells and thus less viability.

Cytotoxicity assay

This assay was performed only in 2D cultures of fibroblasts. The cytotoxicity assay is based on the release of LDH from the cells and accounts not only for cell death occurring by apoptosis but also by necrosis. Fibroblasts were seeded at a density of 6000 cells per well. A standard curve of LDH was prepared in ammonium sulphate, in concentrations ranging from 0 to 0.0225 µg/well (0; 0.0004; 0.0007; 0.0014; 0.0028, 0.0056; 0.0113 and 0.0255). These concentrations were then diluted in culture medium in the assay well, to make their final concentrations in a proportion of 4:100. Two LDH assay solutions (A and B) (Table 7) were prepared separately and then mixed and added to each well of the plate. The assay buffer

contains diaphorase and resazurin. LDH released to the culture medium following loss of membrane integrity catalyses the reduction of NAD^+ to NADH and H^+. In a second step, diaphorase utilizes these newly formed components to catalyse the reduction of resazurin to fluorescence resorufin. After 10 min incubation in the dark at 37 ºC / 5 % CO_2, wavelengths were measured in a plate reader (excitation 530 nm/emission 590 nm). The values of fluorescence were converted in units of LDH (µg/well), utilizing the standard curve values. Higher results of LDH release suggest a compromise of the cell membrane and thus indicate less viability of the cells.

DNA quantification assay

This assay was performed only in 2D cultures of fibroblasts. Fibroblasts were seeded at a density of 6000 cells per well. A standard curve of DNA was prepared in TE buffer (Table 7), in concentrations ranging from 0 to 600 ng/100 µL (0; 50; 100; 200; 300; 400; 500 and 600). Culture media was removed from all the wells and replaced with 100 µL of TE buffer. Two µL of lysis solution (Table 7) were added to each well containing cells to lyse the cells for 10 min at room temperature, in order to release DNA from the cells. After this, thiazole orange (DNA stain) was prepared in TE buffer to provide a final concentration of 1 µg/mL and 100 µL of this solution were added per well. After incubation in the dark at 6 ºC for 10 min, wavelengths were measured in a plate reader (excitation 485 nm/emission 528 nm). The values of fluorescence were converted in units of DNA (ng/well), utilizing the standard curve values.

Immunofluorescence

Immunostaining of 2D and 3D cells cultures was performed in the same manner, only differing in the antibody concentrations, indicated in Table 5. Cells or organoids were seeded in 96 well, black walled, clear bottom, tissue well plates. Cells or organoids were washed twice with 100 µL of PBS for 5 min, fixed with 100 µL of 4 % PFA for 30 min at RT in the dark, washed once with PBS for 5 min and permeabilized with a solution of 0.2 % Triton-X100 in PBS for 20 min at RT in the dark. Blocking was performed with a solution of 1 % BSA in PBS at RT in the dark, for 45 min. After washing 3 times with PBS for 5 min, cells or organoids were incubated with primary antibodies over-night at 4 ºC in a solution of 1 % BSA in PBS. The following day, cells or organoids were washed three times with PBS for 5 min at RT and incubated with secondary antibodies at RT in a solution of 1 % BSA in PBS. Finally, cells or organoids were washed twice with PBS at RT for 5 min and processed for DAPI staining. All

images were acquired using Cytation™ 5 Multi-Mode Cell Imaging reader (BioTek Instruments Inc., VT, USA).

FFPE

Organoid embedding

Because organoids are a small structure compared with tissue samples, the generation of paraffin blocks from organoid cultures was performed by utilization of a technique to generate cell clots. This technique, also named thromboplastin-plasma method, is simple to perform and is generally used to prepare clots of cells, when immunohistochemistry is preferred to immunofluorescence [163,164]. Organoids from 4 wells of a 24 well plate were harvested and washed once in PBS, according to previously described methodology. After resuspension of the pellet in 100 µL of standard plasma, 100 µL of thrombin was added to the suspension. A clot was formed after a couple of seconds and the sample was centrifuged at 300 g for 5 min at RT. The clot was transferred to a histology cassette and submerged in a 4 % PFA solution overnight at 4 ºC. The sample was washed 3 times in PBS, dehydrated, and paraffin embedded. Tissue slices with 4 µm thickness were prepared using a microtome and secured in microscope slides.

Haematoxylin and eosin staining

Microscope slides containing organoid sections were baked for 60 min at 60 ºC, washed 3 times for 4 min in xylol, 3 times for 3 min in isopropanol and dipped 3 times in tap water. Slides were then placed 6 min in haematoxylin, dipped 10 times in tap water, 10 times in HCl alcohol and 10 times in tap water. After 2 dips in a 0.25 % eosin solution (Table 7), slides were dipped 10 times in water, 10 times in isopropanol and 10 times in xylol. The slides were then mounted using a xylol-soluble mounting medium and covered with a cover slip.

Immunohistochemical staining

Microscope slides containing organoid sections were baked for 60 min at 60 ºC, washed 3 times for 4 min in xylol, 3 times for 3 min in isopropanol and 3 times for 3 min in distilled water. Slides were then incubated in a AG-retrieval buffer (Table 7) for 40 min at 95 ºC, cooled down to RT, washed 3 times 3 min in distilled water and 3 times 3 min in PBS-T. Samples were blocked using a DAB peroxidase block kit and incubation for 5 min in the dark, incubated with primary antibody for 1 hour at RT in the dark and with the secondary antibody for 1 hour at RT in the dark (Table 5). In between incubation, slides were washed 3 times 3 min with

PBST. Finally, slides were incubated with DAB reagent for 4 min until stained light brown, washed for 5 min in tap water, processed for H&E staining, and mounted as previously described.

Immunofluorescence assay

Microscope slides containing organoid sections were baked for 60 min at 60 ºC, washed 2 times for 4 min in Histo-clear II, 2 times for 3 min in ethanol and once for 3 min in distilled water. Slides were then incubated in a AG-retrieval buffer for 40 min at 95 ºC, cooled down to RT, washed twice for 3 min in distilled water and twice for 3 min in PBS-T. Samples were blocked using a 1 % BSA solution in PBS for 2 hours, incubated with primary antibody for 1 hour at RT in the dark and with the secondary antibody for 1 hour at RT in the dark. Both primary and secondary antibodies were diluted in a 1% BSA in PBST solution, in concentrations indicated in Table 5. In between incubations, slides were washed 3 times 3 min with PBST. Finally, slides were prepared for DAPI staining, as previously described, covered with a cover slip, and immediately imaged.

Table 5: Antibody list used for immunostaining.

		Antibody	**Host**	**Dilution for 2D cultures**	**Dilution for 3D cultures**	**Manufacturer**
Anti α-smooth muscle actin	53-9760-82	Primary	Mouse	n/**a**	1:300	Invitrogen
Anti α-smooth muscle actin	A5228	Primary	Mouse	1:200	n/a	Sigma-Aldrich
Anti E-cadherin	Sc-31020	Primary	Goat	1:100	1:100	Santa Cruz
Anti-CK18	Ab668	Primary	Mouse	1:100	1:100	Abcam
Anti-Ki67	NB500-170AF594	Conjugate	Rabbit	n/a	1:50	Roche
Anti-Mucin2	Sc-7314	Primary	Mouse	n/a	1:50	Santa Cruz
Anti-Villin	Sc-136119	Primary	Mouse	n/a	1:50	Santa Cruz
Anti-Vimentin	V6630	Primary	Mouse	n/a	1:200	Sigma-Aldrich
Anti-Vimentin	V2258	Primary	Mouse	1:200	n/a	Sigma-Aldrich
Anti-Goat	Sc-3923	Secondary	n/a	1:50	1:50	Sigma-Aldrich
Anti-Mouse	F9259	Secondary	Goat	1:100	n/a	Sigma-Aldrich
Anti-Mouse	F0257	Secondary	Goat	1:50	1:50	Sigma-Aldrich

Anti-Porin (VDAC1)	Primary	n/a	1:2000
Anti-Complex I (NDUFS4)	Primary	n/a	1:1000
Anti-Complex II (SDHA)	Primary	n/a	1:2000
Anti-Complex III (UQCRC2)	Primary	n/a	1:1500
Anti-Complex IV (MTCO1)	Primary	n/a	1:1000
Anti-Complex V (ATP5A1)	Primary	n/a	1:2000

Gene expression analysis

RNA extraction

Total RNA was obtained from two wells of a 24 well plate, using the previously described methods for culture passaging. To remove BME2 residues, the recovered pellet was washed once with DPBS and centrifuged at 300 g, 4 ºC for 5 min. The pellet was resuspended in 700 µL QIAzol lysis reagent, vortexed for 5 seconds and incubate at RT for 5 min. The homogenates were supplemented with 140 µL of chloroform, incubated at RT for 2-3 min and centrifuged for 15 min at 12000 g, 4 ºC. The upper aqueous phase was recovered and supplemented with 1.5 x the volume with 100% ethanol. Total RNA was extracted using the RNeasy mini kit, including a genomic DNA digestion step using RNase free DNase set, following manufacturer's instructions. Total RNA was eluted in 50 µL of RNase-free water and quantified with Quant-iT™ RiboGreen™ RNA assay kit, following manufacturer's instructions.

qRT-PCR assay

Total RNA (0.4 µg per sample) was reverse transcribed to cDNA using the High-Capacity cDNA Reverse Transcription kit and following manufacturer's instructions. Each RNA sample was reverse transcribed in triplicate and one control reaction lacking reverse transcriptase was included to test the contamination with gDNA. Quantitative real-time PCR was performed with the QuantiTest SYBR Green PCR kit, utilizing final concentrations of 10 µL of SYBR^{TM} Green Master Mix, 0.3 µM of each primer, 2 µL of cDNA, 20 µL total reaction in RNAse free water. PCR conditions were 15 seconds at 94 ºC, 35-45 cycles of 30 seconds at 50-65 ºC, stopping with 30 seconds at 72 ºC. PCR was detected with the Light Cycler® 480 System and pre-designed primers were obtained from Sigma-Aldrich (Table 6). Data was analysed using the advanced relative quantification of target and control samples. The

expression values of target samples were normalized to the expression levels of the housekeeping gene GAPDH and presented as fold change to control samples.

Table 6: Primer list used for qRT-PCR

Name	Description	Primer ID	Primer sequence
GAPDH	Glyceraldehyde 3-phosphate dehydrogenase (housekeeping gene)	H_GAPDH_1	F:ACCCACTCCTCCACCTTTGA R:CTGTTGCTGTAGCCAAATTCGT
LGR5	Leucine-rich repeat-containing G-protein coupled receptor 5 (stem cell marker)	H_LGR5_1	F:AAATGCCTTATGCTTACCAG R:ATCTTGAGCCTGAAACATTC
MUC2	Mucin 2 (goblet cell marker)	H_LGR5_1	F:GATTCGAAGTGAAGAGCAAG R:CACTTGGAGGAATAAACTGG
MYC	Proliferation marker	H_MYC_2	F:CTAACAGAAATGTCCTGAGC R:TCCAATTTGAGGCAGTTTAC
CA1	Carbonic anhydrase 1 (mature colonocyte marker)	H_CA1_3	F:GAAGATAATGGCAAGTCCAG R:ATAGGTTTCAGAGAGGTGTC
VIL1	Villin 1 (brush border marker)	BTR_VIL1_1	F:AAGATGGTAGATGATGGGAG R:CAAACGTAGAGCAGGTAATG
CA2	Carbonic anhydrase II (CRC marker)	H_CA2_1	F:GGTGTTGAAATTCCGTAAAC R:TTTGGATACAGACTATGGGAC
APCDD1	Adenomatosis Polyposis Coli Down-Regulated 1 Protein (CRC marker)	H_APCDD1_1	F:AAGTGAATCACATGAAGGTC R:TTTGAAGATCTCGTACTCCG
HK2	Hexokinase 2 (metabolic marker)	H_HK2_1	F:CTAAACTAGACGAGAGTTTCC H:CATCATAACCACAGGTCATC
SLC2A1	Solute Carrier Family 2 Member 1 (metabolic marker for glucose transporter 1)	H_SLC2A1_1	F:ACCTCAAATTTCATTGTGGG R:GAAGATGAAGAACAGAACCAG
PKM2	Pyruvate kinase isozymes M2 (metabolic marker)	H_PKM2_1	F:ATGTTGATATGGTGTTTGCG R:ATTTCATCAAACCTCCGAAC
PROX1	Prospero homeobox protein 1 (CRC marker)	H_PROX1_1	F:AGTTCAACAGATGCATTACC R:TCTCTGGTTATAGACAGCTC
BAMBI	BMP and activin membrane-bound inhibitor homolog (CRC marker)	H_BAMBI_1	F:AAGGTGAAATTCGATGCTAC R:TCAAGAAGTCTAGAGAAGCAG
ATP6	Mitochondrially encoded ATP synthase membrane subunit 6 (metabolic marker)	H_ATP6_1	F:AATTACAGGCTTCCGACACAAAC R:TGGAATTAGTGAAATTGGAGTTCC T
CYTB	Mitochondrially Encoded Cytochrome B (metabolic marker)	H_CYTB_1	F:GCCACCTTGACCCGATTCT R:TTCCTAGGGCCGCGATAAT
ND2	Mitochondrially encoded NADH dehydrogenase 2 (metabolic marker)	H_ND2_1	F:CACGATCAACTGAAGCAGCAA R:ACGATGGCCAGGAGGATAATT

Oxygen consumption rate (OCR) by using the Seahorse XF analyser

Mitochondrial function is a metabolic parameter that can be assessed by several methods, including luminescence ATP assays for detection of total energy metabolism, MTT or alamarBlue assays for metabolic activity and Clark type electrodes to measure oxygen consumption. More recently, the development of the Seahorse XF extracellular flux analyser allows users to measure bioenergetic profiles in real-time and in live cells [165]. As mentioned in the introduction, measurement of cellular respiration is an important parameter to assess mitochondrial metabolism, because during oxidative phosphorylation, ATP synthesis and oxygen consumption are associated. By measuring OCR in conjunction with the administration of chemical effectors such as Oligomycin (inhibitor of complex V), Carbonyl cyanide-4-(trifluoromethoxy)phenylhydrazone (FCCP) (mitochondrial oxidative phosphorylation uncoupler), rotenone (inhibitor of complex I) and Antimycin A (inhibitor of complex III), it is possible to partition respiration rates into different modules [158]. This allows the quantification of the different types of cellular respiration (basal, ATP-linked, reserve capacity, proton leak-linked, maximal of non-mitochondrial) and compare the types of respiration between models or in response to treatments/drugs.

OCR was measured by using the Seahorse Mito Stress Test following manufacturer's instructions, with some alterations for 3D cell cultures as follows. Colon tumour organoids either from control plates or cryopreserved plates, were lifted and split as previously mentioned and seeded in seahorse XF96 cell culture microplates at a ratio of 1:3, in 10 µL domes. Tumour organoids were expanded for 5 days before assay. The day before the assay, the sensor cartridge was hydrated using 200 µL of Seahorse XF calibrant and incubated at 37 ºC in a non-CO_2 incubator overnight. Assay medium was prepared fresh on the day of assay (Table 7), sterile filtered and warmed up to 37 ºC. Culture medium was removed from the microplates, replaced with 180 µL assay medium per well and incubated in a non-CO_2 incubator for 1 hour. Stock solutions of Oligomycin, FCCP and Rotenone were prepared according to manufacturer's instructions to achieve final concentrations of 6 µM (Oligomycin), 2 µM (FCCP) and 0.5 µM Rotenone. These components were added to the corresponding ports of the hydrated cartridge, using only assay medium for control wells. After calibration of the loaded cartridge, the sample plate was added to the machine and the protocol was performed following the subsequent steps: Calibrate; equilibrate; loop start 5x; mix 3 min; wait 2 min; measure 3 min; loop end; inject port A oligomycin; loop start 5x; mix 3 min; wait 2 min; measure 3 min; loop end; inject port

B FCCP; loop start 5x; mix 3 min; wait 2 min; measure 3 min; loop end; inject port C Rotenone; loop start 5x; mix 3 min; wait 2 min; measure 3 min; loop end; end.

Statistical analysis

Statistical tests were run as indicated in the individual figure legends using Sigma Plot 11.0 software. Results were considered significant with p value < 0.05. Results are represented as mean ± SD. P values are given as *p ≤ 0.05.

Solutions, buffers, media, components, and other material

All the solutions, buffers and media utilized, are overviewed in Table 7.

Table 7: Recipes of solutions, buffers, and media

AG-retrieval buffer	EDTA (1 mM), Tween-20 (0.05 %), pH 8
Caspase buffer (2x)	Distilled water, HEPES (47.7 g), Sucrose (200 g), CHAPS (2 g), NaCl (11.7 g), EDTA (0.74 g), DTT (3.09 g), IGEPAL (100 µL)
Chelation buffer	DPBS, EDTA (2 mM), DTT (0.5 mM), Penicillin/Streptomycin (100 µg/mL), Primocin (100 µg/mL)
Colon tissue wash solution	DPBS, Sorbitol (54.9 mM), Sucrose (43.3 mM), Penicillin/Streptomycin (100 µg/mL), Primocin (100 µg/mL)
Colon tumour tissue wash solution	EBSS, Penicillin/Streptomycin (100 µg/mL), Primocin (100 µg/mL)
Complete organoid differentiation medium	Advanced DMEM/F12, BSA (0.01 % w/v), Penicillin/Streptomycin (100 µg/mL), L-glutamine (2 mM), N2 supplement (1x), Primocin (100 µg/mL), HEPES (10 mM), hrEGF (50 ng/mL), [Leu15]-gastrin I (10 nM), B27 supplement without vitamin A (1x), DAPT (5 µM), Y-27632 (10 µM)
Cytotoxicity buffer	Potassium phosphate monobasic (0.544 g), Potassium phosphate dibasic (4.355 g), distilled water
DAB reagent	DAB+substrate buffer (1mL), DAB+Chromogen (1 drop)
Diaphorase solution	Diaphorase (100 U), ammonium sulphate solution (1 mL)
Eosin solution (0.25 %)	Eosin (0.25g), dH_2O (30 mL), 95 % ethanol (70 mL)
Fibroblast medium	DMEM high glucose, FBS (10 %), Fungizone (2.5 µg/mL), HEPES (25 mM), Glutamax (2 mM), Penicillin/Streptomycin (100 µg/mL)
Human colon basal medium	Advanced DMEM/F12, Penicillin/Streptomycin (100 µg/mL), Primocin (100 µg/mL), Glutamax (1x), HEPES (10 mM)
Human colon organoid complete medium	50% Wnt3a conditioned medium (90%), R-spo1-conditioned medium (10%), hrNoggin (25 ng/mL), hr EGF (50 ng/mL), A83-01 (500 nM), SB202190 (10 µM), CHIR99021 (5 µM), [Leu15]-gastrin I (10 nM), Nicotinamide (10 mM), N-acetylcysteine (1 mM), Y-27632 (10 µM), Primocin (100 µg/mL), PGE2 (50 nM)
Human colon tumour organoid complete medium	Advanced DMEM/F12, Penicillin/Streptomycin (100 µg/mL), Primocin (100 µg/mL), Glutamax (1x), HEPES (10 mM), hrNoggin (100ng/mL), hrEGF (50 ng/mL), A-83-01 (500 nM), SB202190 (10 µM), [Leu15]-gastrin I (10 nM),

	Nicotinamide (10 mM), N-acetylcysteine (1.25 mM), PGE2 (10 nM), B27 supplement without vitamin A (1x)
Human tumour organoid digestive medium	EBSS, Liberase (0.0924 mg/mL), Y-27623 (10 µM), Penicillin/Streptomycin (100 µg/mL), Primocin (100 µg/mL), DNaseI (0.1 mg/mL)
L-cell conditioning medium	Advanced DMEM/F12, BSA (1%), Penicillin/Streptomycin (100 µg/mL), L-glutamine (2 mM), N2 supplement (1x), B27 supplement without vitamin A (1x), HEPES (10 mM)
L-cell medium	DMEM high glucose, FBS (10%), Penicillin/Streptomycin (100 µg/mL)
L-cell selective complete medium	DMEM high glucose, FBS (10%), Geneticin (0.4 mg/mL)
LDH assay solution A	Sodium lactate (135 mg), β-NAD, sodium salt (19.5 mg), Diaphorase solution (60 µL), Cytotoxicity buffer (5.94 mL)
LDH assay solution B	Resazurin stock (0.6 mL), PBS (5.4 mL)
Live/Dead staining solution	PBS, FDA (8 µg/ml), PI (20 µg/ml)
Metabolic assay medium	DMEM powder with 15mg/mL phenol red, Pyruvate (1mM), Glutamine (2mM), Glucose (10mM), pH 7.4
PBS (10x)	NaCl (80 g), KCl (2 g), Na_2HPO_4 (11.5 g), KH_2PO_4 (2 g), pH 7.6
PBS-T (0.5 %)	PBS (1x 1L), Tween-20 (5 mL)
Resazurin stock	Resazurin (75 mg), PBS (30 mL)
R-spondin basal growth medium	DMEM high glucose, FBS (10%), Penicillin/Streptomycin (100 µg/mL), Glutamax (1x)
R-spondin conditioning medium	Advanced DMEM/F12, Penicillin/Streptomycin (100 µg/mL), HEPES (10 mM), Glutamax (1x)
R-spondin selection growth medium	DMEM high glucose, FBS (10%), Glutamax (1x), Zeocin (300 µg/mL)
Seahorse assay medium	DMEM, 1 mM pyruvate, 2 mM glutamine, 10 mM glucose, pH 7.4
TE buffer	Tris 1 M (5 mL), EDTA (0.186 g), distilled water (1 L)
Tris (1 M)	Tris (1.2114 g), distilled water (10 mL)

Chemicals, components, antibodies, and kits utilized are described in Table 8.

Table 8: List of chemicals, components, antibodies, and kits.

Component/Kit/Equipment	**Manufacturer**
[Leu^{15}]-gastrin I	Sigma-Aldrich, Irvine, UK
A-83-01	Sigma-Aldrich, Irvine, UK
Advanced DMEM/F12	ThermoFisher Scientific, MA, USA
B27 supplement, without vitamin A	ThermoFisher Scientific, MA, USA
BME2	Amsbio, Abington, UK
BSA	Sigma-Aldrich, Irvine, UK
CellTiter-Glo® 3D cell viability Assay	Promega, WI, USA
CHAPS	Sigma-Aldrich, Irvine, UK
CHIR99021	Sigma-Aldrich, Irvine, UK
Chloroform	Sigma-Aldrich, Irvine, UK
Cryostor ®	Sigma-Aldrich, Irvine, UK

Cytation™ 5 Multi-Mode Cell Imaging reader	BioTek Instruments Inc., VT, USA
DAPT	Merck Millipore, MA, USA
DEVD-Rh1102	AnaSpec, Freemont, CA, USA
Diaphorase	Sigma-Aldrich, Irvine, UK
DNaseI	Sigma-Aldrich, Irvine, UK
Doxorubicin	Sigma-Aldrich, Irvine, UK
DPBS	ThermoFisher Scientific, MA, USA
DTT	Sigma-Aldrich, Irvine, UK
EBSS	ThermoFisher Scientific, MA, USA
EDTA	Sigma-Aldrich, Irvine, UK
EdU HTS Kit 488	Base Click, Munich, Germany
EF600 controlled rate freezer	Asymptote Ltd, Cambridge, UK
FBS	Thermo Fisher Scientific, MA, USA
FDA	Sigma-Aldrich, Irvine, UK
Fluoroshield™	Sigma-Aldrich, Irvine, UK
Fungizone	Sigma-Aldrich, Irvine, UK
Geneticin	Thermo Fisher Scientific, MA, USA
Glutamax	ThermoFisher Scientific, MA, USA
Haematoxylin	Sigma-Aldrich, Irvine, UK
HBSS	Thermo Fisher Scientific, MA, USA
HEPES	Sigma-Aldrich, Irvine, UK
High-Capacity cDNA Reverse Transcription kit	Applied Biosystems, CA, USA
Histo-Clear II	National Diagnostics, Nottingham, UK
hrEGF	Peprotech, London, UK
hrNoggin	Peprotech, London, UK
IGEPAL	Sigma-Aldrich, Irvine, UK
Intesticult™ organoid growth medium (human)	STEMCELL Technologies, Vancouver, Canada
L-glutamine	Sigma-Aldrich, Irvine, UK
Liberase	Sigma-Aldrich, Irvine, UK
Light Cycler® 480 System	Roche, Basel, Switzerland
N2 supplement	Thermo Fisher Scientific, MA, USA
N-acetylcysteine	LKT Labs, MN, USA
NaCl	Sigma-Aldrich, Irvine, UK
Nicotinamide	Sigma-Aldrich, Irvine, UK
PBS	ThermoFisher Scientific, MA, USA
Penicillin/Streptomycin	Sigma-Aldrich, Irvine, UK
PGE	Sigma-Aldrich, Irvine, UK
PI	Sigma-Aldrich, Irvine, UK
Potassium phosphate dibasic	Sigma-Aldrich, Irvine, UK
Potassium phosphate monobasic	Sigma-Aldrich, Irvine, UK
PowerUpTM SYBRTM Green Master Mix	Thermo Fisher Scientific, MA, USA
Primocin	Invivogen, SD, USA
QIAzol lysis reagent	Qiagen, Manchester, UK

QuantiTest SYBR Green PCR kit	Qiagen, Manchester, UK
Quant-iT™ RiboGreen™ RNA assay kit	Invitrogen, MA, USA
Resazurin	Sigma-Aldrich, Irvine, UK
RNase free DNase set	Qiagen, Manchester, UK
RNeasy mini kit	Qiagen, Manchester, UK
SB202190	Sigma-Aldrich, Irvine, UK
Seahorse sensor cartridge and hydration plates	Agilent, SC, USA
Seahorse XF calibrant	Agilent, SC, USA
Seahorse XF96 analyser	Agilent, SC, USA
Seahorse XF96 Cell Culture Microplates	Agilent, SC, USA
Sodium Butyrate	Sigma-Aldrich, Irvine, UK
Sodium lactate	Sigma-Aldrich, Irvine, UK
Sorbitol	Sigma-Aldrich, Irvine, UK
Standard plasma	
Staurosporine	Sigma-Aldrich, Irvine, UK
Sucrose	Sigma-Aldrich, Irvine, UK
Synergy ™ H4 Hybrid Multi-Mode Microplate reader	BioTek, Instruments Inc., VT, USA
Thrombin	
Triton X-100	Sigma-Aldrich, Irvine, UK
TrypLE™ Express	Thermo Fisher Scientific, MA, USA
Trypsin-EDTA	Sigma-Aldrich, Irvine, UK
Ultra-low temperature (ULT) freezer model MDF-C2156VAN-PE	Panasonic, Kadoma, Japan
Y-27632	Cambridge Bioscience, Cambridge, UK
Zeocin	Thermo Fisher Scientific, MA, USA
β-NAD	Sigma-Aldrich, Irvine, UK

References

(1) Kapałczyńska, M.; Kolenda, T.; Przybyła, W.; Zajączkowska, M.; Teresiak, A.; Filas, V.; Ibbs, M.; Bliźniak, R.; Łuczewski, Ł.; Lamperska, K. 2D and 3D Cell Cultures – a Comparison of Different Types of Cancer Cell Cultures. *Arch. Med. Sci.* **2018**, *14* (4), 910–919. https://doi.org/10.5114/aoms.2016.63743.

(2) Duval, K.; Grover, H.; Han, L. H.; Mou, Y.; Pegoraro, A. F.; Fredberg, J.; Chen, Z. Modeling Physiological Events in 2D vs. 3D Cell Culture. *Physiology*. American Physiological Society June 14, 2017, pp 266–277. https://doi.org/10.1152/physiol.00036.2016.

(3) Rodrigues, T.; Kundu, B.; Silva-Correia, J.; Kundu, S. C.; Oliveira, J. M.; Reis, R. L.; Correlo, V. M. Emerging Tumour Spheroids Technologies for 3D in Vitro Cancer Modeling. *Pharmacology and Therapeutics*. Elsevier Inc. April 1, 2018, pp 201–211. https://doi.org/10.1016/j.pharmthera.2017.10.018.

(4) Sachs, N.; Clevers, H. Organoid Cultures for the Analysis of Cancer Phenotypes. *Current Opinion in Genetics and Development*. February 2014, pp 68–73. https://doi.org/10.1016/j.gde.2013.11.012.

(5) Medema, J. P.; Vermeulen, L. Microenvironmental Regulation of Stem Cells in Intestinal Homeostasis and Cancer. *Nature* **2011**, *474* (7351), 318–326. https://doi.org/10.1038/nature10212.

(6) Heath, J. P. Epithelial Cell Migration in the Intestine. *Cell Biol. Int.* **1996**, *20* (2), 139–146. https://doi.org/10.1006/cbir.1996.0018.

(7) Barker, N.; van Es, J. H.; Kuipers, J.; Kujala, P.; van den Born, M.; Cozijnsen, M.; Haegebarth, A.; Korving, J.; Begthel, H.; Peters, P. J.; et al. Identification of Stem Cells in Small Intestine and Colon by Marker Gene Lgr5. *Nature* **2007**, *449* (7165), 1003–1007. https://doi.org/10.1038/nature06196.

(8) Reya, T.; Clevers, H. Wnt Signalling in Stem Cells and Cancer. *Nature*. Nature April 14, 2005, pp 843–850. https://doi.org/10.1038/nature03319.

(9) Kim, K. A.; Kakitani, M.; Zhao, J.; Oshima, T.; Tang, T.; Binnerts, M.; Liu, Y.; Boyle, B.; Park, E.; Emtage, P.; et al. Mitogenic Influence of Human R-Spondin1 on the Intestinal Epithelium. *Science (80-.).* **2005**, *309* (5738), 1256–1259. https://doi.org/10.1126/science.1112521.

(10) Fre, S.; Huyghe, M.; Mourikis, P.; Robine, S.; Louvard, D.; Artavanis-Tsakonas, S. Notch Signals Control the Fate of Immature Progenitor Cells in the Intestine. *Nature* **2005**, *435* (7044), 964–968. https://doi.org/10.1038/nature03589.

(11) Van Es, J. H.; Van Gijn, M. E.; Riccio, O.; Van Den Born, M.; Vooijs, M.; Begthel, H.; Cozijnsen, M.; Robine, S.; Winton, D. J.; Radtke, F.; et al. Notch/γ-Secretase Inhibition Turns Proliferative Cells in Intestinal Crypts and Adenomas into Goblet Cells. *Nature* **2005**, *435* (7044), 959–963. https://doi.org/10.1038/nature03659.

(12) van Es, J. H.; de Geest, N.; van de Born, M.; Clevers, H.; Hassan, B. A. Intestinal Stem Cells Lacking the Math1 Tumour Suppressor Are Refractory to Notch Inhibitors. *Nat. Commun.* **2010**, *1* (1), 18. https://doi.org/10.1038/ncomms1017.

(13) Auclair, B. A.; Benoit, Y. D.; Rivard, N.; Mishina, Y.; Perreault, N. Bone Morphogenetic Protein Signaling Is Essential for Terminal Differentiation of the Intestinal Secretory Cell Lineage. *Gastroenterology* **2007**, *133* (3), 887–896. https://doi.org/10.1053/j.gastro.2007.06.066.

(14) van Dop, W. A.; Uhmann, A.; Wijgerde, M.; Sleddens-Linkels, E.; Heijmans, J.; Offerhaus, G. J.; van den Bergh Weerman, M. A.; Boeckxstaens, G. E.; Hommes, D. W.; Hardwick, J. C.; et al. Depletion of the Colonic Epithelial Precursor Cell Compartment Upon Conditional Activation of the Hedgehog Pathway. *Gastroenterology* **2009**, *136*

(7), 2195-2203.e7. https://doi.org/10.1053/j.gastro.2009.02.068.

(15) Cunningham, D.; Atkin, W.; Lenz, H. J.; Lynch, H. T.; Minsky, B.; Nordlinger, B.; Starling, N. Colorectal Cancer. *The Lancet*. Lancet 2010, pp 1030–1047. https://doi.org/10.1016/S0140-6736(10)60353-4.

(16) Tenesa, A.; Farrington, S. M.; Prendergast, J. G. D.; Porteous, M. E.; Walker, M.; Haq, N.; Barnetson, R. A.; Theodoratou, E.; Cetnarskyj, R.; Cartwright, N.; et al. Genome-Wide Association Scan Identifies a Colorectal Cancer Susceptibility Locus on 11q23 and Replicates Risk Loci at 8q24 and 18q21. *Nat. Genet.* **2008**, *40* (5), 631–637. https://doi.org/10.1038/ng.133.

(17) Tomlinson, I. P. M.; Webb, E.; Carvajal-Carmona, L.; Broderick, P.; Howarth, K.; Pittman, A. M.; Spain, S.; Lubbe, S.; Walther, A.; Sullivan, K.; et al. A Genome-Wide Association Study Identifies Colorectal Cancer Susceptibility Loci on Chromosomes 10p14 and 8q23.3. *Nat. Genet.* **2008**, *40* (5), 623–630. https://doi.org/10.1038/ng.111.

(18) Fearon, E. R.; Vogelstein, B. A Genetic Model for Colorectal Tumourigenesis. *Cell*. June 1, 1990, pp 759–767. https://doi.org/10.1016/0092-8674(90)90186-I.

(19) Clevers, H. Wnt/β-Catenin Signaling in Development and Disease. *Cell*. Cell November 3, 2006, pp 469–480. https://doi.org/10.1016/j.cell.2006.10.018.

(20) Melo, F. D. S. E.; Vermeulen, L.; Richel, D.; Medema, J. P. Targeting Wnt Signaling in Colon Cancer Stem Cells. *Clinical Cancer Research*. Clin Cancer Res February 15, 2011, pp 647–653. https://doi.org/10.1158/1078-0432.CCR-10-1204.

(21) Tetsu, O.; McCormick, F. β-Catenin Regulates Expression of Cyclin D1 in Colon Carcinoma Cells. *Nature* **1999**, *398* (6726), 422–426. https://doi.org/10.1038/18884.

(22) He, T. C.; Sparks, A. B.; Rago, C.; Hermeking, H.; Zawel, L.; Da Costa, L. T.; Morin, P. J.; Vogelstein, B.; Kinzler, K. W. Identification of C-MYC as a Target of the APC Pathway. *Science (80-.).* **1998**, *281* (5382), 1509–1512. https://doi.org/10.1126/science.281.5382.1509.

(23) Van de Wetering, M.; Sancho, E.; Verweij, C.; De Lau, W.; Oving, I.; Hurlstone, A.; Van der Horn, K.; Batlle, E.; Coudreuse, D.; Haramis, A. P.; et al. The β-Catenin/TCF-4 Complex Imposes a Crypt Progenitor Phenotype on Colorectal Cancer Cells. *Cell* **2002**, *111* (2), 241–250. https://doi.org/10.1016/S0092-8674(02)01014-0.

(24) Markowitz, S. D.; Bertagnolli, M. M. Molecular Origins of Cancer: Molecular Basis of Colorectal Cancer. *N. Engl. J. Med.* **2009**, *361* (25), 2449–2460. https://doi.org/10.1056/NEJMra0804588.

(25) Fujii, M.; Shimokawa, M.; Date, S.; Takano, A.; Matano, M.; Nanki, K.; Ohta, Y.; Toshimitsu, K.; Nakazato, Y.; Kawasaki, K.; et al. A Colorectal Tumour Organoid Library Demonstrates Progressive Loss of Niche Factor Requirements during Tumourigenesis. *Cell Stem Cell* **2016**, *18* (6), 827–838. https://doi.org/10.1016/j.stem.2016.04.003.

(26) Sangiorgi, E.; Capecchi, M. R. Bmi1 Is Expressed in Vivo in Intestinal Stem Cells. *Nat. Genet.* **2008**, *40* (7), 915–920. https://doi.org/10.1038/ng.165.

(27) Zhu, L.; Gibson, P.; Currle, D. S.; Tong, Y.; Richardson, R. J.; Bayazitov, I. T.; Poppleton, H.; Zakharenko, S.; Ellison, D. W.; Gilbertson, R. J. Prominin 1 Marks Intestinal Stem Cells That Are Susceptible to Neoplastic Transformation. *Nature* **2009**, *457* (7229), 603–607. https://doi.org/10.1038/nature07589.

(28) Barker, N.; Ridgway, R. A.; Van Es, J. H.; Van De Wetering, M.; Begthel, H.; Van Den Born, M.; Danenberg, E.; Clarke, A. R.; Sansom, O. J.; Clevers, H. Crypt Stem Cells as the Cells-of-Origin of Intestinal Cancer. *Nature* **2009**, *457* (7229), 608–611. https://doi.org/10.1038/nature07602.

(29) Wood, L. D.; Parsons, D. W.; Jones, S.; Lin, J.; Sjöblom, T.; Leary, R. J.; Shen, D.; Boca, S. M.; Barber, T.; Ptak, J.; et al. The Genomic Landscapes of Human Breast and Colorectal Cancers. *Science (80-.).* **2007**, *318* (5853), 1108–1113. https://doi.org/10.1126/science.1145720.

(30) Vermeulen, L.; Sprick, M. R.; Kemper, K.; Stassi, G.; Medema, J. P. Cancer Stem Cells - Old Concepts, New Insights. *Cell Death and Differentiation*. Nature Publishing Group June 15, 2008, pp 947–958. https://doi.org/10.1038/cdd.2008.20.

(31) Vermeulen, L.; Todaro, M.; De Sousa Mello, F.; Sprick, M. R.; Kemper, K.; Perez Alea, M.; Richel, D. J.; Stassi, G.; Medema, J. P. Single-Cell Cloning of Colon Cancer Stem Cells Reveals a Multi-Lineage Differentiation Capacity. *Proc. Natl. Acad. Sci. U. S. A.* **2008**, *105* (36), 13427–13432. https://doi.org/10.1073/pnas.0805706105.

(32) Todaro, M.; Alea, M. P.; Di Stefano, A. B.; Cammareri, P.; Vermeulen, L.; Iovino, F.; Tripodo, C.; Russo, A.; Gulotta, G.; Medema, J. P.; et al. Colon Cancer Stem Cells Dictate Tumour Growth and Resist Cell Death by Production of Interleukin-4. *Cell Stem Cell* **2007**, *1* (4), 389–402. https://doi.org/10.1016/j.stem.2007.08.001.

(33) Todaro, M.; Francipane, M. G.; Medema, J. P.; Stassi, G. Colon Cancer Stem Cells: Promise of Targeted Therapy. *Gastroenterology* **2010**, *138* (6), 2151–2162. https://doi.org/10.1053/j.gastro.2009.12.063.

(34) Tanaka, T.; Kohno, H.; Suzuki, R.; Hata, K.; Sugie, S.; Niho, N.; Sakano, K.; Takahashi, M.; Wakabayashi, K. Dextran Sodium Sulfate Strongly Promotes Colorectal Carcinogenesis in ApcMin/+ Mice: Inflammatory Stimuli by Dextran Sodium Sulfate Results in Development of Multiple Colonic Neoplasms. *Int. J. Cancer* **2006**, *118* (1), 25–34. https://doi.org/10.1002/ijc.21282.

(35) Gould, K. A.; Luongo, C.; Moser, A. R.; McNeley, M. K.; Borenstein, N.; Shedlovsky, A.; Dove, W. F.; Hong, K.; Dietrich, W. F.; Lander, E. S. Genetic Evaluation of Candidate Genes for the Mom1 Modifier of Intestinal Neoplasia in Mice. *Genetics* **1996**, *144* (4).

(36) Takaku, K.; Sonoshita, M.; Sasaki, N.; Uozumi, N.; Doi, Y.; Shimizu, T.; Taketo, M. M. Suppression of Intestinal Polyposis in Apc(Δ716) Knockout Mice by an Additional Mutation in the Cytosolic Phospholipase A2 Gene. *J. Biol. Chem.* **2000**, *275* (44), 34013–34016. https://doi.org/10.1074/jbc.C000586200.

(37) Takaku, K.; Oshima, M.; Miyoshi, H.; Matsui, M.; Seldin, M. F.; Taketo, M. M. Intestinal Tumourigenesis in Compound Mutant Mice of Both Dpc4 (Smad4) and Apc Genes. *Cell* **1998**, *92* (5), 645–656. https://doi.org/10.1016/S0092-8674(00)81132-0.

(38) Kim, B. G.; Li, C.; Qiao, W.; Mamura, M.; Kasperczak, B.; Anver, M.; Wolfraim, L.; Hong, S.; Mushinski, E.; Potter, M.; et al. Smad4 Signalling in T Cells Is Required for Suppression of Gastrointestinal Cancer. *Nature* **2006**, *441* (7096), 1015–1019. https://doi.org/10.1038/nature04846.

(39) Haramis, A. P. G.; Begthel, H.; Van Den Born, M.; Van Es, J.; Jonkheer, S.; Offerhaus, G. J. A.; Clevers, H. De Novo Crypt Formation and Juvenile Polyposis on BMP Inhibition in Mouse Intestine. *Science (80-.).* **2004**, *303* (5664), 1684–1686. https://doi.org/10.1126/science.1093587.

(40) Itzkowitz, S. H.; Yio, X. Inflammation and Cancer IV. Colorectal Cancer in Inflammatory Bowel Disease: The Role of Inflammation. *Am. J. Physiol. Liver Physiol.* **2004**, *287* (1), G7–G17. https://doi.org/10.1152/ajpgi.00079.2004.

(41) Chan, A. T.; Ogino, S.; Fuchs, C. S. Aspirin Use and Survival after Diagnosis of Colorectal Cancer. *JAMA - J. Am. Med. Assoc.* **2009**, *302* (6), 649–658. https://doi.org/10.1001/jama.2009.1112.

(42) Hanahan, D.; Weinberg, R. A. Hallmarks of Cancer: The Next Generation. *Cell* **2011**, *144*.

(43) Hanahan, D.; Weinberg, R. A. The Hallmarks of Cancer. *Cell* **2000**, *100* (1), 57–70.

https://doi.org/10.1007/BF03091804.

(44) Warburg, O.; Wind, F.; Negelein, E. The Metabolism of Tumours in The Body. *J. Gen. Physiol.* **1927**, *8* (6), 519–530.

(45) Hsu, P. P.; Sabatini, D. M. Cancer Cell Metabolism: Warburg and Beyond. *Cell* **2008**, *134* (5), 703–707. https://doi.org/10.1016/j.cell.2008.08.021.

(46) Nolop, K.; Rodhes, C.; LH, B. Why Do Cancers Have High Aerobic Glycolysis? *Nat. Rev. Cancer* **2004**, *4* (11), 891–899. https://doi.org/10.1038/nrc1478.

(47) Gottschalk, S.; Anderson, N.; Hainz, C.; Eckhardt, S. G.; Serkova, N. J. Imatinib (STI571)-Mediated Changes in Glucose Metabolism in Human Leukemia BCR-ABL-Positive Cells. *Clin. Cancer Res.* **2004**, *10* (19), 6661–6668. https://doi.org/10.1158/1078-0432.CCR-04-0039.

(48) Elstrom, R. L.; Bauer, D. E.; Buzzai, M.; Karnauskas, R.; Harris, M. H.; Plas, D. R.; Zhuang, H.; Cinalli, R. M.; Alavi, A.; Rudin, C. M.; et al. Akt Stimulates Aerobic Glycolysis in Cancer Cells. *Cancer Res.* **2004**, *64* (11), 3892–3899. https://doi.org/10.1158/0008-5472.CAN-03-2904.

(49) Nolop, K.; Rodhes, C.; Brudin, L. Glucose Utilization in Vivo by Human Pulmonary Neoplasms. *Lung Cancer* **1989**, *5*, 21. https://doi.org/10.1016/0169-5002(89)90373-5.

(50) Christofk, H. R.; Vander Heiden, M. G.; Harris, M. H.; Ramanathan, A.; Gerszten, R. E.; Wei, R.; Fleming, M. D.; Schreiber, S. L.; Cantley, L. C. The M2 Splice Isoform of Pyruvate Kinase Is Important for Cancer Metabolism and Tumour Growth. *Nature* **2008**, *452* (7184), 230–233. https://doi.org/10.1038/nature06734.

(51) Dang, C. V; Semenza, G. L. Oncogenic Alterations of Metabolism. *Trends Biochem. Sci.* **1999**, *24* (2), 68–72.

(52) Ramanathan, A.; Wang, C.; Schreiber, S. L. Perturbational Profiling of a Cell-Line Model of Tumourigenesis by Using Metabolic Measurements. *Proc. Natl. Acad. Sci. U. S. A.* **2005**, *102* (17), 5992–5997. https://doi.org/10.1073/pnas.0502267102.

(53) Manning, B. D.; Cantley, L. C. AKT/PKB Signaling: Navigating Downstream. *Cell* **2007**, *129* (7), 1261–1274. https://doi.org/10.1016/j.cell.2007.06.009.

(54) Gordan, J. D.; Thompson, C. B.; Simon, M. C. HIF and C-Myc: Sibling Rivals for Control of Cancer Cell Metabolism and Proliferation. *Cancer Cell* **2007**, *12* (2), 108–113. https://doi.org/10.1016/j.ccr.2007.07.006.

(55) Matoba, S.; Kang, J.-G.; Patino, W. D.; Wragg, A.; Boehm, M.; Gavrilova, O.; Hurley, P. J.; Bunz, F.; Hwang, P. M. P53 Regulates Mitochondrial Respiration. *Science* **2006**, *312* (5780), 1650–1653. https://doi.org/10.1126/science.1126863.

(56) Jones, R. G.; Thompson, C. B. Tumour Suppressors and Cell Metabolism: A Recipe for Cancer Growth. *Genes Dev.* **2009**, *23* (5), 537–548. https://doi.org/10.1101/gad.1756509.

(57) Jiménez, B.; Mirnezami, R.; Kinross, J.; Cloarec, O.; Keun, H. C.; Holmes, E.; Goldin, R. D.; Ziprin, P.; Darzi, A.; Nicholson, J. K. 1H HR-MAS NMR Spectroscopy of Tumour-Induced Local Metabolic "Field-Effects" Enables Colorectal Cancer Staging and Prognostication. *J. Proteome Res.* **2013**, *12* (2), 959–968. https://doi.org/10.1021/pr3010106.

(58) Chan, E. C. Y.; Koh, P. K.; Mal, M.; Cheah, P. Y.; Eu, K. W.; Backshall, A.; Cavill, R.; Nicholson, J. K.; Keun, H. C. Metabolic Profiling of Human Colorectal Cancer Using High-Resolution Magic Angle Spinning Nuclear Magnetic Resonance (HR-MAS NMR) Spectroscopy and Gas Chromatography Mass Spectrometry (GC/MS). *J. Proteome Res.* **2009**, *8* (1), 352–361. https://doi.org/10.1021/pr8006232.

(59) Haber, R. S.; Rathan, A.; Weiser, K. R.; Pritsker, A.; Itzkowitz, S. H.; Bodian, C.; Slater, G.; Weiss, A.; Burstein, D. E. GLUT1 Glucose Transporter Expression in Colorectal Carcinoma: A Marker for Poor Prognosis. *Cancer* **1998**, *83* (1), 34–40. https://doi.org/10.1002/(SICI)1097-0142(19980701)83:1<34::AID-CNCR5>3.0.CO;2-E.

(60) Abdullah, M.; Rani, A. A.; Simadibrata, M.; Fauzi, A.; Syam, A. F. The Value of Fecal Tumour M2 Pyruvate Kinase as a Diagnostic Tool for Colorectal Cancer Screening. *Acta Med. Indones.* **2012**, *44* (2), 94–99.

(61) Altenberg, B.; Greulich, K. O. Genes of Glycolysis Are Ubiquitously Overexpressed in 24 Cancer Classes. *Genomics* **2004**, *84* (6), 1014–1020. https://doi.org/10.1016/j.ygeno.2004.08.010.

(62) Koukourakis, M. I.; Giatromanolaki, A.; Simopoulos, C.; Polychronidis, A.; Sivridis, E. Lactate Dehydrogenase 5 (LDH5) Relates to up-Regulated Hypoxia Inducible Factor Pathway and Metastasis in Colorectal Cancer. *Clin. Exp. Metastasis* **2005**, *22* (1), 25–30. https://doi.org/10.1007/s10585-005-2343-7.

(63) Izuishi, K.; Yamamoto, Y.; Sano, T.; Takebayashi, R.; Nishiyama, Y.; Mori, H.; Masaki, T.; Morishita, A.; Suzuki, Y. Molecular Mechanism Underlying the Detection of Colorectal Cancer by 18F-2-Fluoro-2-Deoxy-D-Glucose Positron Emission Tomography. *J. Gastrointest. Surg.* **2012**, *16* (2), 394–400. https://doi.org/10.1007/s11605-011-1727-z.

(64) Chekulayev, V.; Mado, K.; Shevchuk, I.; Koit, A.; Kaldma, A.; Klepinin, A.; Timohhina, N.; Tepp, K.; Kandashvili, M.; Ounpuu, L.; et al. Metabolic Remodeling in Human Colorectal Cancer and Surrounding Tissues: Alterations in Regulation of Mitochondrial Respiration and Metabolic Fluxes. *Biochem. Biophys. Reports* **2015**, *4*, 111–125. https://doi.org/10.1016/j.bbrep.2015.08.020.

(65) Kaldma, A.; Klepinin, A.; Chekulayev, V.; Mado, K.; Shevchuk, I.; Timohhina, N.; Tepp, K.; Kandashvili, M.; Varikmaa, M.; Koit, A.; et al. An in Situ Study of Bioenergetic Properties of Human Colorectal Cancer: The Regulation of Mitochondrial Respiration and Distribution of Flux Control among the Components of ATP Synthasome. *Int. J. Biochem. Cell Biol.* **2014**, *55*, 171–186. https://doi.org/10.1016/j.biocel.2014.09.004.

(66) Pavlides, S.; Whitaker-menezes, D.; Castello-cros, R.; Witkiewicz, A. K.; Frank, P. G.; Casimiro, M. C.; Wang, C.; Fortina, P.; Addya, S.; Pestell, R. G.; et al. The Reverse Warburg Effect : Aerobic Glycolysis in Cancer Associated Fibroblasts and the Tumour Stroma. *Cell Cycle* **2009**, *8* (23). https://doi.org/10.4161/cc.8.23.10238.

(67) Vincent, A. S.; Phan, T. T.; Mukhopadhyay, A.; Lim, H. Y.; Halliwell, B.; Wong, K. P. Human Skin Keloid Fibroblasts Display Bioenergetics of Cancer Cells. *J. Invest. Dermatol.* **2008**, *128* (3), 702–709. https://doi.org/10.1038/sj.jid.5701107.

(68) Whitaker-Menezes, D.; Martinez-Outschoorn, U. E.; Lin, Z.; Ertel, A.; Flomenberg, N.; Witkiewicz, A. K.; Birbe, R.; Howell, A.; Pavlides, S.; Gandara, R.; et al. Evidence for a Stromal-Epithelial "Lactate Shuttle" in Human Tumours. *Cell Cycle* **2011**, *10* (11), 1772–1783. https://doi.org/10.4161/cc.10.11.15659.

(69) Martinez-Outschoorn, U. E.; Lin, Z.; Trimmer, C.; Flomenberg, N.; Wang, C.; Pavlides, S.; Pestell, R. G.; Howell, A.; Sotgia, F.; Lisanti, M. P. Cancer Cells Metabolically "Fertilize" the Tumour Microenvironment with Hydrogen Peroxide, Driving the Warburg Effect. *Cell Cycle* **2011**, *10* (15), 2504–2520. https://doi.org/10.4161/cc.10.15.16585.

(70) Curry, J. M.; Tuluc, M.; Whitaker-Menezes, D.; Ames, J. A.; Anantharaman, A.; Butera, A.; Leiby, B.; Cognetti, D.; Sotgia, F.; Lisanti, M. P.; et al. Cancer Metabolism, Stemness and Tumour Recurrence. *Cell Cycle* **2013**, *12* (9), 1371–1384. https://doi.org/10.4161/cc.24092.

(71) Sotgia, F.; Martinez-Outschoorn, U. E.; Lisanti, M. P. The Reverse Warburg Effect in Osteosarcoma. *Oncotarget* **2014**, *5* (18), 7982–7983. https://doi.org/10.18632/oncotarget.2352.

(72) Nieman, K. M.; Kenny, H. A.; Penicka, C. V; Ladanyi, A.; Buell-Gutbrod, R.; Zillhardt, M. R.; Romero, I. L.; Carey,

M. S.; Mills, G. B.; Hotamisligil, G. S.; et al. Adipocytes Promote Ovarian Cancer Metastasis and Provide Energy for Rapid Tumour Growth. *Nat. Med.* **2011**, *17* (11), 1498–1503. https://doi.org/10.1038/nm.2492.

(73) Barretina, J.; Caponigro, G.; Stransky, N.; Venkatesan, K.; Margolin, A. A.; Kim, S.; Wilson, C. J.; Lehár, J.; Kryukov, G. V.; Sonkin, D.; et al. The Cancer Cell Line Encyclopedia Enables Predictive Modelling of Anticancer Drug Sensitivity. *Nature* **2012**, *483* (7391), 603–607. https://doi.org/10.1038/nature11003.

(74) Garnett, M. J.; Edelman, E. J.; Heidorn, S. J.; Greenman, C. D.; Dastur, A.; Lau, K. W.; Greninger, P.; Thompson, I. R.; Luo, X.; Soares, J.; et al. Systematic Identification of Genomic Markers of Drug Sensitivity in Cancer Cells. *Nature* **2012**, *483* (7391), 570–575. https://doi.org/10.1038/nature11005.

(75) Yada, E.; Wada, S.; Yoshida, S.; Sasada, T. Use of Patient-Derived Xenograft Mouse Models in Cancer Research and Treatment. *Futur. Sci. OA* **2018**, *4* (3). https://doi.org/10.4155/FSOA-2017-0136.

(76) Centenera, M. M.; Raj, G. V.; Knudsen, K. E.; Tilley, W. D.; Butler, L. M. Ex Vivo Culture of Human Prostate Tissue and Drug Development. *Nature Reviews Urology*. Nat Rev Urol August 2013, pp 483–487. https://doi.org/10.1038/nrurol.2013.126.

(77) Tentler, J. J.; Tan, A. C.; Weekes, C. D.; Jimeno, A.; Leong, S.; Pitts, T. M.; Arcaroli, J. J.; Messersmith, W. A.; Eckhardt, S. G. Patient-Derived Tumour Xenografts as Models for Oncology Drug Development. *Nature Reviews Clinical Oncology*. NIH Public Access June 2012, pp 338–350. https://doi.org/10.1038/nrclinonc.2012.61.

(78) Griffith, L. G.; Swartz, M. A. Capturing Complex 3D Tissue Physiology in Vitro. *Nat. Rev. Mol. Cell Biol.* **2006**, *7* (3), 211–224. https://doi.org/10.1038/nrm1858.

(79) Astashkina, A.; Grainger, D. W. Critical Analysis of 3-D Organoid in Vitro Cell Culture Models for High-Throughput Drug Candidate Toxicity Assessments. *Adv. Drug Deliv. Rev.* **2014**, *69–70*, 1–18. https://doi.org/10.1016/j.addr.2014.02.008.

(80) Simian, M.; Bissell, M. J. Organoids: A Historical Perspective of Thinking in Three Dimensions. *J. Cell Biol.* **2017**, *216* (1), 31–40. https://doi.org/10.1083/jcb.201610056.

(81) Fatehullah, A.; Tan, S. H.; Barker, N. Organoids as an in Vitro Model of Human Development and Disease. *Nature Cell Biology*. Nature Publishing Group February 25, 2016, pp 246–254. https://doi.org/10.1038/ncb3312.

(82) Drost, J.; Clevers, H. Organoids in Cancer Research. *Nat. Rev. Cancer* **2018**, *18* (7), 407–418. https://doi.org/10.1038/s41568-018-0007-6.

(83) Silva-Almeida, C.; Ewart, M. A.; Wilde, C. 3D Gastrointestinal Models and Organoids to Study Metabolism in Human Colon Cancer. *Seminars in Cell and Developmental Biology*. Elsevier Ltd February 1, 2020, pp 98–104. https://doi.org/10.1016/j.semcdb.2019.05.019.

(84) Tuveson, D.; Clevers, H. Cancer Modeling Meets Human Organoid Technology. *Science*. American Association for the Advancement of Science June 7, 2019, pp 952–955. https://doi.org/10.1126/science.aaw6985.

(85) Pauli, C.; Hopkins, B. D.; Prandi, D.; Shaw, R.; Fedrizzi, T.; Sboner, A.; Sailer, V.; Augello, M.; Puca, L.; Rosati, R.; et al. Personalized in Vitro and in Vivo Cancer Models to Guide Precision Medicine. *Cancer Discov.* **2017**, *7* (5), 462–477. https://doi.org/10.1158/2159-8290.CD-16-1154.

(86) Van De Wetering, M.; Francies, H. E.; Francis, J. M.; Bounova, G.; Iorio, F.; Pronk, A.; Van Houdt, W.; Van Gorp, J.; Taylor-Weiner, A.; Kester, L.; et al. Prospective Derivation of a Living Organoid Biobank of Colorectal Cancer Patients. *Cell* **2015**, *161* (4), 933–945. https://doi.org/10.1016/j.cell.2015.03.053.

(87) Weeber, F.; van de Wetering, M.; Hoogstraat, M.; Dijkstra, K. K.; Krijgsman, O.; Kuilman, T.; Gadellaa-van

Hooijdonk, C. G.; van der Velden, D. L.; Peeper, D. S.; Cuppen, E. P.; et al. Preserved Genetic Diversity in Organoids Cultured from Biopsies of Human Colorectal Cancer Metastases. *Proc Natl Acad Sci U S A* **2015**, *112* (43), 13308–13311. https://doi.org/10.1073/pnas.1516689112.

(88) Schütte, M.; Risch, T.; Abdavi-Azar, N.; Boehnke, K.; Schumacher, D.; Keil, M.; Yildiriman, R.; Jandrasits, C.; Borodina, T.; Amstislavskiy, V.; et al. Molecular Dissection of Colorectal Cancer in Pre-Clinical Models Identifies Biomarkers Predicting Sensitivity to EGFR Inhibitors. *Nat. Commun.* **2017**, *8*. https://doi.org/10.1038/ncomms14262.

(89) Nozaki, K.; Mochizuki, W.; Matsumoto, Y.; Matsumoto, T.; Fukuda, M.; Mizutani, T.; Watanabe, M.; Nakamura, T. Co-Culture with Intestinal Epithelial Organoids Allows Efficient Expansion and Motility Analysis of Intraepithelial Lymphocytes. *J. Gastroenterol.* **2016**, *51* (3), 206–213. https://doi.org/10.1007/s00535-016-1170-8.

(90) Yan Kelvin Yip, H.; Tan, C. W.; Hirokawa, Y.; Burgess, A. W. Colon Organoid Formation and Cryptogenesis Are Stimulated by Growth Factors Secreted from Myofibroblasts. *PLoS One* **2018**, *13* (6). https://doi.org/10.1371/journal.pone.0199412.

(91) Hirokawa, Y.; Yip, K. H. Y.; Tan, C. W.; Burgess, A. W. Colonic Myofibroblast Cell Line Stimulates Colonoid Formation. *Am. J. Physiol. - Gastrointest. Liver Physiol.* **2014**, *306* (7). https://doi.org/10.1152/ajpgi.00267.2013.

(92) Kabiri, Z.; Greicius, G.; Madan, B.; Biechele, S.; Zhong, Z.; Zaribafzadeh, H.; Edison; Aliyev, J.; Wu, Y.; Bunte, R.; et al. Stroma Provides an Intestinal Stem Cell Niche in the Absence of Epithelial Wnts. *Development* **2014**, *141* (11), 2206–2215. https://doi.org/10.1242/dev.104976.

(93) Pastuła, A.; Middelhoff, M.; Brandtner, A.; Tobiasch, M.; Höhl, B.; Nuber, A. H.; Demir, I. E.; Neupert, S.; Kollmann, P.; Mazzuoli-Weber, G.; et al. Three-Dimensional Gastrointestinal Organoid Culture in Combination with Nerves or Fibroblasts: A Method to Characterize the Gastrointestinal Stem Cell Niche. *Stem Cells Int.* **2016**, *2016*, 1–16. https://doi.org/10.1155/2016/3710836.

(94) Hubert, C. G.; Rivera, M.; Spangler, L. C.; Wu, Q.; Mack, S. C.; Prager, B. C.; Couce, M.; McLendon, R. E.; Sloan, A. E.; Rich, J. N. A Three-Dimensional Organoid Culture System Derived from Human Glioblastomas Recapitulates the Hypoxic Gradients and Cancer Stem Cell Heterogeneity of Tumours Found In Vivo. *Cancer Res.* **2016**, *76* (8), 2465–2477. https://doi.org/10.1158/0008-5472.CAN-15-2402.

(95) Choi, N. W.; Cabodi, M.; Held, B.; Gleghorn, J. P.; Bonassar, L. J.; Stroock, A. D. Microfluidic Scaffolds for Tissue Engineering. *Nat. Mater.* **2007**, *6* (11), 908–915. https://doi.org/10.1038/nmat2022.

(96) Bruzewicz, D. A.; McGuigan, A. P.; Whitesides, G. M. Fabrication of a Modular Tissue Construct in a Microfluidic Chip. *Lab Chip* **2008**, *8* (5), 663. https://doi.org/10.1039/b719806j.

(97) Weeber, F.; Ooft, S. N.; Dijkstra, K. K.; Voest, E. E. Tumour Organoids as a Pre-Clinical Cancer Model for Drug Discovery. *Cell Chem. Biol.* **2017**, *24* (9), 1092–1100. https://doi.org/10.1016/j.chembiol.2017.06.012.

(98) Vlachogiannis, G.; Hedayat, S.; Vatsiou, A.; Jamin, Y.; Fernández-Mateos, J.; Khan, K.; Lampis, A.; Eason, K.; Huntingford, I.; Burke, R.; et al. Patient-Derived Organoids Model Treatment Response of Metastatic Gastrointestinal Cancers. *Science (80-.).* **2018**, *359* (6378), 920–926. https://doi.org/10.1126/science.aao2774.

(99) Verissimo, C. S.; Overmeer, R. M.; Ponsioen, B.; Drost, J.; Mertens, S.; Verlaan-Klink, I.; Gerwen, B. van; van der Ven, M.; Wetering, M. van de; Egan, D. A.; et al. Targeting Mutant RAS in Patient-Derived Colorectal Cancer Organoids by Combinatorial Drug Screening. *Elife* **2016**, *5*. https://doi.org/10.7554/eLife.18489.

(100) Dekkers, J. F.; Wiegerinck, C. L.; De Jonge, H. R.; Bronsveld, I.; Janssens, H. M.; De Winter-De Groot, K. M.; Brandsma, A. M.; De Jong, N. W. M.; Bijvelds, M. J. C.; Scholte, B. J.; et al. A Functional CFTR Assay Using Primary Cystic Fibrosis Intestinal Organoids. *Nat. Med.* **2013**, *19* (7), 939–945. https://doi.org/10.1038/nm.3201.

(101) Dekkers, J. F.; Berkers, G.; Kruisselbrink, E.; Vonk, A.; De Jonge, H. R.; Janssens, H. M.; Bronsveld, I.; Van De Graaf, E. A.; Nieuwenhuis, E. E. S.; Houwen, R. H. J.; et al. Characterizing Responses to CFTR-Modulating Drugs Using Rectal Organoids Derived from Subjects with Cystic Fibrosis. *Sci. Transl. Med.* **2016**, *8* (344), 344ra84-344ra84. https://doi.org/10.1126/scitranslmed.aad8278.

(102) Vidovic, D.; Carlon, M. S.; Da Cunha, M. F.; Dekkers, J. F.; Hollenhorst, M. I.; Bijvelds, M. J. C.; Ramalho, A. S.; Van Den Haute, C.; Ferrante, M.; Baekelandt, V.; et al. RAAV-CFTRDR Rescues the Cystic Fibrosis Phenotype in Human Intestinal Organoids and Cystic Fibrosis Mice. *Am. J. Respir. Crit. Care Med.* **2016**, *193* (3), 288–298. https://doi.org/10.1164/rccm.201505-0914OC.

(103) Boehnke, K.; Iversen, P. W.; Schumacher, D.; Lallena, M. J.; Haro, R.; Amat, J.; Haybaeck, J.; Liebs, S.; Lange, M.; Schäfer, R.; et al. Assay Establishment and Validation of a High-Throughput Screening Platform for Three-Dimensional Patient-Derived Colon Cancer Organoid Cultures. *J. Biomol. Screen.* **2016**, *21* (9), 931–941. https://doi.org/10.1177/1087057116650965.

(104) Wilding, J. L.; Bodmer, W. F. Cancer Cell Lines for Drug Discovery and Development. *Cancer Research*. American Association for Cancer Research Inc. January 5, 2014, pp 2377–2384. https://doi.org/10.1158/0008-5472.CAN-13-2971.

(105) Behjati, S.; Huch, M.; Van Boxtel, R.; Karthaus, W.; Wedge, D. C.; Tamuri, A. U.; Martincorena, I.; Petljak, M.; Alexandrov, L. B.; Gundem, G.; et al. Genome Sequencing of Normal Cells Reveals Developmental Lineages and Mutational Processes. *Nature* **2014**, *513* (7518), 422–425. https://doi.org/10.1038/nature13448.

(106) Sato, T.; Vries, R. G.; Snippert, H. J.; van de Wetering, M.; Barker, N.; Stange, D. E.; van Es, J. H.; Abo, A.; Kujala, P.; Peters, P. J.; et al. Single Lgr5 Stem Cells Build Crypt-Villus Structures in Vitro without a Mesenchymal Niche. *Nature* **2009**, *459* (7244), 262–265. https://doi.org/10.1038/nature07935.

(107) Sato, T.; Stange, D. E.; Ferrante, M.; Vries, R. G. J.; Van Es, J. H.; Van Den Brink, S.; Van Houdt, W. J.; Pronk, A.; Van Gorp, J.; Siersema, P. D.; et al. Long-Term Expansion of Epithelial Organoids from Human Colon, Adenoma, Adenocarcinoma, and Barrett's Epithelium. *Gastroenterology* **2011**, *141* (5), 1762–1772. https://doi.org/10.1053/j.gastro.2011.07.050.

(108) Eastman, A. Improving Anticancer Drug Development Begins with Cell Culture: Misinformation Perpetrated by the Misuse of Cytotoxicity Assays. *Oncotarget* **2017**, *8* (5), 8854–8866. https://doi.org/10.18632/oncotarget.12673.

(109) Junttila, M. R.; De Sauvage, F. J. Influence of Tumour Micro-Environment Heterogeneity on Therapeutic Response. *Nature*. Nature 2013, pp 346–354. https://doi.org/10.1038/nature12626.

(110) Ootani, A.; Li, X.; Sangiorgi, E.; Ho, Q. T.; Ueno, H.; Toda, S.; Sugihara, H.; Fujimoto, K.; Weissman, I. L.; Capecchi, M. R.; et al. Sustained in Vitro Intestinal Epithelial Culture within a Wnt-Dependent Stem Cell Niche. *Nat. Med.* **2009**, *15* (6), 701–706. https://doi.org/10.1038/nm.1951.

(111) De Lau, W.; Barker, N.; Low, T. Y.; Koo, B. K.; Li, V. S. W.; Teunissen, H.; Kujala, P.; Haegebarth, A.; Peters, P. J.; Van De Wetering, M.; et al. Lgr5 Homologues Associate with Wnt Receptors and Mediate R-Spondin Signalling. *Nature* **2011**, *476* (7360), 293–297. https://doi.org/10.1038/nature10337.

(112) Gregorieff, A.; Pinto, D.; Begthel, H.; Destrée, O.; Kielman, M.; Clevers, H. Expression Pattern of Wnt Signaling Components in the Adult Intestine. *Gastroenterology* **2005**, *129* (2), 626–638. https://doi.org/10.1016/j.gastro.2005.06.007.

(113) Sato, T.; Van Es, J. H.; Snippert, H. J.; Stange, D. E.; Vries, R. G.; Van Den Born, M.; Barker, N.; Shroyer, N. F.; Van De Wetering, M.; Clevers, H. Paneth Cells Constitute the Niche for Lgr5 Stem Cells in Intestinal Crypts. *Nature*

2011, *469* (7330), 415–418. https://doi.org/10.1038/nature09637.

(114) Dignass, A. U.; Sturm, A. Peptide Growth Factors in the Intestine. *European Journal of Gastroenterology and Hepatology*. Eur J Gastroenterol Hepatol 2001, pp 763–770. https://doi.org/10.1097/00042737-200107000-00002.

(115) Denu, J. M. Vitamin B3 and Sirtuin Function. *Trends in Biochemical Sciences*. Elsevier Ltd 2005, pp 479–483. https://doi.org/10.1016/j.tibs.2005.07.004.

(116) Frisch, S. M.; Francis, H. Disruption of Epithelial Cell-Matrix Interactions Induces Apoptosis. *J. Cell Biol.* **1994**, *124* (4), 619–626. https://doi.org/10.1083/jcb.124.4.619.

(117) Grossmann, J. Molecular Mechanisms of "Detachment-Induced Apoptosis - Anoikis." *Apoptosis*. Kluwer Academic Publishers 2002, pp 247–260. https://doi.org/10.1023/A:1015312119693.

(118) Hofmann, C.; Obermeier, F.; Artinger, M.; Hausmann, M.; Falk, W.; Schoelmerich, J.; Rogler, G.; Grossmann, J. Cell-Cell Contacts Prevent Anoikis in Primary Human Colonic Epithelial Cells. *Gastroenterology* **2007**, *132* (2), 587–600. https://doi.org/10.1053/j.gastro.2006.11.017.

(119) Sasaki, T.; Giltay, R.; Talts, U.; Timpl, R.; Talts, J. F. Expression and Distribution of Laminin A1 and A2 Chains in Embryonic and Adult Mouse Tissues: An Immunochemical Approach. *Exp. Cell Res.* **2002**, *275* (2), 185–199. https://doi.org/10.1006/excr.2002.5499.

(120) Tojo, M.; Hamashima, Y.; Hanyu, A.; Kajimoto, T.; Saitoh, M.; Miyazono, K.; Node, M.; Imamura, T. The ALK-5 Inhibitor A-83-01 Inhibits Smad Signaling and Epithelial-to-Mesenchymal Transition by Transforming Growth Factor-β. *Cancer Sci.* **2005**, *96* (11), 791–800. https://doi.org/10.1111/j.1349-7006.2005.00103.x.

(121) Düzgün, Ş. A.; Yerlikaya, A.; Zeren, S.; Bayhan, Z.; Okur, E.; Boyacı, İ. Differential Effects of P38 MAP Kinase Inhibitors SB203580 and SB202190 on Growth and Migration of Human MDA-MB-231 Cancer Cell Line. *Cytotechnology* **2017**, *69* (4), 711–724. https://doi.org/10.1007/s10616-017-0079-2.

(122) Manthey, C. L.; Wang, S. W.; Kinney, S. D.; Yao, Z. SB202190, a Selective Inhibitor of P38 Mitogen-Activated Protein Kinase, Is a Powerful Regulator of LPS-Induced MRNAs in Monocytes. *J. Leukoc. Biol.* **1998**, *64* (3), 409–417. https://doi.org/10.1002/jlb.64.3.409.

(123) Drost, J.; van Jaarsveld, R. H.; Ponsioen, B.; Zimberlin, C.; van Boxtel, R.; Buijs, A.; Sachs, N.; Overmeer, R. M.; Offerhaus, G. J.; Begthel, H.; et al. Sequential Cancer Mutations in Cultured Human Intestinal Stem Cells. *Nature* **2015**, *521* (7550), 43–47. https://doi.org/10.1038/nature14415.

(124) Matano, M.; Date, S.; Shimokawa, M.; Takano, A.; Fujii, M.; Ohta, Y.; Watanabe, T.; Kanai, T.; Sato, T. Modeling Colorectal Cancer Using CRISPR-Cas9–Mediated Engineering of Human Intestinal Organoids. *Nat. Med.* **2015**, *21* (3), 256–262. https://doi.org/10.1038/nm.3802.

(125) Semenza, G. L. Regulation of Metabolism by Hypoxia-Inducible Factor 1. *Cold Spring Harb. Symp. Quant. Biol.* **2011**, *76* (0), 347–353. https://doi.org/10.1101/sqb.2011.76.010678.

(126) Fischbach, C.; Chen, R.; Matsumoto, T.; Schmelzle, T.; Brugge, J. S.; Polverini, P. J.; Mooney, D. J. Engineering Tumours with 3D Scaffolds. *Nat. Methods* **2007**, *4* (10), 855–860. https://doi.org/10.1038/nmeth1085.

(127) Rodenhizer, D.; Gaude, E.; Cojocari, D.; Mahadevan, R.; Frezza, C.; Wouters, B. G.; McGuigan, A. P. A Three-Dimensional Engineered Tumour for Spatial Snapshot Analysis of Cell Metabolism and Phenotype in Hypoxic Gradients. *Nat. Mater.* **2016**, *15* (2), 227–234. https://doi.org/10.1038/nmat4482.

(128) Merker, S. R.; Weitz, J.; Stange, D. E. Gastrointestinal Organoids: How They Gut It Out. *Dev. Biol.* **2016**, *420* (2), 239–250. https://doi.org/10.1016/J.YDBIO.2016.08.010.

(129) Gattazzo, F.; Urciuolo, A.; Bonaldo, P. Extracellular Matrix: A Dynamic Microenvironment for Stem Cell Niche. *Biochimica et Biophysica Acta - General Subjects*. Elsevier 2014, pp 2506–2519. https://doi.org/10.1016/j.bbagen.2014.01.010.

(130) Fujii, S.; Suzuki, K.; Kawamoto, A.; Ishibashi, F.; Nakata, T.; Murano, T.; Ito, G.; Shimizu, H.; Mizutani, T.; Oshima, S.; et al. PGE2 Is a Direct and Robust Mediator of Anion/Fluid Secretion by Human Intestinal Epithelial Cells. *Sci. Rep.* **2016**, *6* (1), 1–15. https://doi.org/10.1038/srep36795.

(131) Muzny, D. M.; Bainbridge, M. N.; Chang, K.; Dinh, H. H.; Drummond, J. A.; Fowler, G.; Kovar, C. L.; Lewis, L. R.; Morgan, M. B.; Newsham, I. F.; et al. Comprehensive Molecular Characterization of Human Colon and Rectal Cancer. *Nature* **2012**, *487* (7407), 330–337. https://doi.org/10.1038/nature11252.

(132) Vlachogiannis, G.; Hedayat, S.; Vatsiou, A.; Jamin, Y.; Fernández-Mateos, J.; Khan, K.; Lampis, A.; Eason, K.; Huntingford, I.; Burke, R.; et al. Patient-Derived Organoids Model Treatment Response of Metastatic Gastrointestinal Cancers. *Science (80-.).* **2018**, *359* (6378), 920–926. https://doi.org/10.1126/science.aao2774.

(133) Luo, Z. W.; Zhu, M. G.; Zhang, Z. Q.; Ye, F. J.; Huang, W. H.; Luo, X. Z. Increased Expression of Ki-67 Is a Poor Prognostic Marker for Colorectal Cancer Patients: A Meta Analysis. *BMC Cancer* **2019**, *19* (1), 123. https://doi.org/10.1186/s12885-019-5324-y.

(134) Walsh, M. D.; Clendenning, M.; Williamson, E.; Pearson, S. A.; Walters, R. J.; Nagler, B.; Packenas, D.; Win, A. K.; Hopper, J. L.; Jenkins, M. A.; et al. Expression of MUC2, MUC5AC, MUC5B, and MUC6 Mucins in Colorectal Cancers and Their Association with the CpG Island Methylator Phenotype. *Mod. Pathol.* **2013**, *26* (12), 1642–1656. https://doi.org/10.1038/modpathol.2013.101.

(135) Fritzmann, J.; Morkel, M.; Besser, D.; Budczies, J.; Kosel, F.; Brembeck, F. H.; Stein, U.; Fichtner, I.; Schlag, P. M.; Birchmeier, W. A Colorectal Cancer Expression Profile That Includes Transforming Growth Factor β Inhibitor BAMBI Predicts Metastatic Potential. *Gastroenterology* **2009**, *137* (1), 165–175. https://doi.org/10.1053/j.gastro.2009.03.041.

(136) Takahashi, M.; Fujita, M.; Furukawa, Y.; Hamamoto, R.; Shimokawa, T.; Miwa, N.; Ogawa, M.; Nakamura, Y. Isolation of a Novel Human Gene, APCDD1, as a Direct Target of the B-Catenin/ T-Cell Factor 4 Complex with Probable Involvement in Colorectal Carcinogenesis. *Cancer Res.* **2003**, 6116–6120.

(137) Morgan, R. G.; Mortensson, E.; Williams, A. C. Targeting LGR5 in Colorectal Cancer: Therapeutic Gold or Too Plastic? *British Journal of Cancer*. Nature Publishing Group May 1, 2018, pp 1410–1418. https://doi.org/10.1038/s41416-018-0118-6.

(138) Uhlen, M.; Fagerberg, L.; Hallstrom, B. M.; Lindskog, C.; Oksvold, P.; Mardinoglu, A.; Sivertsson, A.; Kampf, C.; Sjostedt, E.; Asplund, A.; et al. Tissue-Based Map of the Human Proteome. *Science (80-.).* **2015**, *347* (6220), 1260419–1260419. https://doi.org/10.1126/science.1260419.

(139) Fan, Y.-Y.; Davidson, L. A.; Callaway, E. S.; Wright, G. A.; Safe, S.; Chapkin, R. S. A Bioassay to Measure Energy Metabolism in Mouse Colonic Crypts, Organoids, and Sorted Stem Cells. *Am. J. Physiol. - Gastrointest. Liver Physiol.* **2015**, *309* (1), G1–G9. https://doi.org/10.1152/ajpgi.00052.2015.

(140) Sato, T.; Clevers, H. Growing Self-Organizing Mini-Guts from a Single Intestinal Stem Cell: Mechanism and Applications. *Science*. American Association for the Advancement of Science 2013, pp 1190–1194. https://doi.org/10.1126/science.1234852.

(141) Barker, N.; Van Es, J. H.; Kuipers, J.; Kujala, P.; Van Den Born, M.; Cozijnsen, M.; Haegebarth, A.; Korving, J.; Begthel, H.; Peters, P. J.; et al. Identification of Stem Cells in Small Intestine and Colon by Marker Gene Lgr5. *Nature*

2007, *449* (7165), 1003–1007. https://doi.org/10.1038/nature06196.

(142) Onozato, D.; Yamashita, M.; Nakanishi, A.; Akagawa, T.; Kida, Y.; Ogawa, I.; Hashita, T.; Iwao, T.; Matsunaga, T. Generation of Intestinal Organoids Suitable for Pharmacokinetic Studies from Human Induced Pluripotent Stem Cells. *Drug Metab. Dispos.* **2018**, *46* (11), 1572–1580. https://doi.org/10.1124/dmd.118.080374.

(143) Ozawa, T.; Takayama, K.; Okamoto, R.; Negoro, R.; Sakurai, F.; Tachibana, M.; Kawabata, K.; Mizuguchi, H. Generation of Enterocyte-like Cells from Human Induced Pluripotent Stem Cells for Drug Absorption and Metabolism Studies in Human Small Intestine. *Sci. Rep.* **2015**, *5* (1), 1–11. https://doi.org/10.1038/srep16479.

(144) Töpfer, E.; Pasotti, A.; Telopoulou, A.; Italiani, P.; Boraschi, D.; Ewart, M. A.; Wilde, C. Bovine Colon Organoids: From 3D Bioprinting to Cryopreserved Multi-Well Screening Platforms. *Toxicol. Vitr.* **2019**, *61*, 1–8. https://doi.org/10.1016/j.tiv.2019.104606.

(145) Takahashi, T. Organoids for Drug Discovery and Personalized Medicine. *Annual Review of Pharmacology and Toxicology*. Annual Reviews Inc. January 6, 2019, pp 447–462. https://doi.org/10.1146/annurev-pharmtox-010818-021108.

(146) Qiao, L.; Koutsos, M.; Tsai, L. L.; Kozoni, V.; Guzman, J.; Shiff, S. J.; Rigas, B. Staurosporine Inhibits the Proliferation, Alters the Cell Cycle Distribution and Induces Apoptosis in HT-29 Human Colon Adenocarcinoma Cells. *Cancer Lett.* **1996**, *107* (1), 83–89. https://doi.org/10.1016/0304-3835(96)04346-7.

(147) Lüpertz, R.; Wätjen, W.; Kahl, R.; Chovolou, Y. Dose- and Time-Dependent Effects of Doxorubicin on Cytotoxicity, Cell Cycle and Apoptotic Cell Death in Human Colon Cancer Cells. *Toxicology* **2010**, *271* (3), 115–121. https://doi.org/10.1016/j.tox.2010.03.012.

(148) Xiong, S.; Xiao, G. W. Reverting Doxorubicin Resistance in Colon Cancer by Targeting a Key Signaling Protein, Steroid Receptor Coactivator. *Exp. Ther. Med.* **2018**, *15* (4), 3751–3758. https://doi.org/10.3892/etm.2018.5912.

(149) Tailor, D.; Hahm, E.-R.; Kale, R. K.; Singh, S. V; Singh, R. P. Sodium Butyrate Induces DRP1-Mediated Mitochondrial Fusion and Apoptosis in Human Colorectal Cancer Cells. *Mitochondrion* **2014**, *16*, 55–64. https://doi.org/10.1016/j.mito.2013.10.004.

(150) Scharlau, D.; Borowicki, A.; Habermann, N.; Hofmann, T.; Klenow, S.; Miene, C.; Munjal, U.; Stein, K.; Glei, M. Mechanisms of Primary Cancer Prevention by Butyrate and Other Products Formed during Gut Flora-Mediated Fermentation of Dietary Fibre. *Mutat. Res. - Rev. Mutat. Res.* **2009**, *682* (1), 39–53. https://doi.org/10.1016/j.mrrev.2009.04.001.

(151) Sengupta, S.; Muir, J. G.; Gibson, P. R. Does Butyrate Protect from Colorectal Cancer? *J. Gastroenterol. Hepatol.* **2006**, *21* (1 Pt 2), 209–218. https://doi.org/10.1111/j.1440-1746.2006.04213.x.

(152) Haraguchi, N.; Ohkuma, M.; Sakashita, H.; Matsuzaki, S.; Tanaka, F.; Mimori, K.; Kamohara, Y.; Inoue, H.; Mori, M. CD133+CD44+ Population Efficiently Enriches Colon Cancer Initiating Cells. *Ann. Surg. Oncol.* **2008**, *15* (10), 2927–2933. https://doi.org/10.1245/s10434-008-0074-0.

(153) Augeron, C.; Laboisse, C. L. Emergence of Permanently Differentiated Cell Clones in a Human Colonic Cancer Cell Line in Culture after Treatment with Sodium Butyrate. *Cancer Res.* **1984**, *44* (9).

(154) Souleimani, A.; Asselin, C. Regulation of C-Myc Expression by Sodium Butyrate in the Colon Carcinoma Cell Line Caco-2. *FEBS Lett.* **1993**, *326* (1–3), 45–50. https://doi.org/10.1016/0014-5793(93)81758-R.

(155) Freshney, R. I. Basic Principles of Cell Culture. In *Culture of Cells for Tissue Engineering*; Vunjak-Novakovic, G., Freshney, R. I., Eds.; 2005; pp 1–21. https://doi.org/doi:10.1002/0471741817.ch1.

(156) Yamamoto, S.; Rafique, T.; Priyantha, W. S.; Fukui, K.; Matsumoto, T.; Niino, T. Development of a Cryopreservation Procedure Using Aluminium Cryo-Plates. *Cryo Letters* **2011**, *32* (3), 256–265.

(157) Bahari, L.; Bein, A.; Yashunsky, V.; Braslavsky, I. Directional Freezing for the Cryopreservation of Adherent Mammalian Cells on a Substrate. *PLoS One* **2018**, *13* (2), 1–17. https://doi.org/10.1371/journal.pone.0192265.

(158) Divakaruni, A. S.; Paradyse, A.; Ferrick, D. A.; Murphy, A. N.; Jastroch, M. Analysis and Interpretation of Microplate-Based Oxygen Consumption and PH Data. In *Methods in Enzymology*; Academic Press Inc., 2014; Vol. 547, pp 309–354. https://doi.org/10.1016/B978-0-12-801415-8.00016-3.

(159) John Morris, G.; Acton, E. Controlled Ice Nucleation in Cryopreservation - A Review. *Cryobiology*. April 2013, pp 85–92. https://doi.org/10.1016/j.cryobiol.2012.11.007.

(160) Cellink. CELLINK LAMININK 521 - Cellink Global https://www.cellink.com/global/product/cellink-laminink-521/ (accessed Oct 8, 2020).

(161) Ashammakhi, N.; Ahadian, S.; Xu, C.; Montazerian, H.; Ko, H.; Nasiri, R.; Barros, N.; Khademhosseini, A. Bioinks and Bioprinting Technologies to Make Heterogeneous and Biomimetic Tissue Constructs. *Materials Today Bio*. Elsevier B.V. January 1, 2019, p 100008. https://doi.org/10.1016/j.mtbio.2019.100008.

(162) Sato, T.; Van Es, J. H.; Snippert, H. J.; Stange, D. E.; Vries, R. G.; Van Den Born, M.; Barker, N.; Shroyer, N. F.; Van De Wetering, M.; Clevers, H. Paneth Cells Constitute the Niche for Lgr5 Stem Cells in Intestinal Crypts. *Nature* **2011**, *469* (7330), 415–418. https://doi.org/10.1038/nature09637.

(163) Castro-Villabon, D.; Avello, Y.; Ruiz, N.; Rodríguez-Urrego, P. Implementation of Routine Thromboplastin-Plasma Cell Block Technique in the Evaluation of Non-Gynecologic Specimens: A Methodologic Comparison with Conventional Cytology. *J. Microsc. Ultrastruct.* **2014**, *2* (3), 177. https://doi.org/10.1016/j.jmau.2014.05.001.

(164) Poojan, S.; Kim, H. S.; Yoon, J. W.; Sim, H. W.; Hong, K. M. Determination of Protein Expression Level in Cultured Cells by Immunocytochemistry on Paraffin-Embedded Cell Blocks. *J. Vis. Exp.* **2018**, *2018* (135), 57369. https://doi.org/10.3791/57369.

(165) Wu, M.; Neilson, A.; Swift, A. L.; Moran, R.; Tamagnine, J.; Parslow, D.; Armistead, S.; Lemire, K.; Orrell, J.; Teich, J.; et al. Multiparameter Metabolic Analysis Reveals a Close Link between Attenuated Mitochondrial Bioenergetic Function and Enhanced Glycolysis Dependency in Human Tumour Cells. *Am. J. Physiol. - Cell Physiol.* **2007**, *292* (1). https://doi.org/10.1152/ajpcell.00247.2006.